Surface Modification and Characterization of Cellulose Nanocrystals For Biomedical Applications

by

Seyedeh Parinaz Akhlaghi

A thesis
presented to the University of Waterloo
in fulfillment of the
thesis requirement for the degree of
Doctor of Philosophy
in
Chemical Engineering-Nanotechnology

Waterloo, Ontario, Canada, 2014

Author's Declaration

I hereby declare that I am the sole author of this thesis. This is a true copy of the thesis, including any required final revisions, as accepted by my examiners.

I understand that my thesis may be made electronically available to the public.

Abstract

There is an ever-increasing desire to develop novel materials that could control the release of active compounds and increase their stability. Replacing petroleum-based synthetic polymers with sustainable materials has many advantages, such as reducing the dependence on fossil fuels, and diminishing environmental pollution. Recently, cellulose nanocrystal (CNC) obtained by acid hydrolysis of cellulose fibres has gained a lot of interest. The high mechanical strength, large and negatively charged surface area, and the presence of several hydroxyl groups that allow for modification with different functionalities make CNC an excellent candidate for various applications in the biomedical field. This thesis explores (i) the surface modification and characterization of modified CNC and (ii) the biomedical applications of these novel sustainable nanomaterials.

In the first part, amine functionalized CNC was prepared. Ammonium hydroxide was reacted with epichlorohydrin (EPH) to produce 2-hydroxy-3-chloro propylamine (HCPA), which was then grafted to CNC using an etherification reaction. A series of reactions were carried out to determine the optimal conditions. The final product (CNC-NH_2(T)) was dialyzed for one week. Further purification via centrifugation yielded the sediment (CNC-NH_2(P)) and supernatant (POLY-NH_2). The presence of amine groups was confirmed by FT-IR and the amine content was determined by potentiometric titration and elemental analysis. A high amine content of 2.2 and 0.6 mmol amine/g was achieved for CNC-NH_2(T) and CNC-NH_2(P), respectively. Zeta potential measurements confirmed the charge reversal of amine CNC from negative to positive when the pH was decreased from 10 to 3. TEM images showed similar structural properties of the nanocrystals along with some minor aggregation. This simple, yet effective synthesis method can be used for further conjugation as required for various biomedical applications. Moreover, the surface of CNC was modified with chitosan oligosaccharide (CS_{OS}). First, the primary alcohol groups of CNC were selectively oxidized to carboxyl groups using the catalyst, 2,2,6,6-tetramethylpiperidine-1-oxyl radical (TEMPO), and were then reacted with the amino groups of CS_{OS} via the carbodiimide reaction using N-hydroxysuccinimide (NHS) and 1-Ethyl-3-(3-dimethylaminopropyl)-carbodiimide (EDC). The appearance of C=O peak in FT-IR spectrum of oxidized CNC (CNC-OX), accompanied by calculations based on potentiometric titration revealed that CNC was successfully oxidized with a degree of oxidation of 0.28. The grafting of CS_{OS} on oxidized CNC was confirmed by the following observations: (i) the reduction of the C=O peak in FT-IR of CNC-CS_{OS} and the appearance of new amide peaks; (ii) the significant reduction of the carbonyl peak at 175 ppm in the ^{13}C NMR spectrum for CNC-CS_{OS}; (iii) a higher decomposition temperature in TGA of CNC-CS_{OS}; (iv) a positive zeta potential of CNC-CS_{OS} at acidic pH; and (v) a degree of

substitution of 0.26, which is close to the DO (0.28), indicating that $\sim$ 90% of COOH groups on CNC-OX were involved in the formation of amide bonds with CS_{OS}. TEM and AFM studies also revealed a completely different morphology for CNC-CS_{OS}.

In the second part, the potential of exploiting CNCs as delivery carriers for two cationic model drugs, procaine hydrochloride (PrHy) and imipramine hydrochloride (IMI), were investigated. IMI displayed a higher binding to CNC derivatives compared to PrHy. Isothermal titration calorimetry (ITC), transmittance and zeta potential measurements were used to elucidate the complexation between model drugs and CNC samples. It was observed that the more dominant exothermic peak observed in the ITC isotherms leading to the formation of larger particle-drug complexes could explain the increased binding of IMI to CNC samples. Drug selective membranes were prepared for each model drug that displayed adequate stability and rapid responses. Different *in vitro* release profiles at varying pH conditions were observed due to the pH responsive properties of the systems. Both drugs were released rapidly from CNC samples due to the ion-exchange effect, and CNC-CS_{OS} displayed a more sustained release profile. Furthermore, the antioxidant properties of CNC samples and the potential of CNC-CS_{OS} as a carrier for the delivery of vitamin C was investigated. CNC-CS_{OS}/vitamin C complexes (CNCS/VC) were formed between CNC-CS_{OS} and vitamin C via ionic complexation using sodium tripolyphosphate (TPP). The complexation was confirmed via DSC and UV-Vis absorbance measurements. TEM images showed complexes with a size of approximately 1 μm. The encapsulation efficiency of vitamin C was higher ($\sim$ 91%) at pH 5 compared to pH 3 ($\sim$ 72%). The *in vitro* release of vitamin C from CNCS/VC complexes exhibited a sustained release of up to 3 weeks, with the released vitamin C displaying higher stability compared to a control vitamin C solution. Antioxidant activity and kinetics of various CNC samples were studied using the 2,2-diphenyl-1-picrylhydrazyl (DPPH) assay. CNC-CS_{OS} possessed a higher scavenging activity and faster antioxidant activity compared to its precursors, CNC-OX and CS_{OS}, and their physical mixture. Therefore, by loading vitamin C into CNC-CS_{OS} particles, a dynamic antioxidant system was produced. Vitamin C can be released over a prolonged time period displaying enhanced and sustained antioxidant properties since the carrier CNC-CS_{OS} also possesses antioxidant properties.

As a result of this doctoral study, knowledge on the surface modification of CNC with amine groups and CS_{OS} have been advanced. The *in vitro* drug release and antioxidant studies suggest that systems comprising of CNC could be further explored as potential carriers in biomedical applications.

Acknowledgements

As I begin to write the Acknowledgements section of my thesis, I cannot stop thinking of the long journey I have taken and the many wonderful people I have met along the way who have made it possible for me to become the person I am today. For me doing my PhD was not just about becoming a better scientist but was more of a personal journey to practice endurance, patience and trust.

I am thankful to my supervisor Professor Michael Tam for all his endless support and encouragement from the very first day I became his student. He believed in me and hired a pharmacist into an engineering program and taught me so many things. Most of all he helped me discover my passions and my potentials by helping me step out of my comfort zone. Thank you Professor Tam for everything! I would like to thank my committee members Prof. Anderson, Prof. Duhamel, Prof. Zhao and Prof. Charpentier for their valuable comments and suggestions regarding my research and my thesis. I would like to thank Prof. Bill Power who helped me analyze my NMR results and kindly explained everything to me. People like him inspire me to become a better teacher and a better person.

My wonderful labmates have been my source of energy and motivation throughout my studies. Masuduz Zaman and Rasim Batmaz came up with the idea of increasing the amine content on the amine CNC and optimized the reaction. They shared their knowledge with me and were great people to work with. Nishil Mohamed has been a great partner who collaborated with me on several projects. His patience and kindness along with his attention to details made working with him a pleasure. Debbie Wu has brightened my days so many times and helped me with several parts of my research. Her artistic side and great talent has helped me in improving my presentations and the quality of my images. All my other labmates in the Laboratory for Functional Colloids and Nanomaterials, whom I have had the pleasure to work with are dearly appreciated. This thesis would have not been possible without the help of my talented co-op students and undergraduate research assistants Paola Pochmann, Derek Sun, Anthony Wang, Moin Ahmed and Daryl Tiong. I believe that they have taught me a lot more than I have taught them and I have great memories of working with each one of them.

I would like to thank all my great friends in Waterloo and around the world for supporting me in every possible way. Mahsa Shayan, who I consider to be the sister I never had, Sophie Chen, my dance and yoga buddy, Parisa Sadamousavi, Lena Ahmadi and Ngan Huang who have always been there for me and cheered me up several times. I would also like to thank Neil Gibson for all the wonderful chats we had and how he helped me learn

a lot about myself and aim for the stars. All the support and encouragement of Kristin Meier who has helped me grow both personally and academically is dearly acknowledged. I would also like to thank Cesar Brinatti who has helped me in several aspects of my PhD and made the completion of my studies possible. His valuable comments on my ITC results, all his support and kindness in proofreading my thesis twice and carefully listening to my four PhD defence rehearsals is truly appreciated. Obrigada!

Last but not least, I would like to thank my family. My cousin Pooya Bayenat who made a cold winter in Canada not so cold with her warm presence and big heart and my amazing talented brother who would take care of all my high tech computer stuff. My late dear grand father "Baba Akhlaghi" who always believed in me and prayed for me every single day is truly acknowledged. At the end I would like to thank my beautiful mother Shiva Shahabi for teaching me patience and endurance and my role model, my father Dr. Farshad Akhlaghi for being my guide in my life. Their love for me has made me do all the things that I once thought were impossible! kheili doosetun daram va merci!

Dedication

To my lovely parents Shiva and Farshad.

Table of Contents

List of Tables

List of Figures

Chapter 1

Introduction

1.1 Overview

Current interests in nanotechnology have led to the development and design of many types of nanomaterials. Functionalization of various types of nanomaterials to achieve novel or improved properties, that take advantage of their synergistic effects would be worthy of exploration. However, currently most of the chemicals used in the synthesis of these nanomaterials are derived from petroleum-based sources. Because of the continuing concerns of global warming arising from greenhouse gases emitted from the production of such feedstocks, there is a growing trend to focus on the development of polymeric nanostructures derived from renewable resources [1]. The potential applications of materials derived from natural sources are being extensively investigated as many biomedical applications are discovered, such as drug delivery. There is ongoing research in developing novel drug carriers that can deliver drugs to their active site with higher therapeutic effects and lower toxicity. New technologies are required to deliver insoluble or unstable therapeutic compounds, localize the delivery of potent drugs, and improve the compliance of patients [2]. The desire towards designing novel products for various applications from renewable resources has led to increased research activity on abundant, natural, biodegradable and biocompatible polymers over the last decade.

Polysaccharides have many advantages that make them suitable for biomedical applications and have gained a lot of interest as surface coatings for pharmaceutical carriers [3]. Small, hydrophilic and biocompatible drug carriers have also shown extended blood circulation times [4]. Polysaccharide drug carriers demonstrate an extended blood circulation time and possess several hydroxyl groups on their surface, which can be functionalized

by chemical coupling reactions. Cellulose fibre is the most abundant natural biomaterial that is comprised of amorphous and crystalline domains. The acid hydrolysis of cellulose fibre disrupts its amorphous regions and releases individual rod-like rigid crystallites called cellulose nanocrystals (CNC) that possess high mechanical strength. The treatment of native cellulose with sulfuric acid introduces negative charges on its surface due to the formation of sulfate ester groups. Interest in CNC has arisen over the last decade because of its availability, low cost and high surface area per volume. CNC possesses many benign properties, such as non-toxicity, biodegradability, and biocompatibility, which make it an excellent candidate for pharmaceutical applications [5]. Due to the presence of several hydroxyl groups, the surface of CNC can be modified with different functional groups, which expands its usefulness in many formulations [6].

The primary hydroxyl groups can be converted to aldehyde, carboxylic acid, and amine functionalities. Cationic modification of cellulose and its derivatives is of interest due to their utility in several key industrial sectors. Cationic CNC has been prepared by a reaction with epoxypropyltrimethylammonium chloride [7] and 4-(1-bromoethyl/bromomethyl) benzoic acid [8]. Amine functionalization of CNC not only introduces cationic charge on the surface of CNC in an acidic medium, but it can also be used for the conjugation of biomolecules to CNC for biomedical applications [9]. In recent years, amine functionalized CNCs have been produced via different synthetic routes. Dong et al. prepared amine CNC by first decorating the surface of CNC with epoxide groups via a reaction with epichlorohydrin (EPH) in sodium hydroxide at $60\,^{\circ}C$. Dialyzing the reaction mixture and opening the epoxide rings using ammonium hydroxide at 60 $^{\circ}C$, then introduced the amine groups on the surface of CNC [10]. However, this reaction was not optimized and the amine content reported was low. Therefore, there is a need to improve the synthetic method and optimize the reaction parameters.

The potential applications of CNC in pharmaceuticals have been studied and efforts have been devoted to develop nanocrystal based drug delivery systems [5, 6, 11, 12, 13]. The ability to form stable aqueous suspensions has given CNC a number of potential applications in controlled release systems as well as in the delivery of drugs. Due to its large surface area and negative charge, cationic drugs can be bound to the surface of CNC with high payloads, providing the potential for optimal dosage control [14].

The second most abundant polymer in nature is chitosan (CS) which is obtained from shrimps and crabs. It is non-toxic, biocompatible, and biodegradable. Different drugs or polymeric systems can bind to CS due to the presence of several amino groups which make it positively charged. Therefore, CS is an excellent potential candidate for delivering drugs and allows the manipulation of their release profiles. Despite the notable properties of CS, there are some problems associated with its *in-vivo* applications due to its, high viscosity,

high molecular weight, large aggregation formation, and low solubility at physiological pHs (7.2-7.4) [15]. The solubility problems can be overcome by utilizing low molecular weight CS, known as chitosan oligosaccharides (CS_{OS}) [16]. There are limited studies on systems consisting of CNC and CS for biomedical applications in the literature. In a relevant study, Wang and coworkers studied polyelectrolyte macroion complex (PMC) formation between CS and CNC for oral drug delivery applications. The particles were formed by electrostatic interactions because of the strong mismatch between the opposite charges of CNC and CS [17].

CNC was first reported as a drug excipient by Jackson and coworkers [14]. Unmodified and surfactant modified CNC was used for the loading of hydrophobic and hydrophilic drugs, respectively. In several studies, Kolakovic and coworkers examined the potential applications of Nanofibrilar Cellulose (NFC) for sustained drug delivery. NFC consists of alternating crystalline and amorphous domains. The release kinetics depended on the solubility of the drug in the medium and its affinity to NFC. In their study, the unbound drug fraction was relatively high, and they attributed it to the fraction that was weakly bound and accessible to water [18]. In another study, their results showed that drugs could be released from the NFC films over prolonged time because of the presence of tight fibre networks that act as a barrier for drug diffusion [19]. Recently, Kolakovic and coworkers used isothermal titration calorimetry (ITC) to study the interactions between NFC and different model drugs of different molecular weights and charge characteristics. The ITC studies showed that the drugs bind to NFC in a pH dependent manner. [20]. Different drugs have been loaded into charged particles as observed in ion-exchange resins [21]. The high charges on these biopolymers allow a strong binding between the drug and its carrier, leading to a slower release [22].

Vitamin C (L-ascorbic acid) is an important antioxidant. It serves as a cofactor in hydroxylation reactions and scavenges reactive oxygen species [23]. Vitamin C has many benefits for the skin (e.g. whitening, anti-aging, depigmenting, etc) [24] and has been used in different cosmetic formulations [25]. However, the formulation of vitamin C is challenging as this compound is unstable and can be easily oxidized [26]. In order to achieve applicable vitamin C formulations, developing methods to increase the stability of vitamin C is required. One way to increase the stability of vitamin C is to encapsulate vitamin C into nanoparticles that have the potential to protect the sensitive bioactive compound from chemical and enzymatic degradation during storage and *in vivo* [27]. CS nanoparticles have been used for the delivery of vitamins [28]. In one study, Jang and coworkers characterized vitamin C-loaded CS nanoparticles and studied their stability [29].

1.2 Research Objectives

The main goal of this study is to develop novel, biocompatible, biodegradable, and non-toxic systems for the delivery of active compounds suitable for biomedical applications. Moreover, to the best of our knowledge, no attempts have been made in exploiting the combined advantages of modifying the surface of CNC with CS_{OS}. By using CS_{OS}, the insolubility problem of CS at physiological pH is addressed. To date, no studies have been published on the antioxidant properties of CNC and its derivatives. In addition, it was expected that chemically modified CNCs would exhibit a more desirable drug release profile compared to unmodified CNC. The other approach in this doctoral thesis is to study the drug loading and *in vitro* release profile of two cationic model drugs from CNC and its derivatives. A detailed study to elucidate the mechanisms of encapsulation and release of drug molecules from CNC was pursued. To the best of our knowledge, no studies have examined the pH dependent drug binding to CNC and its derivatives and the characterization of the CNC-drug complexes. Moreover, the potentials of CNC-CS_{OS} as a drug carrier need to be explored. To this date, no studies have been reported on applying CNC and its derivatives for the delivery of vitamin C. Since vapours are not able to penetrate through the crystalline domains of CNC, it can be used as vapour-proof barriers [30]. This could potentially limit the exposure of unstable vitamin C to oxygen. Moreover, there are no studies reported on the antioxidant activity of CNC and CNC-CS_{OS}.

Therefore, based on a comprehensive literature review, the following objectives were formulated for this thesis:

- Synthesize, optimize and characterize amine functionalized CNC with a high amine content.
- Develop and characterize a robust system based on the surface modification of CNC with CS_{OS}.
- Evaluate the drug interactions and *in vitro* drug release properties of CNC, CNC-OX, and CNC-CS_{OS} for two cationic model drugs.
- Investigate the antioxidant properties of CNC-CS_{OS} and evaluate its effectiveness as a suitable carrier for vitamin C.

1.3 Thesis Outline

This thesis consists of 7 chapters. The research results are reported in manuscript format in chapters 3 through 6. The scope of the chapters are listed as follows: Chapter 1 briefly introduces CNC and the importance of its surface modifications and biomedical applications. The research objectives of the thesis and its organization are also included. Chapter 2 covers the literature review and provides an introduction to drug delivery systems and pharmaceutical carriers along with the motivation for applying nanotechnology in designing novel drug delivery systems. The advantages and disadvantages of nano drug delivery systems and their properties are described. In this chapter, different types of polymers used in drug delivery and their properties are discussed. The production, physicochemical properties, and surface modification routes of CNC are discussed. Furthermore, the biomedical applications of CNC are reviewed. Chapter 3 introduces an improved method for producing amine functionalized CNC and its characterization. Chapter 4 reports the modification and characterization of CNC with CS_{OS}. Chapter 5 investigates the interactions of CNC and two of its derivatives (CNC-OX and CNC-CS_{OS}) with two cationic model drugs and their drug release properties. Chapter 6 reports the antioxidant properties of CNC, CNC-OX and CNC-CS_{OS} and investigates the potential of CNC-CS_{OS} as an effective carrier for the delivery of vitamin C. Chapter 7 summarizes the key conclusions and major contributions of the author along with recommendations for future studies.

Chapter 2

Literature Review*

2.1 Introduction

This chapter reviews the literature related to the research performed in this thesis. First nanoparticles and their properties in drug delivery are discussed and then a background on different polymers used in the biomedical field is reviewed. A review on cellulose and chitosan is presented. Preparation and properties of cellulose nanocrystals (CNCs) is described in detail. Furthermore, surface modification of CNC is described with a more detailed focus on TEMPO-mediated oxidation applied in this thesis. Finally, different biomedical applications of CNC are reviewed.

2.2 Drug Delivery

The method of administering a pharmaceutical compound in humans or animals is known as drug delivery. A pharmaceutical drug is a chemical compound used for diagnosis, cure, treatment or prevention of a disease or a condition. In order to achieve a therapeutic effect, the pharmaceutical compound must be delivered to the active sites at the right time and with the right concentration. The efficacy of many drugs depends on their delivery method.

*This chapter is partially adapted from S. P. Akhlaghi, B. Peng, Z. Yao, K. C. Tam, "Sustainable Nanomaterials Derived from Polysaccharides and Amphiphilic Compounds", *Soft Matter*, 2013, 9:7905-7918 and S. P. Akhlaghi, M. Zaman, B. Peng, K. C. Tam, "Cationic Cellulose and Chitin Nanocrystals for Novel Therapeutic Applications", Accepted as a book chapter in "Cationic Polymers in Regenerative Medicine", *RSC publication.*

The therapeutic index (TI) of a drug is the optimum concentration range in which the drug has the most benefit. Concentrations above the TI can be toxic whereas concentrations below TI may not display any therapeutic effect [31]. Drug delivery systems (DDS) are new strategies based on multi-disciplinary studies such as pharmaceutics, molecular biology, polymer science, and chemistry that have been developed in recent years [32].

Drug delivery systems have the following goals [31, 33]: (i) Modifications of drug pharmacodynamics and pharmacokinetics i.e., release profile, absorption, distribution and elimination. (ii) Improving the TI of current drugs by increasing their efficacy and reducing toxicity. (iii) Increasing patient compliance. (iv) Overcoming the limitations of biomacromolecular therapeutics (proteins, peptides, oligonucleotides, and plasmids), i.e., low stability, immunogenicity, and short plasma half-life. (v) Targeted drug delivery for increasing the amount of drug at its site of action, i.e., inflammation, infection and tumor sites.

2.2.1 Routes of Administration

Delivery of a pharmaceutical compound to a patient is called administration. A drug can be administered in various dosage forms, such as capsules, tablets, creams, suppositories, and drops. The drug can also be administered via different routes as follows [33, 34]: (i) Enteral: oral, rectal, and sublingual. (ii) Parenteral: intravascular, intramuscular, subcutaneous, and inhalation. (iii) Topical: mucosal membranes and skin.

Drug delivery can also be categorized as follows [33]: (a) Systemic: absorbed into systemic blood circulation. (b) Local: substance is applied directly where the treatment is desired. Various parameters that impact the choice of a specific route of administration, are (i) the properties of the drug (e.g., solubility), (ii) efficacy in the treatment of a specific disease, (iii) accessibility to the disease site, and (iv) patient acceptability [34].

2.2.2 Novel Delivery Systems

Most of the conventional drug delivery systems used today are administered in multiple doses with specific time intervals and they are not optimal for the treatment of diseases. Many of the current drugs are comprised of peptides and hormones produced by genetic engineering techniques. These drugs used for the treatment of diseases, such as cancer, diabetes, and autoimmune diseases are susceptible to degradation by enzymes in our body. The susceptibility of these drugs highlights the importance of developing novel drug delivery systems. Traditional drug delivery systems have little control over the time, site and drug release rates. Also, the drug concentration in the blood varies frequently which causes the

concentration to exceed the TI, which may lead to either a toxic effect or lack of efficacy. Novel drug delivery systems including controlled drug delivery vehicles are able to control the rate, site and time of the drug release. In these systems the drug is released over a period of time in a controlled manner. Several stimuli-responsive and targeting drug delivery systems are being studied. The purpose of targeted drug delivery is to deliver most of the drug to its site of action. The purpose of this delivery is for the drug to be only active in the targeted area of the body (e.g., in cancerous cells). Stimuli-responsive polymers have more advantages over traditional release delivery systems. They follow a pattern similar to the conditions in the body and respond to different stimuli, such as pH, temperature, light, magnetic field, etc. The application of nanotechnology in the delivery of drugs has opened a new horizon for drug delivery development which will be discussed in the following section [32].

2.2.3 Nanotechnology in the Delivery of Active Compounds

Nanotechnology refers to the engineering of materials at the molecular and atomic scale. It consists of the interactions of cellular and molecular components. The National Nanotechnology Initiative has defined nanotechnology as structures with 1-100 nm size in at least one dimension. However, this is a strict definition and nanotechnology more commonly refers to structures developed by bottom-up or top-down engineering of individual components with the size of up to several hundreds of nanometers [35]. The potential benefits of nanotechnology in the development of novel drug delivery systems have been explored by researchers for more than two decades [32]. Nanoscale drug delivery systems have enabled targeted and controlled release of conventional drugs, vaccines, recombinant proteins, and nucleic acids. They regulate the pharmacokinetics of drugs and enhance their TI. Nano-scale drug delivery systems can be rationally designed from biological or synthetic materials and applied in various drug delivery routes such as, inhalable, implantable, injectable, topical, transdermal, and oral [33].

2.2.3.1 Advantages

Nanotechnology offers great advantages for drug delivery, targeting and release. It also has the potential to combine diagnosis and therapy and therefore, acts as one of the major tools in nanomedicine. Reducing the size of current drugs to the nanometer scale is considered a useful method for increasing drug solubility. This is because of the larger surface area-to-volume ratios of smaller particles, which in turn results in increased particle dissolution rates thereby increasing their bioavailability by overcoming the solubility problems. It also

increases the adhesion of drugs to the epithelial of the intestine that is useful in the oral delivery of drugs. The chemical encapsulation of drugs in their nanocarriers increases their stability in different biological environments such as the acidic medium of the gut. The size range of nanoparticles along with their surface properties also enables targeted delivery by increasing their penetration through various biological barriers and cell membranes. The nanoscale range of nanoparticles also reduces their uptake by the reticuloendothelial system (RES) and minimizes the risk of undesired clearance from the body through the spleen or liver [36].

2.2.3.2 Disadvantages

Despite several advantages of nanoparticles for drug delivery, they possess some disadvantages. The small particle size and the resulting high surface area present some limitations in drug loading capacity and cause a burst release of drugs. Also, in some cases the small particle size leads to aggregation of particles and difficulties in the delivery of dosage forms. Therefore, it is important to develop some practical solutions to these problems before commercializing the nanoscale drug delivery products and their application in the clinic. Cytotoxicity is a major concern of nanoparticles and their degradation products. Therefore, improving the biocompatibility of nanoparticles is of great importance [34].

2.2.4 Nanoparticle Carriers

Pharmaceutical carriers have different morphologies such as microparticles, liposomes, oil emulsions, micelles, dendrimers, liquid crystals and nanoparticles (Figure 2.1).

The nanoparticle properties will be discussed in more detail.

2.2.4.1 Nanoparticle Properties

Modification of different properties of nano drug delivery systems can be achieved by altering specific factors as listed below [37]: (i) Size and shape: different materials and chemistry. (ii) Surface characteristics. (iii) Drug loading: physical and/or chemical interaction between drug and carrier. (iv) Drug release: physical interaction between carrier and drug and/or chemical breakage of covalent linker. (v) Solubility: hydrophilicity and/or addition of solubilizing materials. (vi) Biodegradability: spacer, backbone. (vii) Biocompatibility: electrical charge and addition of bioinert groups. (viii) Biodistribution: addition of targeting moiety, molecular weight (MW).

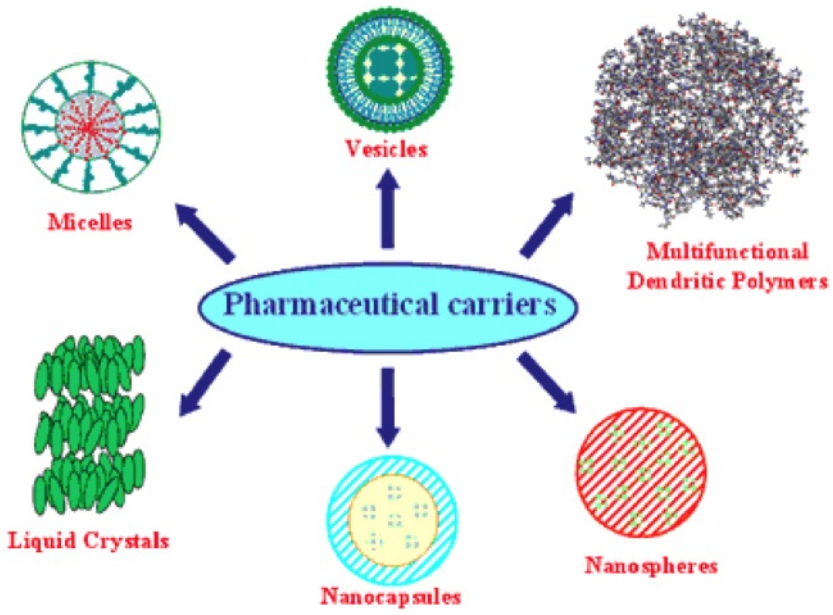

Figure 2.1: Different morphologies of pharmaceutical carriers [32].

The first four properties are discussed in more detail in the following sections.

2.2.4.2 Size

Particle size and size distribution are the most important properties of nanoscale drug delivery systems. They strongly impact the biodistribution, bioavailability, toxicity and efficacy of nanoparticles in reaching their active sites. Different studies have listed the advantages of nanoscale delivery systems compared to micro delivery systems. Generally, the increased mobility of smaller sized nanoscale delivery systems results in better uptake by cells and therefore, the drug can readily reach the active sites. The nanoparticle size also affects its drug release properties. Smaller particles have a higher surface-to-volume ratio and therefore most of the drug is located on or near the surface of the particles, leading to rapid drug release. On the other hand, larger particles have more space for drug entrapment and slow diffusive release of drug [38].

As discussed previously, drugs can be administered systemically or locally. The drug encapsulated in its vehicle can be released inside or outside the target cells. Larger drug delivery systems result in high drug concentrations near the target cells whereas smaller drug delivery systems can enter the cell directly via endocytosis [37]. The bioavailability and blood circulation time are strongly affected by differences in the size even at the nanoscale range. The nanoparticle size ranges and their consequent bioavailability following systemic administration are listed below [39]: (a) Particle size < 10 nm: rapid removal through renal clearance. (b) $10 <$ Particle size < 70 nm: penetration in very small capillaries. (c) $70 <$ Particle size < 200 nm: most prolonged circulation times. (d) Particle size > 200 nm: isolated by the spleen and finally removed through phagocytosis.

Based on the information above and due to the fact that nanoparticles smaller than 100 nm can be enclosed in endocytic vesicles, the preferred size range for systemic nanoparticle drug delivery systems is 10 to 100 nm [33]. In topical applications, it is generally observed that smaller particles can penetrate the skin more easily. If the active compound is required to penetrate through the skin and reach the dermis, the particle size should be less than 40 nm [40, 41].

2.2.4.3 Surface Characteristics

The intravenous injection of nanoparticles usually leads to their detection by the immune system and rapid clearance by the macrophages in the blood. The size and hydrophobicity of nanoparticles determine the amount of proteins called opsonins that attach to the

nanoparticles in the blood stream. This attachment is called opsonisation and is an intermediate pathway between nanoparticles and phagocytes. Therefore, in order to increase the success of nanoparticles reaching their active site, one should increase the circulation time of nanoparticles in the blood by minimizing opsonisation [42]. To achieve the above goals, the surface of nanoparticles can be covered with hydrophilic polymers or surfactants. Moreover, nanoparticles can be formulated with biodegradable copolymers containing hydrophilic segments such as polyethylene glycol [43].

The surface charge of nanoparticles is determined by their zeta potential, which depends on the structure of the particles and their dispersion medium. Nanoparticles with zeta potentials above ± 30 mV are stable in the dispersing medium. The zeta potential can also be an indicator of whether an active charged substance is encapsulated inside the nanoparticles or adsorbed on their surface [44].

2.2.4.4 Bioactive Compound Loading

Ideally, a successful nanoparticulate system should have a high loading capacity. Loading of the bioactive compound can be conducted by two methods [45]: (i) Incorporation method: Drug loading is done simultaneously with the process of nanoparticle formation. (ii) Absorption/adsorption method: After the formation of nanoparticles, they are incubated with a concentrated solution of drug.

Drug loading and encapsulation efficiency highly depend on the solubility of the drug in the polymer or substances composing the nanoparticles. This is related to the polymer structure, molecular weight, interaction between the drug and polymer and the presence of functional groups, such as ester or carboxyl in the polymer [46, 47].

2.2.4.5 Bioactive Compound Release

In order to produce a successful nanoparticle-based drug delivery system, drug release and polymer degradation are two important factors that need to be considered. Generally, drug release rate depends on parameters such as, drug solubility, separation of drug from the surface or the bound drug, diffusion of the drug in the nanoparticle matrix, diffusion through the carrier wall (in nanocapsules), degradation of nanoparticle matrix, and combination of diffusion/degradation [32].

Therefore, dissolution, diffusion and biodegradability of the matrix within the nanoparticles are the main factors that control drug release. If the diffusion of the drug in the matrix is faster than the degradation of the matrix, drug release is mainly controlled by diffusion.

The initial rapid release or burst release is mainly attributed to drugs that are weakly attached or bound to a large surface of nanoparticles [48]. If the nanoparticle is coated with a polymer, drug release is controlled by the diffusion of drug from the polymer membrane. The coating polymer layer acts as a barrier against drug release and thus, diffusion and dissolution of drug in the polymer will act as an indicative factor in the drug release process. Also, ionic interactions between drug and excipients can affect drug release. If the drug forms large insoluble complexes with the materials in the nanoparticles, the drug release can be reduced or hindered [45].

2.3 Polymers in Biomedical Field

Polymers are the most versatile class of materials that have changed our lives over the past several decades. However, it has been only forty years since a distinction between permanent and temporary biomedical applications of polymers was made [49]. For many years, the application of polymers as biomaterials has attracted the interest of pharmacists and surgeons. Polymer therapeutics consist of polymer-drug and polymer-protein conjugates, rationally designed macromolecular drugs, polymeric micelles and polyplexes for DNA delivery. These systems have various advantages such as the ability for customizing surface functionalities, chemical modification, and the potential for creating three dimensional structures [37]. Polymeric delivery systems are mostly used for achieving either spatial or temporal control of drug delivery [49]. Due to the diversity in chemistry, topology, and dimensions, polymers are a class of materials suitable for applications in nano drug delivery systems. Drugs can be either physically entrapped inside polymer matrices or covalently bound to the polymer backbones. The most important properties for a polymer used in a drug delivery system are: the ability to diffuse drugs, the effect of the polymer on the immune response, the ability to protect the drug molecules from degradation, biocompatibility, biodegradability and the ability to release the active ingredients. Polymers used in clinical therapies can be categorized based on their origin, stability and other additional properties. In the following, these categories are described in more detail. (i) Origin: (a) Synthetic: The birth of synthetic polymers was the dawn of a new era in the field of human therapy [51]. Examples are poly(ethylene glycol),poly(vinylpyrrolidone), poly(ethyleneimine) and linear polyamidoamines. (b) Natural: Despite the advantages of natural polymers such as availability and cost, these polymers have not been widely used for drug delivery. This is due to the variations in their purity and the necessity of crosslinking which may denature the embedded drug [52]. Examples are: Polysaccharides (dextran, dextrin, cellulose, hyaluronic acid and chitosan), proteins (collagen, gelatin, al-

bumin, fibrin). (c) Pseudosynthetic: examples are the man-made poly(amino acids) and polyaspartamides [50]. (ii) Backbone stability: (a) Biostable: These polymer structures that are stable in the body and are resistant against degradation, are used when permanent aids are needed. Polymers such as polyethylene and poly(methyl methacrylate) are two examples of biostable polymers. These polymers should be physiologically inert in tissues and should keep their mechanical properties for decades. (b) Biodegradable: These polymers are intended for temporary aids such as sutures, drug delivery devices and tissue supporting scaffolds. They stay in the body for a specific time and are then degraded to soluble molecules that can be excreted from the body. Therefore, there is no need for another surgery to remove the polymeric system [53]. These polymers will be discussed in more detail in the next section. (iii) Architecture: Polymers can have a variety of architectures such as linear, branched, graft, crosslinked, star shaped, multivalent, and dendronized. In drug delivery, the polymer architecture affects the drug loading efficiency, drug release rate and biodistribution as well as the physicochemical properties of the carrier [54]. (iv) Chemical Composition: Polymers can have different chemical compositions such as polyester, polyamide, polyanhydride. (v) Water solubility: Polymers can be either hydrophilic or hydrophobic and (vi) other properties such as, bioadhesion and biocompatibility.

2.3.1 Biodegradable Polymers

Polymer degradation is known as chemical reactions that result in a breakage of bonds in the main polymer chain that produce shorter oligomers, monomers and other low molecular weight by-products. Other terms such as resorbable, absorbable, and erodible have also been used in the literature to indicate biodegradation. In a biodegradable polymer, the degradation is due to environmental actions such as biocatalytic processes (involving fungi, enzyme, bacteria, etc), radical and/or chemical reactions (UV irradiation, oxidation, or hydrolysis). Most of the biodegradable polymers that have been discovered or synthesized in the past few decades have bonds that can be hydrolyzed such as ester, ortho-ester, anhydride, carbonate, amide, and urea. Due to the high biocompatibility and suitable physicochemical and biological properties, aliphatic polyesters containing ester bonds are one of the most common biodegradable polymers [55].

Since these polymers are absorbed in the body, they do not have the problems associated with non-biodegradable polymers such as the necessity to remove the polymers after drug release and the probability of increasing toxicity. Therefore, their applications have increased over the past decades. Also, biodegradable polymers have two major advantages over non-biodegradable polymers. First, since they are gradually absorbed by the human

body, and do not leave any residual implantation sites, they do not demonstrate chronic foreign-body reactions. Second, some of these polymers have been found to be able to regenerate tissues (called tissue engineering) by the interaction of their biodegradation with immunologic cells like macrophages. Therefore, they can be used as temporary scaffold for tissue engineering in surgical implants [56]. They have received considerable attention as medical devices (e.g., sutures, implants, dental, etc) and for the controlled release of different active ingredients for various applications (i.e., pharmaceutical, pesticide, veterinary). Among these systems, biodegradable micro-and nano-systems have been studied as drug delivery systems for controlled release applications [57].

Mechanisms such as diffusion and/or erosion impact the release kinetics of drugs from these systems. These mechanisms are influenced by the degradation rate of polymer and depend on the polymer and active ingredient properties [57]. The biodegradation rate of a polymer depends on different factors such as polymer chemistry, molecular weight, molecular architecture, and morphology. Other factors are geometry, porosity, and size, as well as surrounding conditions (i.e., temperature and pH) [51].

Based on their chemical origin, biodegradable polymeric biomaterials can be divided into the following groups: (i) linear aliphatic polyesters (e.g., polylactide) and their copolymers within the aliphatic polyester family such as poly(glycolide-ϵ-caprolactone) copolymer (ii) biodegradable copolymers of linear aliphatic polyesters in linear aliphatic polyesters and monomers other than linear aliphatic polyesters like, poly(L-lactic acid-L-lysine) copolymer (iii) biodegradable polysaccharides like chitosan, chitin and hyaluronic acid (iv) poly(ester-ethers) like poly-p-dioxanone, olyamino acids such as poly-L-lysine (v) Inorganic biodegradable polymers such as polyphosphaene, which have a nitrogen-phosphorus backbone instead of ester linkage (vi) poly(orthoesters) and (vii) polyanhydrides [56].

2.3.2 Biocompatible Polymers

Since polymers are often internalized by cells, biocompatibility is of great importance [58]. Biocompatibility is defined as "the ability of a material to perform with an appropriate host response in a specific application" [59]. Polycations are usually hemolytic, cytotoxic and activate the complement system, whereas polyanions can induce cytokine release and anticoagulant activity but are less cytotoxic.

General requirements for a biocompatible polymer are non-carcinogenicity, non-toxicity, non-allergenicity, non-mutagenicity, being free of contaminants (such as synthesis residues, solvents, and additives), having biocompatible degradation products, no immunological responses and bioresorbability. The term bioresorbable refers to polymers that are degraded

into products which can be removed from the body by natural pathways or are ideally involved in the metabolic pathway. Biocompatibility also depends on the site of injection and surface topography of the polymer. This is because different tissues in the body have different sensitivity to irritation; sharp edges or corners can irritate and increase the local tissue response [51].

2.3.3 Bioadhesive Polymers

One of the ways to increase the absorption of drugs is the application of bioadhesive systems. Bioadhesive polymers enhance drug delivery systems by increasing their residence time in several routes of administration. Improvements in local drug delivery and enhanced bioavailability of some drugs can be achieved by prolonged contact. A bioadhesive is defined as a material that adheres to a biological substrate and remains on that surface for a prolonged time. These systems create concentration gradients between the drug delivery system and the absorptive membrane and lead to the inactive absorption of drugs. They also increase the penetration of drugs. Drug delivery systems containing bioadhesives usually adhere to the mucin layer coating or the membrane surfaces. Most of the targeted areas used in drug delivery have coatings of mucus. Due to the adhesion of bioadhesive polymers to mucus, they are commonly called mucoadhesive. Examples of bioadhesives with their water solubility and charge are listed below [60]: (i) water soluble bioadhesive: The contact time between the adhesive and mucus is limited to a few hours depending on the type of adhesive and flow of biological fluid at the site of administration. The different types of water-soluble bioadhesives are cationic (polylysine), anionic (carboxymethyl cellulose (sodium)), and neutral (polyethylene glycol), (ii) water insoluble bioadhesive: These bioadhesives remain on their site until the tissue or mucin replaces itself and they usually stay for about 4 to 72 h. Examples are cationic (L gelatin), anionic (crosslinked poly(methyl acrylic acid)), and neutral (poly(methyl methacrylate)).

Most bioadhesive drug delivery systems are applied topically to a targeted tissue. These systems can be applied to several parts of the body such as dermal areas, oral cavity, ocular, vaginal, rectal, intestinal, and gastric. The biological membranes of these tissues have unique properties such as immunology, permeability and enzymatic activity. These factors should be taken into consideration for improved bioavailability of the drug and successful bioadhesion.

The contact between mucosal membrane or its coating and the adhesive is seen as a two-step process: (i) initial contact between substrate and the bioadhesive: Successful initial contact is accompanied with wetting of the substrate surface and depends on the

similarities of the physicochemical properties of two surfaces and (ii) Subsequent formation of bonds between the two surfaces: These bonds can be hydrogen bonds, hydrophobic, or electrostatic which permit the bioadhesive drug delivery system to attach to the substrate [60].

2.4 Polysaccharides

2.4.1 Cellulose

Cellulose is the most abundant organic biopolymer on earth and is the primary structural component of cell walls of higher plants. It was first characterized in 1838 by Anselme Payen [61]. Cellulose is one of the few natural compounds that have a similar structure despite its various sources such as grass (i.e., papyrus and bamboo), cotton, wood, or other plants. Other sources of cellulose are some sea animals (tunicates), some algae, some fungi, oomycetes (water mould) and acetic acid bacteria (Acetobacter xylinum). However, the cellulose content in different sources varies notably. The highest amount of cellulose is found in cotton balls (90-99%), while wood contains 40-50% cellulose. In nature, cellulose occurs in the form of highly crystalline (crystallinity 65-95%) microscopic fibres 2-20 nm in width and different lengths depending on its origin [62].

2.4.1.1 Cellulose Molecular Structure

Cellulose is a high molecular-weight (162 g/mol or more) linear homopolysaccharide of $\beta(1-4)$ linked D-glucopyranose (Glc) residues. The removal of water from each glucose molecule results in an anhydride glucose unit (AGU) that is polymerized into long cellulose units with 5,000-10,000 repeating units. The basic repeating unit of cellulose is called a disaccharide cellobiose unit composed of two AGUs (Figure 2.2). As shown in Figure 2.2, cellulose polymer has two chemically different side chain ends:

- Reducing end group: contains a D-glucopyranose unit in which the anomeric carbon atom is part of a cyclic hemiacetal. This terminal hemiacetal group is in an equilibrium where a small proportion is an aldehyde acting as a reducing group.
- Non-reducing end group: contains a D-glucopyranose unit in which the anomeric carbon atom is involved in a closed ring structure.

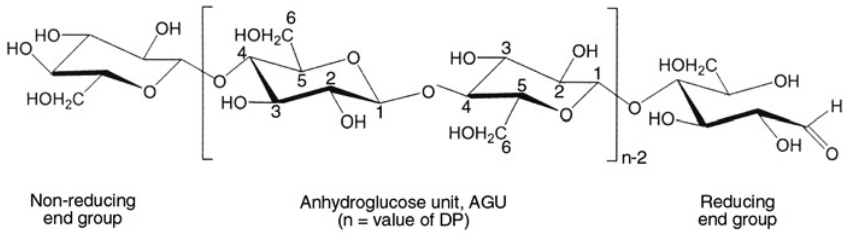

Figure 2.2: Molecular structure of cellulose [63].

2.4.1.2 Cellulose Properties

Cellulose is a biodegradable and hydrophilic polymer. It is odorless and has no taste. Treatment of this long chain colloidal carbohydrate polymer with specific enzymes or concentrated acids at high temperature can break it into its glucose subunits. Many properties of cellulose depend on its chain length or degree of polymerization. Another important factor that affects the properties of cellulose is the strong hydrogen bond network within the cellulose chains [64].

Cellulose Degree of Polymerization The average number of glucose residues per cellulose molecule is known as degree of polymerization (DP), which affects many properties of cellulose. Cellulose has different DPs depending on its source and the DPs are not very well established. The reason is that the isolation of pure cellulose includes different steps such as pulping, partial hydrolysis, dissolution, re-precipitation, and extraction with organic solvents. These procedures usually break cellulose chains and lead to underestimated DP values depending on the method used. Cellulose from wood pulp has DPs between 300 and 1,700 whereas cotton and other plant fibers and also bacterial cellulose have DPs of 800 to 10,000. Acid hydrolysis of cellulose can produce molecules with very low DPs known as cellodextrins [65].

Cellulose Solubility and Hydrogen Bonding The free hydroxyl groups in the equatorial positions of cellulose can participate in hydrogen bonds leading to the formation of different crystalline arrangements. These hydrogen bonds organize the chains in highly ordered crystalline structures. Therefore, by inhibiting the free rotation of the pyranose rings, the strength of the polymer is increased and the flexibility is reduced. Hydrogen

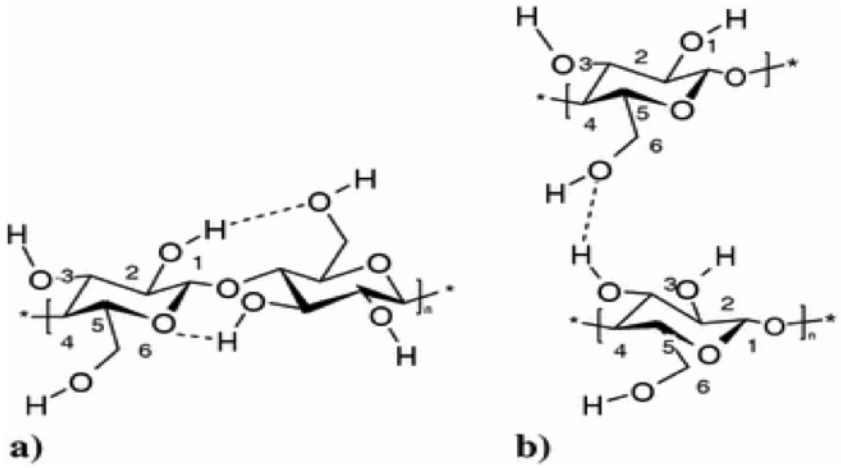

Figure 2.3: Hydrogen bonding of cellulose (a) intramolecular and (b) intermolecular [69].

bonding is the reason for properties such as, swelling, absorption and optical behavior in cellulose chains. The general structure of cellulose contains aggregated particles with extensive pores capable of capturing large amounts of water by capillary forces. As mentioned, between the crystalline regions of cellulose amorphous regions are present. The less ordered or amorphous regions in cellulose polymer are less tightly packed and are thus, more available for hydrogen bonding to other molecules, such as water. Due to the extensive and strong hydrogen bonding in the crystalline regions of cellulose, it is insoluble in most common solvents [66].

Hydrogen bonding with water does not dissolve cellulose but rather makes cellulose swell. The hydrogen bond network also increases the thermal stability of cellulose. The hydrogen bonding can be intra- and inter-molecular [67]:

- Intra-chain hydrogen bonding: between C3-OH and O5 and/or the C6-OH and C2-OH [68](Figure 2.3a).
- Inter-chain hydrogen bonding: This type of binding is believed to be the main factor in holding cellulose chains together. The inter-chain hydrogen bonding occurs between the C6-OH of one chain and the C3-OH of the adjacent chain (Figure 2.3b).

2.4.1.3 Cellulose Derivatives

Several morphological and chemical modifications are possible on cellulose due to its unique molecular and supramolecular architecture via derivatization. Modifications are performed on cellulose to either reinforce its original properties or to add new functionalities. Throughout history, different chemical and physical modifications have been performed on cellulose. The insolubility of cellulose in most common solvents requires the modification reactions to occur in heterogeneous media. This decreases the overall reaction efficiency by hindering the accessibility of the reagents and solvents to penetrate. Solvents and reagents reach the amorphous regions more easily than the crystalline regions.

Using the hydroxyl groups, cellulose can fully or partially react with reagents yielding derivatives suitable for applications in industry. Most of the cellulose derivatives are synthesized based on alcohol chemistry. The most typical cellulose modifications are etherification and esterification. Etherifications are performed using different types of alkylating reagents such as methyl chloride. Esterifications involve acetylations with acetic acid or acetic anhydride leading to the production of cellulose acetate. Other types of modification reactions are ionic and radical grafting, oxidation and deoxyhalogenation (Figure 2.4). However, the crystalline structure of cellulose causes a steric hindrance that decreases the reactivity of hydroxyl groups. Degree of substitution (DS) is a value used to study the reactivity of cellulose. Based on the hydroxyl groups on the three AGUs, DS ranges from 0 to 3. Usually DS is lower than 3 due to the poor accessibility of the crystalline regions in cellulose, indicating the partial reactions within the amorphous regions [63].

2.4.1.4 Cellulose Applications

Industrial Applications Cellulose has many applications as an emulsifier, stabilizer, anti-caking agent, dispersing agent, thickener and gelling agent. Its most important use is in the retention of water [70]. The amorphous domains of cellulose become soft and flexible after water absorption. Cellulose can also act as a fat replacer in sauces and dressings by improving volume and texture. Viscous cellulose solutions have potentials in various industrial sectors, such as paper-coating and textile finishes. One third of purified cellulose is used for derivatization reactions that have many applications based on the DS [71]. As described previously, derivatization of cellulose interrupts the orderly crystal-forming hydrogen bonding, so that even hydrophobic derivatives may increase the apparent solubility in water. Cellulose derivatives can be used as thickening agents in food, adhesives, explosives, and moisture-proof coatings.

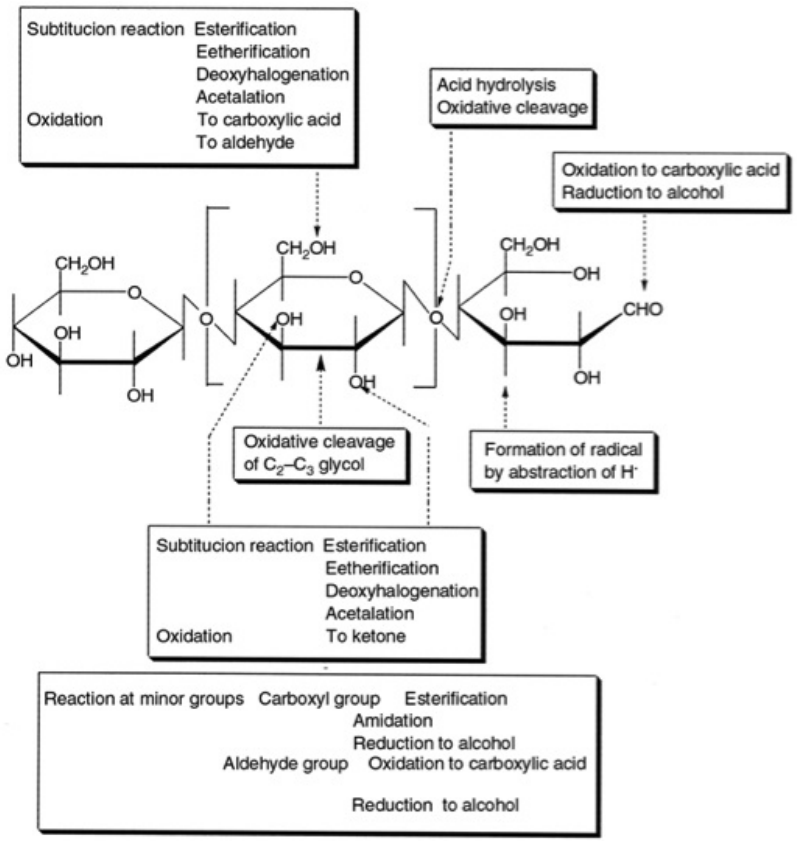

Figure 2.4: Position in cellulose structure for chemical modifications [63].

Cellulose Biomedical Applications Cellulose, being the most abundant biopolymer in nature, is a popular biomaterial for pharmaceutical applications. As discussed previously, due to its insolubility in water arising from the intensive intra- and inter-molecular hydrogen bonding between the individual chains [72], chemical modifications are desirable. These cellulose derivatives (cellulosics) can be used in pharmaceutical applications because of their several advantages such as, biocompatibility, strength, low cost, reproducibility and recyclability. They are usually used for film formation, water retention, emulsifying and suspending agents, thickening agents, tablet binders and modifying the release of drugs from formulations. A summary of some pharmaceutical applications along with the cellulose derivatives are given below [63]: (i) Controlled delivery systems: hydroxypropyl cellulose and microcrystalline cellulose (MCC). (ii) Coating tablets: MCC, sodium carboxymethyl cellulose, hydroxypropylmethyl cellulose. (iii) Enteric coating of tablets: cellulose acetate phthalate and hydroxymethyl cellulose phthalate. (iv) Colon targeting of drugs following oral administration and delayed absorption (binders that swell in gastric media): hydrated form of hydroxypropylmethyl cellulose and hydroxypropyl cellulose. (v) Stabilizing agents (adjusting the viscosity of syrups: carboxymethyl cellulose. (vi) Diluent and disintegrating agent for release of solid dosage forms: MCC. (vii) Applications in matrix systems: (a) Hydrophilic: hydroxypropyl cellulose and hydroxyethyl cellulose. (b) Hydrophobic: ethyl cellulose.

Despite a long history of use in tableting, there is still extensive research into the use of MCC and other types of cellulose in advanced pelleting systems. The tablet disintegration and drug release rate might be controlled by microparticle inclusion, excipient layering or tablet coating [14].

2.4.2 Chitosan

Chitosan is the second most abundant natural polymer that is produced by the partial deacetylation of chitin under enzymatic hydrolysis using chitin deacetylase or under alkaline conditions. Chitin is a linear homopolysaccharide of $\beta(1-4)$ linked 2-acetamido-2-deoxy-D-glucopyranose (GlcNAc) residues (Figure 2.5). Chitin is obtained from the cell walls of yeast and fungi or from exoskeletons of arthropods [73]. However, the main source of industrial chitosan is shrimp and crab shell wastes [74].

2.4.2.1 Chitosan Preparation

Upon boiling chitin in a concentrated potassium hydroxide solution, Rouget first reported chitosan in 1859 [76]. A century later, detailed studies were reported on chitosan [77]. A

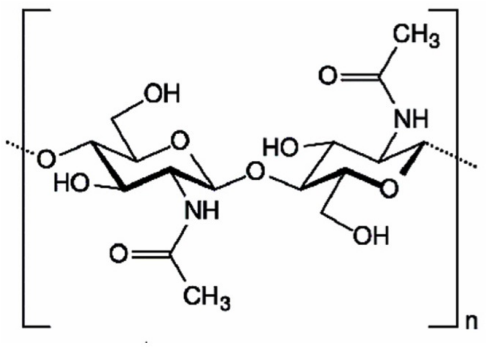

Figure 2.5: Chemical structure of chitin [75]

schematic on the manufacturing process of chitosan is shown in Figure 2.6. In this easy and inexpensive process, sequential treatment of ground crustacean shells with alkali and acid leads to the demineralization and deproteinization of the shells. Afterwards, chitin is extracted and deacetylated to chitosan at high temperature by alkaline hydrolysis [78].

2.4.2.2 Chitosan Structure

Molecular Structure Chitosan is an aminoglucopyran composed of $\beta(1-4)$ linked N-acetyl glucosamine (GlcNAc) and glucosamine (GlcN) residues (Figure 2.7). The structure of chitosan is similar to cellulose. In chitosan the hydroxyl groups in the C-2 position of cellulose have been replaced with amino groups.

Solid State Structure Chitosan is a semi-crystalline polymer and the degree of crystallinity depends on the degree of deacetylation. The solid-state structure of chitosan depends on its molecular properties, such as, the sequence, proportions, and number of GlcN and GlcNAc units [80]. The maximum crystallinity of chitosan is observed when it is either chitin (0% deacetylated) or fully deacetylated (i.e., 100%). Complete deacetylation produces single crystals of chitosan [73]. Chitosan with short chain length (low molecular weight) and high proportion of GlcN residues is highly crystalline. The crystalline form of chitosan has a fully extended two-fold helical structure. Crystalline chitosan has two distinguished forms: anhydrous and hydrated [81]. At intermediate degrees of deacetylation, minimum crystallinity is achieved [80]. Chitosan with a random sequence and equal proportions of GlcN and GlcNAc is completely amorphous and highly soluble in water.

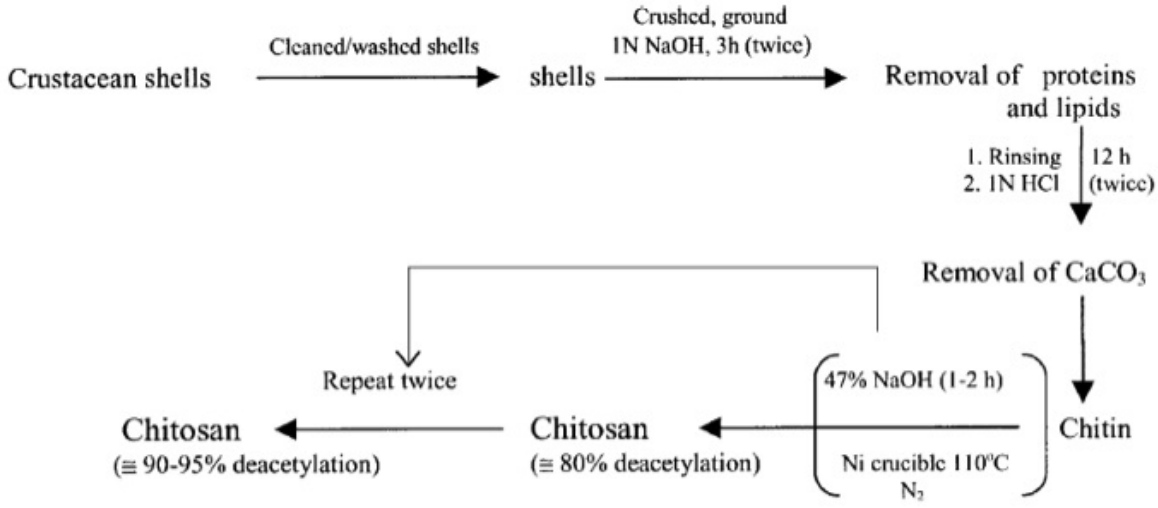

Figure 2.6: Chitosan production [79].

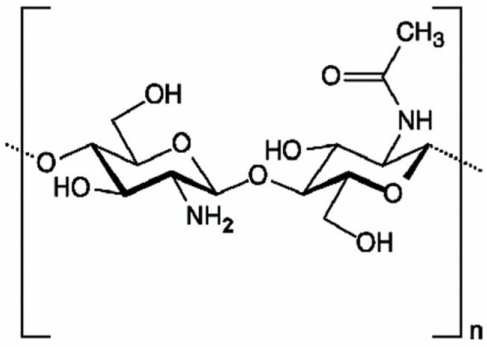

Figure 2.7: Chemical structure of chitosan [75]

Conformation in Solution Polysaccharides have a tendency to form intra- and inter-chain hydrogen bonds, due to the many hydroxyl groups on their structure, leading to insolubility or molecular aggregation in solutions [82]. Also, polysaccharides have hydrophobic properties due to CH groups, which are the basis for hydrophobic interactions [73].

Commonly, it is believed that chitosan chains act as stiff wormlike chains. Generally, two kinds of parameters affect the conformation of chitosan molecules in solution [83]: (i) Parameters related to the molecular structure such as proportions of GlcN and GlcNAc residues and chain length (molecular weight). In a study [84], the researchers observed random coil conformations for chitosan chains with molecular weights equal to or greater than 223 kDa and extended rod-like conformation for chitosan chains with molecular weights of 148 kDa or lower. Differences in charge distributions and intramolecular hydrogen bonding patterns caused the changes in conformation below and above the transition. (ii) Parameters related to the molecular environment such as, solvent type, ionic strength and pH: At low pH values, chitosan is positively charged due to the protonation of the GlcN residues. Therefore, the repulsion between the positive charges along the chain reduce the molecular flexibility and lead to a more extended conformation [85].

Later studies showed the significant effect of proportions of GlcN and GlcNAc and ionic strength on the chain conformation. Temperature and pH had substantial effects on chitosan molecules [84, 86].

2.4.2.3 Chitosan Physicochemical Properties

Molecular Weight As discussed previously, the alkaline hydrolysis of chitin at high temperatures leads to the production of chitosan. The molecular weight of chitin is several million Daltons which is reduced to molecular weights in the range of 10-1,000 kDa in chitosan by harsh treatment with alkali [78]. Commercial chitosans from Fluka (biochemika, Switzerland) are classified as below:

- High molecular weight: $\sim 2,000$ kDa
- Medium molecular weight: ~ 750 kDa
- Low molecular weight: ~ 70 kDa

Degree of Deacetylation The average number of GlcN residues per 100 residues in chitosan is known as the degree of deacetylation (DD) and is usually expressed as a percentage [87]. Commercial chitosans vary in DD from about 70 to 95% depending on the determination methods and manufacturing process. DD is an important factor for chitosan applications. Sometimes DD is expressed as degree of acetylation (DA), DA=100-DA. When DD is higher than 40% in dilute acidic solutions, chitosan is soluble [88].

Solubility In acidic aqueous media due to the protonation of amino groups in the presence of H^+ ions chitosan is soluble. A number of papers state that chitosan is soluble below pH 6 and can be easily dissolved in 1 v/v % acetic acid. The pKa of chitosan ranges from 6.2 to 7. If the pH of the solution approaches the pKa, the amino groups become deprotonated and chitosan precipitates. However, apart from pH, other factors such as degree of deacetylation, acetyl group distribution, ionic strength of medium, the type of acid used, and intra-molecular hydrogen bonds between hydroxyl groups and final drying conditions for chitosan preparation affect the solubility of chitosan [73].

2.4.2.4 Chitosan Biological Properties and Applications in Biomedical Field

Chitosan has attracted interest in the biomedical field due to several advantages such as unique physicochemical properties, high biocompatibility, complete biodegradability, abundance, renewability as well as low toxicity [16]. It has interesting biological properties such as, mucoadhesion, analgesic, hemostatic, antioxidant, antibacterial, and antitumor properties [89]. Thus, it is suitable for a wide range of biomedical and pharmaceutical applications [90, 91, 92].

Chitosan is a linear polyelectrolyte, a cationic polyamine that possesses a high charge density below pH=6.5 and can attach to negatively charged surfaces and form chelates with metal ions. It has active hydroxyl and amino groups that make it suitable for chemical reactions and salt formation. The functional properties of chitosan depend on its chain length, charge density and distribution [93]. Chitosan and its derivatives have properties such as film formation, high mucoadhesion, gel formation, opening the cellular tight junctions, and non-toxic effect in the body. Due to its polyelectrolyte nature at low pH, it has many potential applications in the form of aqueous solutions, hydrogels, sponges, fibers, and films. Therefore, it can be applied as the gel coating in drugs, granules micro- and nanoparticles for applications in drug delivery systems from several routes such as oral, injection, inhalation, and dermal. Chitosan has applications in cosmetics and studies are focused on applying it in several pharmaceutical formulations.

The suitable functionality of chitosan as a part of pharmaceutical formulations for drug delivery has been proven in several studies. Some of the several advantages of chitosan for drug delivery are controlled release properties for drugs, rapid release properties for drugs, applications in bioadhesive drug delivery systems, improvements in peptide drug delivery, applications as colonic drug delivery systems, and applications in gene delivery[16, 93]

Table 2.1 summarizes the principal characteristics of chitosan and its related biomedical applications.

Table 2.1: Principal properties of chitosan in relation to its use in biomedical applications [73]

Potential Biomedical Applications	**Principal Characteristics of Chitosan**
Surgical sutures	Biocompatible
Dental implants	Biodegradable
Artificial skin	Renewable
Bone rebuilding	Film-forming
Corneal contact lenses	Hydrating agent
Time release drugs	Non-toxic, biological tolerance
Encapsulating material	Hydrolyzed by lysozyme, wound healing properties, efficient against bacteria, viruses, fungi

2.4.3 Chitosan Oligosaccharide (CS_{OS})

Despite several attractive functional properties of chitosan in many applications, its high viscosity, high molecular weight, ease of aggregation and low solubility at physiological pH values (7.2-7.4), make it difficult to use in *in vivo* applications [94]. To overcome the solubility problem, chitosans has been modified into water-soluble analogues such as PEGylated chitosan and glycol chitosan. Another approach for addressing the chitosan solubility issues is the use of low molecular weight chitosans known as chitosan oligosaccharides (CS_{OS}) [16].

The enzymatic degradation of chitosan followed by ultrafiltration leads to the production of short chain chitosans with low molecular weight (i.e., 3-6 kDa), called CS_{OS}. Unlike chitosan, CS_{OS} is soluble in water below pH=7.4. It also has reactive amino and hydroxyl groups therefore, by chemically altering its properties, many derivatives can be obtained for pharmaceutical applications [94]. Another major advantage of CS_{OS} compared to water-insoluble chitosan is its higher *in vivo* antibacterial properties [92].

2.5 Cellulose Nanocrystals (CNC)

2.5.1 CNC Preparation

Natural cellulose contains both crystalline and amorphous domains. The access of chemicals to the crystalline domains is restricted due to the highly ordered, hydrogen bonded and extended packing of the cellulose chains. Therefore, acid hydrolysis mostly affects the amorphous regions. Stable suspensions of colloidal sized cellulose crystals prepared by sulfuric acid hydrolysis of cotton and wood cellulose were first reported in 1950 by Ranby and Ribi [95]. The acid hydrolysis of cellulose microfibrils is a heterogeneous and complex reaction. In a heterogeneous acid hydrolysis reaction, the primary fibrils are first broken into highly crystalline fragments by the penetration of acid into the amorphous regions. After the hydrolysis of a certain amount of glycosidic bonds, the reaction rate slows down significantly and results in a degree of polymerization. The acid hydrolysis of cellulose fibers produces highly crystalline rod-like particles called cellulose nanocrystals (CNC) (Figure 2.8) [5, 96].The rate of acid hydrolysis is different for various sources. For instance, studies have shown that wood cellulose is depolymerized faster than cotton cellulose. Amorphous cellulose domains can be selectively removed by proper selection of reaction conditions. The optimum condition for CNC production entails an acid hydrolysis reaction at 45 °C for 60 min. Under these reaction conditions, all the amorphous regions are completely hydrolyzed with residual crystalline particles left with a length of approximately 200 nm [97].

The acid hydrolysis mechanism for the disruption of $\beta(1-4)$ glycosidic bonds is comprised of three steps [68, 97] as shown in Figure 2.9. First a conjugate acid is formed by the rapid interaction of acid with glycosidic oxygen and protonization of acetal oxygen linking the two sugar residues together. An electron pair is shifted to the anomeric carbon which breaks the C-O bond. Lastly, a neutral end group and a proton are produced by the interaction of water and carbonium ion. The intermediate carbonium ion is formed more rapidly at the end than in the middle of the polysaccharide chain. Therefore, after partial hydrolysis, the number of monosaccharides produced is higher than the calculated value based on random bond cleavage [99].

2.5.2 CNC Properties

CNC is a biodegradable, relatively cheap biomaterial with superior mechanical properties. For instance, CNC is considered to be stiffer than aluminum and stronger than steel [101].

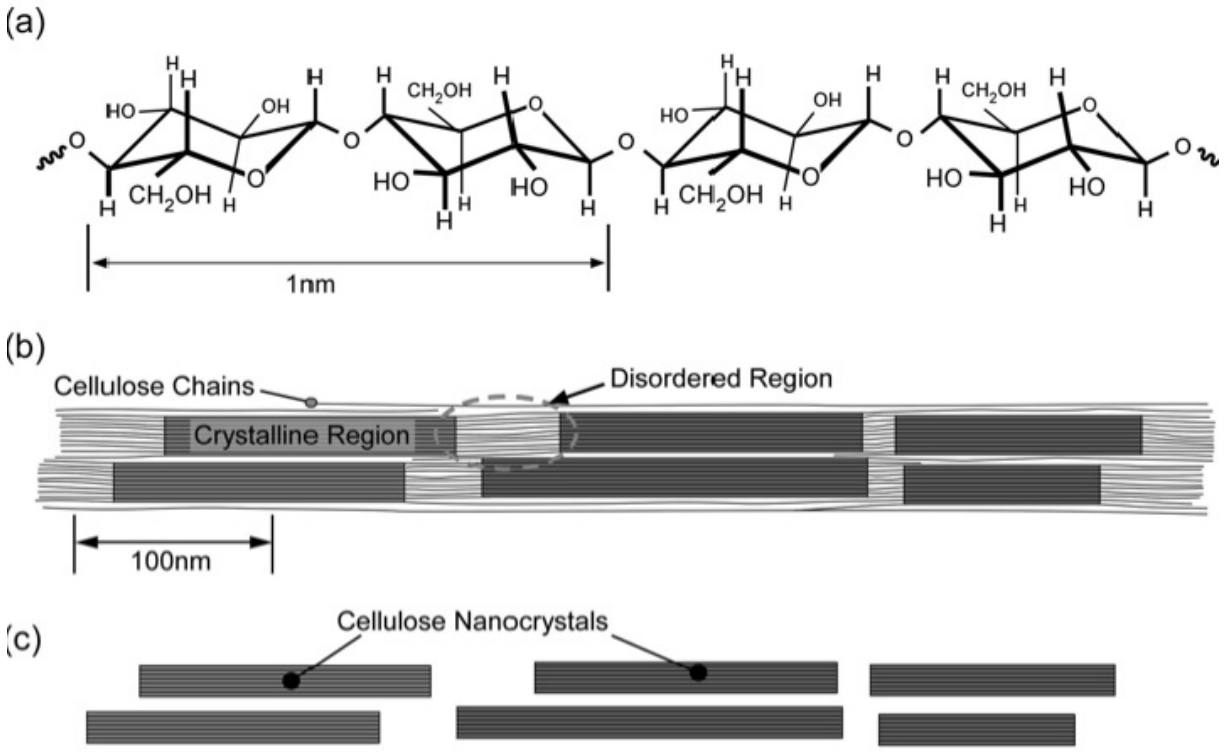

Figure 2.8: Schematics of (a) single cellulose chain, (b) a cellulose microfibril showing ordered (crystalline) and disordered (amorphous) regions, and (c) cellulose nanocrystals after acid hydrolysis which dissolved the disordered regions [98].

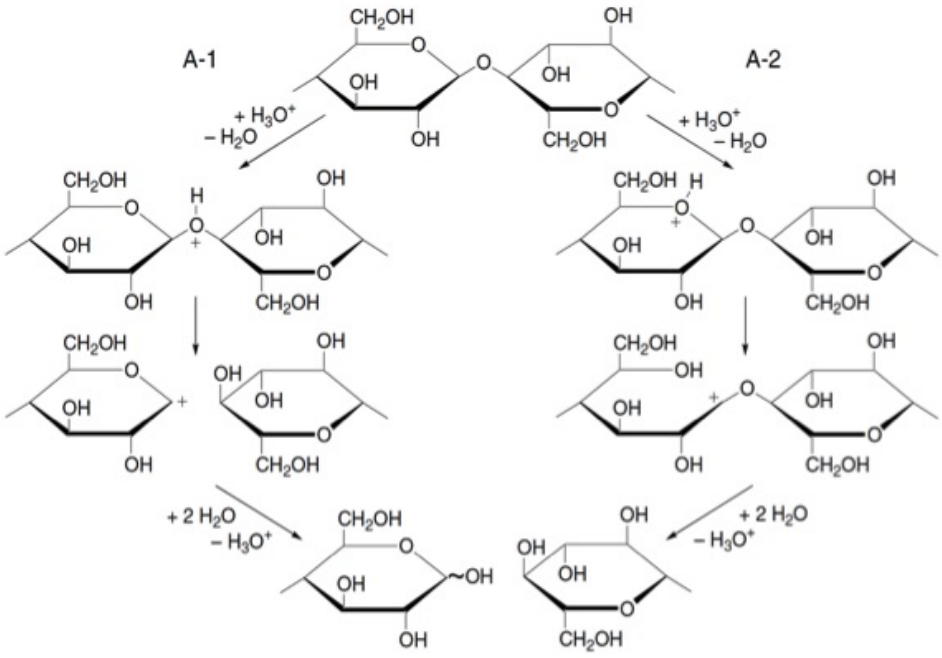

Figure 2.9: Mechanisms of the acidic hydrolysis of cellulose [100].

It also has a high aspect-ratio (i.e. length/diameter) of 30 to 150 depending on its source [96]. Other important properties of CNC are discussed hereafter.

2.5.2.1 Size

In wood, cellulose molecules form long crystalline elements with cross-sectional dimensions around 2-5 nm called elementary fibrils. The aggregation of these fibrils forms larger structures called microfibrils with lateral dimensions of around tens of nanometers (Figure 2.10) [102]. The preparation method and cellulose origin generate CNCs with different dimensions. For instance, lengths from 100 nm to a few micrometers and a diameter of 8-10 nm and 10-20 nm, have been reported for CNCs derived from cotton and tunicate, respectively [103]. By ultrasonicating CNC solutions, the aggregates formed are broken down whilst no reduction is observed in the average length of the particles [104].

There is a challenge in determining the exact dimensions of cellulose microfibrils. However, in the past decade several analytical methods have been used such as, Transmission Electron Microscope (TEM) [105], Scanning Electron Microscope (SEM) [106, 107], Field Emission Scanning Electron Microscope (FE-SEM) [105], dynamic and static light scattering techniques [5], and AFM [103, 108].

2.5.2.2 Surface Charge

The sulfuric acid hydrolysis of cellulose fibers introduces sulfate ester groups on the surface of CNC (Figure 2.11). Factors such as temperature, time, acid concentration, and acid to substrate ratio can affect the sulfur content in CNC in the range of 0.5-2%. The deprotonation of sulfate ester groups in aqueous solutions gives CNC a negative charge [110, 111].

2.5.2.3 Suspension Properties

Due to the repulsion between the negatively charged particles, CNCs form stable aqueous solutions [113]. The ionic strength of the solution affects the forces between the particles [110]. Above a critical concentration ($\sim 5-7\%$ cellulose), CNC suspensions form chiral nematic ordered phases in solutions without salt.

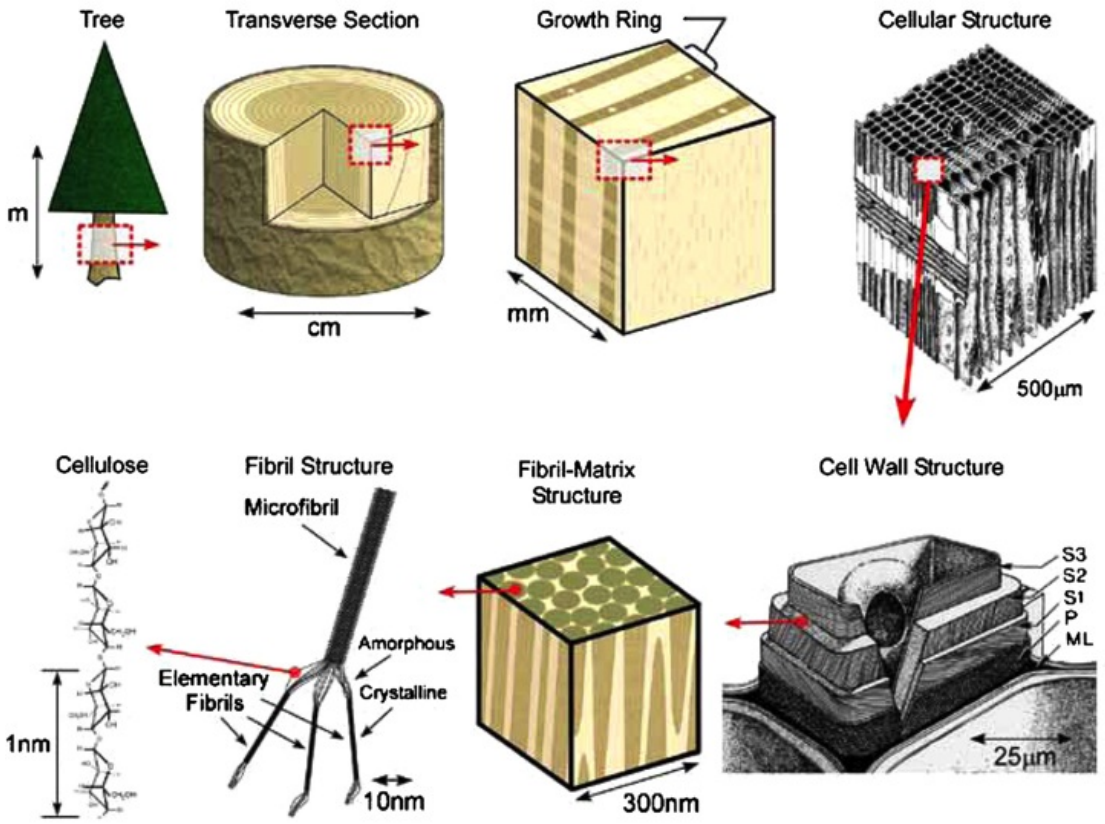

Figure 2.10: Structure of wood from the tree to CNCs. ML=middle lamellae between tracheids, P=primary cell wall, S1, S2, S3=cell wall layers [109].

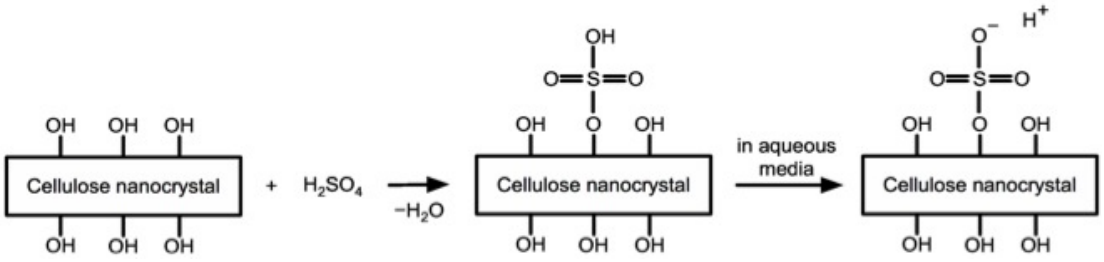

Figure 2.11: Partial esterification of surface hydroxyl groups by sulfuric acid during cellulose hydrolysis [112]

2.6 CNC Surface Modification

The rigid rod-like structure of sustainable CNC offers many potential modifications in gels, coatings and composites. However, due to the hydrophilic nature of CNC, it is limited to applications involving polar solvents. In order to explore the full potential of CNC in various fields, the surface of CNC has to be modified with different compounds to enhance the interfacial compatibility and add new functionalities. The presence of several functional groups on CNC, provides the opportunity of surface functionalization of CNC via different chemistries [114]. Similar to cellulose, CNC possesses many hydroxyl groups on its surface. Therefore, the same reactions can be conducted on CNC (Figure 2.12) and several novel nanomaterials have been produced [115, 116]. The properties of CNC-modified nanomaterials can be manipulated by the structure of polymer chains grafted on it (i.e., polymer type, architecture, hydrophobicity, thermal behavior, chain flexibility, and chain length), the size of CNC, and the density and location of grafting.

CNC has been covalently grafted with several polymers for different applications. In all of these studies, the reactions were random without site specificity and did not affect the architecture and morphology of cellulose. In one study, cellulose microcrystals were grafted with PEG to produce steric stabilizing effects and increase the stability of such suspensions [118]. In a recent study, pH-responsive CNC was obtained via grafting 4-vinylpyridine through surface-initiated graft polymerization using ceric(IV) ammonium nitrate. By changing the pH, poly(4-vinylpyridine) grafted CNC could undergo reversible sedimentation and flocculation. The authors proposed that their system could have potential applications as flocculating agents in the pulp and paper industry and as clarifying agents and triggered release delivery systems in the biomedical field [119].

In the production of CNC, varying the acid hydrolysis reaction parameters of cellulose not only alters the dimensions of CNC but also creates nanocrystals with one end containing concentrated reducing end groups. Therefore, the asymmetrical structure of CNC allows the creation of novel nanomaterials by selective grafting of polymer chains onto one end of their rigid structure. Small molecules have been selectively grafted onto one end of cellulose microcrystals [120].

In the following, anionic modification of CNC through TEMPO-mediated oxidation is described in more detail.

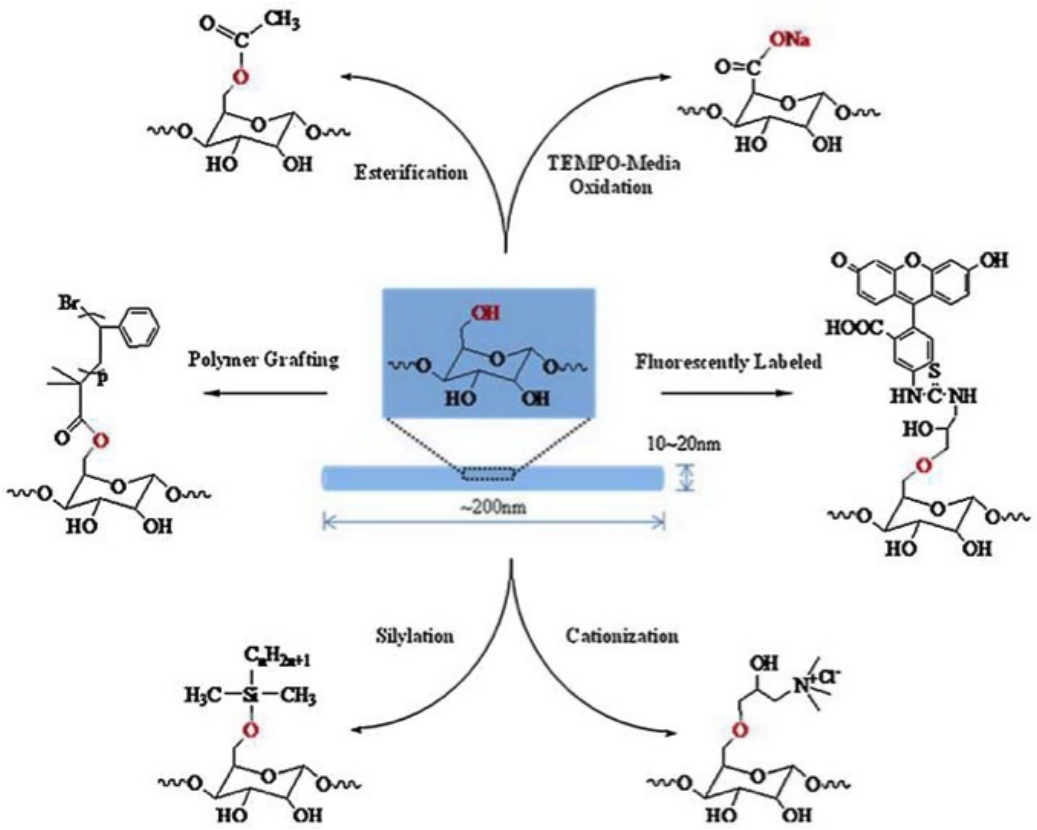

Figure 2.12: Schematic diagram illustrating the various types of chemical modifications on CNC surface [117].

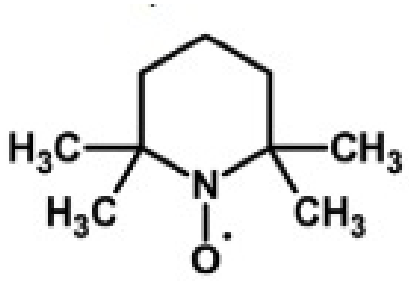

Figure 2.13: Structure of 2,2,6,6-tetramethylpiperidine-1-oxyl (TEMPO).

2.6.1 TEMPO-Mediated Oxidation

2,2,6,6-Tetramethylpiperidine-1-oxyl (TEMPO) belongs to the highly stable nitroxide radical or nitroxyl class of compounds (Figure 2.13). The use of TEMPO for the selective oxidation of primary alcohols in the presence of secondary ones was first introduced by Semmelhack and coworkers [121]. Several papers have been published on the TEMPO oxidation of carbohydrates (including cellulose) including an extensive review [122].

2.6.1.1 Reaction Process and Proposed Mechanisms

Most of the TEMPO-mediated oxidation reactions of cellulose are performed in aqueous media at alkaline pH $(9-11)$. The degree of oxidation depends on the amount of NaOCl added in the TEMPO/NaOCl/NaBr system. After the oxidation process of CNC to CNC-OX with the structure of $\beta-1,4-$linked polyglucuronic acid sodium salt (cellouronic acid Na salt), the solution becomes clear [123]. A simplified schematic of the TEMPO mediated oxidation based on the mechanism proposed in the literature [124] is shown in Figure 2.14. In order to transform a single anhydroglucose primary alcohol to its carboxylate derivative, two molar equivalents of primary oxidant, hypochlorite, are required. Because TEMPO and NaBr are regenerated in the course of the reaction, only catalytic amounts are required to complete the reaction. During the reaction, protons are continuously being released therefore the pH has to be maintained by adding dilute alkali solution.

The cellulose chains are packed in its crystalline unit cell in a manner where only half of the primary hydroxyl groups (hydroxymethyl) are extended out of the crystalline structure and are accessible for oxidation (Figure 2.15). The regio-selective oxidation of hydroxyl groups on the surface of CNC to carboxylic acid is due to the fact that half of the cellulose chains on the surface are buried inside the crystalline domains of the nanocrystals whereas the other half on the exterior of the aggregates are available for oxidation [125].

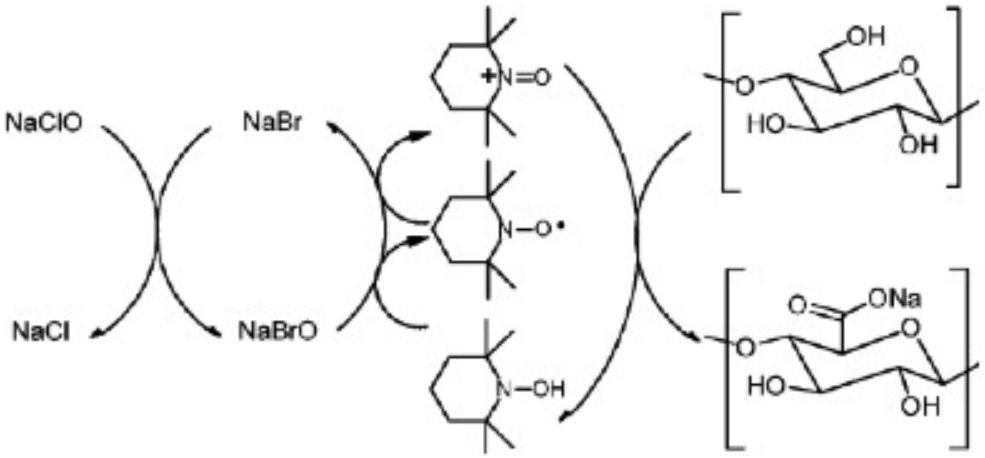

Figure 2.14: Simplified TEMPO mediated oxidation scheme [124].

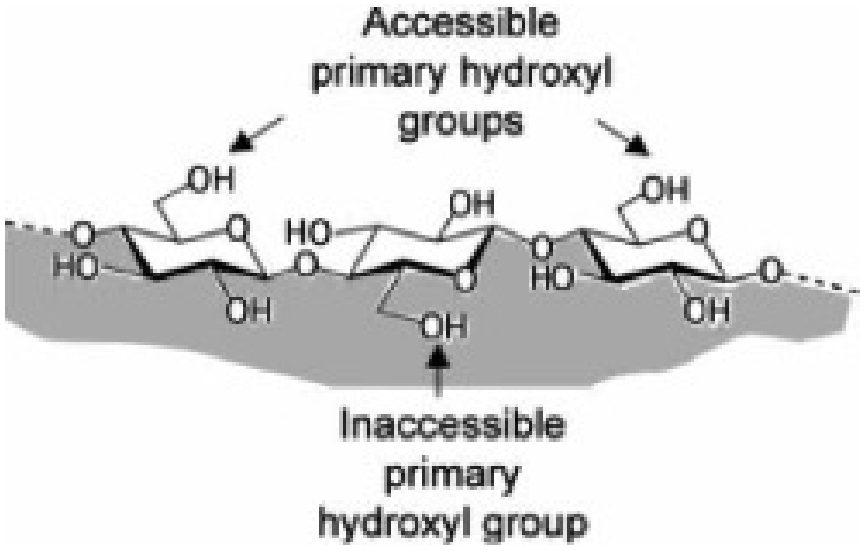

Figure 2.15: Schematic of a cellulose chain at the surface of a cellulose crystal [125].

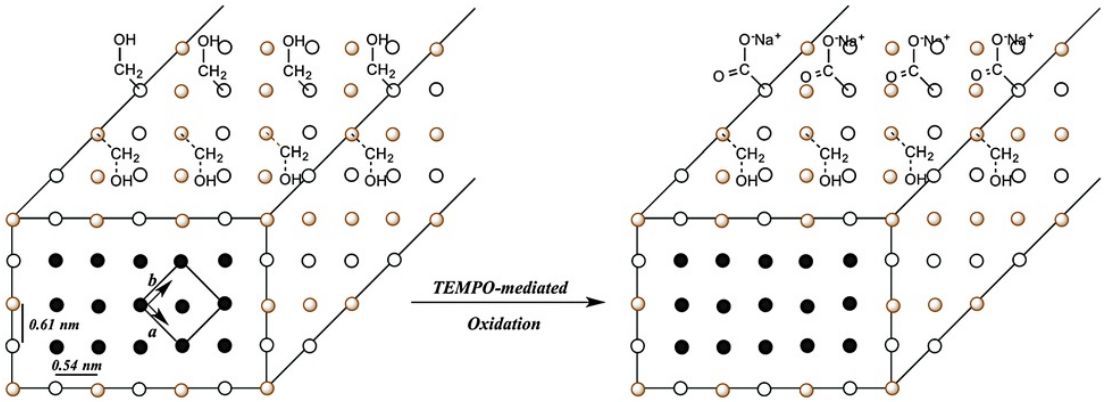

Figure 2.16: Schematic representation of a cellulose whisker cross-section [126].

Habibi and coworkers have suggested the arrangement of cellulose chains in its crystalline unit cell (Figure 2.16). Based on this representation, the carboxylic acid groups produced by TEMPO reaction are 0.8 nm apart in the lateral direction and 1.0 nm apart in the longitudinal direction. The introduction of carboxylic acid groups on the surface of CNC without changing its crystalline structure provides a unique platform for further modification on CNC. One can create various novel compounds by further manipulating these functional groups [126].

The conversion of primary hydroxyl groups to carboxylic acids is known to be pH dependent. The pH of the reaction medium also affects the time of oxidation and a pH of 10 has been shown to result in the shortest oxidation time [126]. Also, at acidic pH the secondary hydroxyl group might be oxidized [122]. At pH values higher than 10, the cellulose could be degraded by a β-elimination [127] .

2.6.1.2 Characteristics of TEMPO-oxidized Celluloses

TEMPO-mediated oxidation of cellulose also allows several modifications. The crystallinity of cellulose significantly affects its degree of oxidation by TEMPO [122]. Due to the high crystallinity index of native cellulose compared to mercerized/ regenerated celluloses, it resists high levels of conversion [128, 129]. The partial oxidation of native cellulose does not change its core crystalline characteristics and only produces superficial modification of microfibril surfaces [130].

2.6.1.3 Potential Applications of TEMPO-oxidized Celluloses

Due to the presence of several chemical functional groups on the surface of TEMPO-oxidized cellulose fibers, they have the capability for heterogeneous derivatization. In one study, sterically stabilized colloidal suspensions of functionalized microcrystalline celluloses were prepared using TEMPO-mediated oxidized cellulose fibers [118]. Amine-terminated PEG chains were grafted onto carboxylic sites of the TEMPO-oxidized microcrystals, which caused stable suspensions in high concentration electrolyte (2M NaCl) in comparison to unmodified microcrystals. Non-polar groups have also been successfully grafted onto TEMPO-oxidized celluloses [127, 131]. Carboxyl functionalized celluloses have also been used to co-adsorb some organic hydrophobic compounds and surfactants onto the surface of cellulose microfibrils [132]. The aggregation of surfactants onto charged solid substrates has various applications in different fields such as cosmetic formulations [133]. Based on their findings it is concluded that the adsorption of non-polar compounds onto the fibrils depends highly on the degree of oxidation during the TEMPO reaction.

2.7 CNC Biomedical Applications

CNC is becoming an important class of renewable nanomaterials with many applications in different areas including biomedicine. In the following, a number of biomedical applications of CNC are discussed.

2.7.1 Bionanocomposites

The small dimensions of CNC, its high aspect-ratio and high mechanical strength have also made it a reinforcing material for polymers [134]. One of the main applications of CNC is as reinforcing fillers in nanocomposite materials. Nanocomposite materials with superior mechanical properties compared to conventional fillers have been produced by mixing polymer latexes with CNC derived from tunicate cellulose [96]. Incorporating CNC into various polymeric matrices develops numerous bionanocomposite materials with potential bioapplications. Capadona et al. [135] reported on various novel stimuli-responsive polymer nanocomposites based on CNC, and they showed that the mechanical properties of the material can be selectively and reversibly controlled. CNC has also been incorporated in bionanocomposites that mimic the structure of a class of echinoderms called sea cucumbers. These creatures have the ability to reversibly and rapidly alter the stiffness of the dermis in response to different chemicals. This modulus is regulated by changes in interactions

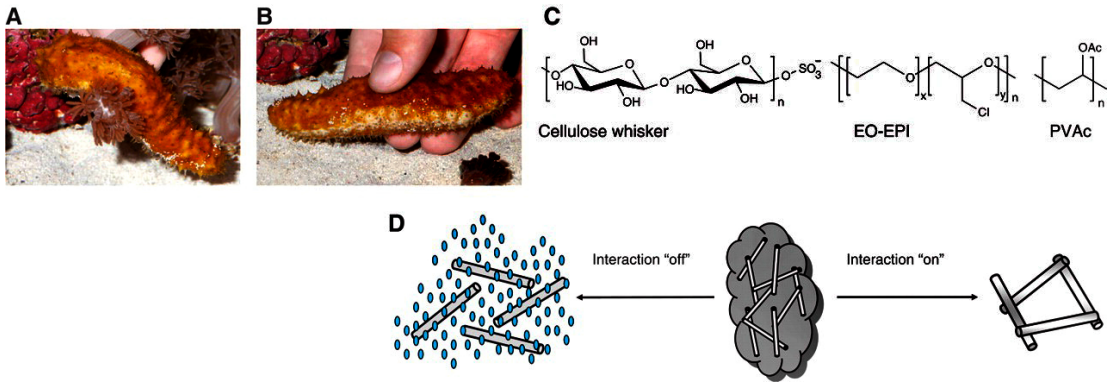

Figure 2.17: Natural model and bioinspired design of chemomechanical nanocomposites. Pictures of a D sea cucumber in relaxed (A) and stiffened (B) Interaction "off" Interaction "on" state demonstrating the firming of dermal tissue in the vicinity of the contacted area. (C) Chemical structure of cellulose whiskers isolated through sulfuric acid hydrolysis of tunicate cellulose pulp and the EO-EPI and PVAc matrix polymers used. (D) Schematic representation of the architecture and switching mechanism in the artificial nanocomposites with dynamic mechanical properties. In the "on" state, strong hydrogen bonds between rigid, percolating nanofibers maximize stress transfer and therewith the overall modulus of the nanocomposite. The interactions are switched "off" by the introduction of a chemical regulator that allows for competitive hydrogen bonding. AB [135].

between the collagen fibrils. CNC was incorporated in a bionanocomposite with a rubbery host polymer with a suitable thermal transition range and upon chemical stimulation, the interaction between the nanocrystals was altered. CNCs have a strong tendency to aggregate due to strong interactions between their surface hydroxyl groups. The presence of sulfate ester groups on the surface of CNC can moderate the interactions between the nanocrystals allowing its dispersion in hydrogen-bond-forming solvents. Taking advantage of this key factor between the balance of attraction and repulsion forces in CNC nanocomposites, the modulus of CNC bionanocomposites can be dynamically altered by a chemical regulator, which in this case changes the hydrogen bonding between the nanocrystals similar to sea cucumbers. During the processing, good dispersion is achieved by "switching off" the interactions between the nanocrystals by competitive binding with a solvent that forms hydrogen bonds. The interactions between the nanocrystals are "switched on" when the solvent is evaporated and they are assembled into percolating networks (Figure 2.17) [135].

In another study using in situ free radical polymerization, CNC was used to reinforce

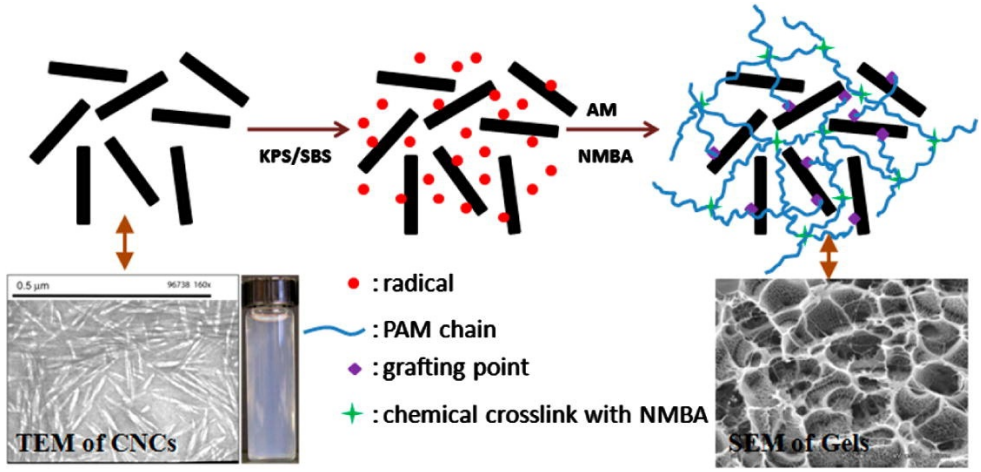

Figure 2.18: Scheme of the gelation mechanisms of PAM-CNC nanocomposite hydrogels [136].

polyacrylamide (PAM) hydrogels. They proposed a mechanism for the formation of the hydrogels (Figure 2.18). CNCs were homogeneously dispersed in solution followed by the addition of redox initiators of potassium persulfate (KPS) and sodium bisulfite (SBS) which induced the production of free radicals from the OH groups on the surface of CNCs. After the addition of acrylamide (AM) monomer and crosslinker N,N‘-methylenebisacrylamide (NMBA), the free radicals formed on the surface of CNCs reacted with the double bonds of AM monomer resulting in grafting points (covalent bond C-O) between CNCs and PAM chains. The homopolymerization of AM to grow PAM chains was initiated by other free radicals in solution, which were also crosslinked by NMBA. Finally, the PAM network including CNCs was formed. The grafting points denoted the hydrogen bonding between PAM and CNCs besides the covalent bonding (Figure 2.18). Investigations were done on the chemical structure, morphology and swelling properties of nanogels. It was observed the effective crosslink density increased and that accelerated the hydrogel formation through grafting copolymerization of acrylamide monomer on the surface of CNC as reinforcing materials. It was suggested that this biocompatible, strong nanocomposite hydrogel could potentially be used in bone tissue engineering and bone-defect repair [136].

In a recent study, injectable hydrogels of dextran and carboxymethyl cellulose were reinforced with CNC and aldehyde modified CNC (CHO-CNC). Shortly after the hydrogel components were extruded from a double-barrel syringe, gelation occurred and CNCs were shown to be distributed evenly throughout the hydrogel composites as observed by electron microscopy techniques. Figure 2.19 shows a schematic of the composite hydrogel formation.

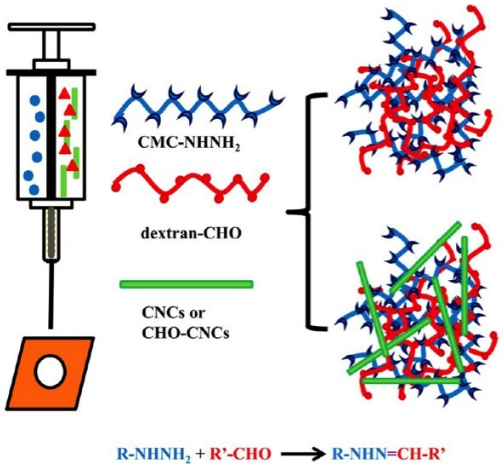

Figure 2.19: Schematic representation of injectable hydrogels reinforced with cellulose nanocrystals (CNCs), prepared using a double-barrel syringe. The crosslinking hydrogel components include hydrazide- functionalized carboxymethyl cellulose (CMC-$NHNH_2$), aldehyde- functionalized dextran (dextran-CHO), and either unmodified CNCs or aldehyde-modified CNCs (CHO-CNCs) [137].

CNC acted as filler while CHO-CNC acted as both filler and chemical crosslinker exhibiting enhanced elastic moduli. The composite hydrogels were stable for more than two months in buffer solution and they showed no significant toxicity to NIH 3T3 fibroblast cells. The CNC-reinforced hydrogels could have potential applications in tissue engineering and delivery of active compounds [137].

2.7.2 Electrochemical Biosensors

CNC is an amphiphilic, eco-friendly, biocompatible, high surface area material that can be easily functionalized. CNC has been used alone or in combination with other nanomaterials for the optimization of biosensor designs. Different peptides and proteins can be attached to the surface of CNC with retained bioactivity, which can be useful in the design of biosensors. Edwards et al. fabricated calorimetric and fluorescent biosensors by conjugating elastase substrate peptide on CNC. Elastase is the biomarker for various inflammatory diseases including chronic wounds. The spatio-stoichiometric features of CNC provide a useful platform for the interaction with the ligand [138]. In a previous study by the same group, the researchers had attached hydrolase to CNC and reported very high lysozyme activity [139].This suggested that the bioactivity of antimicrobial enzymes can be augmented

when they are attached to the surface of CNC. These systems have potential applications for the detection and inhibition of the formation of microbial biofilms [140]. Furthermore, a novel nanocomposite consisting of CNC and gold nanoparticles was recently investigated as a matrix for enzyme/protein immobilization [141], which exhibits significant biocatalytic activity. Site-specific or regio-selective functionalization of CNC can create promising materials that can be self-organized into higher assemblies. Karaaslan et al. demonstrated site-specific immobilization of a model protein at one tip of CNC. Mushroom-like conjugated nanoparticles were obtained by click chemistry in which, the reducing ends of rod-like functionalized CNC with azide groups were reacted with acetylene groups of spherical b-casein micelles. These hybrid protein-polysaccharide nanoparticles could be self-assembled into different nanobiomaterials with potential applications in immunoassay, nanomedicine and drug delivery [142].

2.7.3 Drug Delivery

CNC has attracted increasing attention in biomedical applications considering its properties as well as its safety and efficacy. U.S. Food and Drug Administration (FDA) has listed CNC as a "Generally Regarded As Safe" (GRAS) material. The toxicity assessment of CNC in the microvascular endothelial cells of human brain was conducted and CNC was found to be non-toxic to cells and therefore could be used as carriers in the targeted delivery of therapeutics [143]. CNC particles were incorporated into hydrogels based on cyclodextrin/polymer inclusion [144], and the new nanocomposite hydrogels seemed to be useful as controlled delivery vehicles.

Jackson and co-workers reported on the use of CNC for the binding and release of both hydrophilic and hydrophobic drugs, where the encapsulation and release of drug molecules can be controlled. First, they loaded CNC with water soluble, ionizable antibiotic drugs such as, tetracycline and doxorubicin. A significant quantity of these drugs was shown to bind to CNC with a fast release over one day. In order to study the potentials of CNC as a carrier for hydrophobic drugs, the surface of CNC was modified with cetyl trimethylammonium bromide (CTAB), a cationic surfactant. Modification of CNC with CTAB increased the zeta potential from -55 to 0 mV. Hydrophobic anticancer drugs, such as paclitaxel, docetaxel, and etoposide were significantly bound to CNC-CTAB and released in a more controlled manner over 2 days. They also studied the cellular uptake of the CNC-CTAB particles loaded with hydrophobic drugs to the KU-7 bladder cancer cells by probing the drugs with fluorescein using fluorescence microscopy [14].

In a recent study, Rescignano et al. formed a novel hybrid bionanocomposite of CNC-poly(vinyl alcohol)-poly(d,l-lactide-co-glycolide) (CNC-PVA-PLGA). They aimed at im-

proving the biocompatibility, thermal, and mechanical properties of PVA by incorporating CNC and PLGA nanoparticles loaded with bovine serum albumin fluorescein isothiocynate conjugate (FITC-BSA). This system takes advantage of both the biocompatibility and high mechanical strength of PVA/CNC as well as the control release of protein from the PLGA nanoparticles. These bionanocomposite films are considered suitable candidates for the successful delivery of biopolymeric nanoparticles to bone marrow mesenchymal stem cells. The binary and ternary PVA nanocomposite films were investigated for their biocompatibility and release of BSA to mesenchymal stem cells. Their results showed that the nanoparticles were easily taken up by the nanoparticles dissolved in the culture medium after the dissolution of PVA from the binary films, or by direct contact modality of ternary films. The bionanocomposites are excellent candidates for different localized and fast controlled drug delivery applications [145].

In another study, researchers incorporated polysaccharide nanocrystals, such as rod-like cellulose nanocrystals (CN), platelet-like starch nanocrystals (SN) and chitin whiskers (CHW) into sodium alginate (SA) nanocomposite microspheres by conventional crosslinking of Ca^{2+} with the goal of regulating drug release pattern and enhancing mechanical strength. They characterized the nanocomposites with rheological testing, FT-IR, and SEM. They observed increased stability of the network structure, improved mechanical performance and crystalline properties, higher encapsulation efficiency, more consistent swelling behaviors and desirable sustained release profiles of drugs. By analyzing the drug release mechanism they concluded that the dispersion of these nanocrystals in the microgel inhibits the diffusion of their drug theophylline and slows the dissolution and collapse of microgels which leads to an improvement in the drug loading and release profile. Therefore, the bio-nanocomposite microspheres could be used as a drug carrier for controlled delivery and release of drugs [146].

2.8 Summary

In this chapter a background on nanoparticles in drug delivery is presented. Also, polymers used in the biomedical field i.e. biodegradable, biocompatible, and bioadhesive polymers are reviewed. Cellulose and chitosan as naturally occurring polysaccharides are described. The production and properties of cellulose nanocrystal along with its surface modification techniques is reviewed. Among different surface modification techniques, TEMPO-mediated oxidation is described in more detail. Finally, the biomedical applications of CNC in bionanocomposites, biosensors, and delivery of active compounds is presented. Based on the current literature review, it can be concluded that studies on surface modification of

CNC for various applications, is one of the main domains of interest of researchers. Moreover, surface modified CNC can address the desire to design novel carriers for the delivery of active compounds. Therefore, our goal is to design and characterize novel CNC derivatives with improved biological properties suitable for delivery of bioactive compounds.

Chapter 3

Synthesis and Characterization of Amine Functionalized Cellulose Nanocrystals *

A simple protocol was used to prepare amine functionalized CNC. In the first step, epichlorohydrin (EPH) was reacted with ammonium hydroxide to produce 2-hydroxy-3-chloro propylamine (HCPA). In the next step, HCPA was grafted to CNC using etherification reaction in an organic solution media. Various reactions with varying different parameters, such as time, temperature, and reactants molar ratio were performed to determine the optimal reaction conditions. The final product (CNC-NH_2(T)) was dialyzed for a week. Further purification via centrifugation yielded the sediment (CNC-NH_2(P)) and supernatant (POLY-NH_2). The presence of amine groups on the surface of modified CNC was confirmed by FT-IR and the amine content was determined by potentiometric titration and elemental analysis. A high amine content of 2.2 and 0.6 mmol amine/g was achieved for CNC-NH_2(T) and CNC-NH_2(P), respectively. Zeta potential measurements confirmed the charge reversal of amine CNC from negative to positive when the pH was decreased from 10 to 3. This simple versatile synthesis method leading to high amine content can be used for further conjugation as required for various applications.

*This chapter is adapted from a paper "S.P. Akhlaghi, M. Zaman, N. Mohammed, C. Brinatti, R. Batmaz, R. Berry, W. Loh, K.C. Tam, Synthesis of Amine Functionalized Cellulose Nanocrystals: Optimization and Characterization", Submitted to *Carbohydrate Research*.

3.1 Introduction

Cellulose nanocrystals, rigid rod-like nanoparticles obtained by acid hydrolysis of pulp fibres have received increasing interest over the last 10 years. The non-toxicity, biocompatibility, and biodegradability of CNC along with its robust physical properties such as large surface area, mechanical strength, and the presence of abundant surface hydroxyl groups offer an interesting opportunity for their use in different fields [5]. In addition, further surface modification of CNC expands its usefulness in many product formulations. The primary hydroxyl groups could be converted to aldehyde, carboxylic acid and amine functionalities. Cationic modification of cellulose and its derivatives is of interest due to their utility in several key industrial sectors, such as water treatment [147]. In one study, cationic CNC was prepared by reaction with epoxypropyltrimethylammonium chloride. The cationic functionalization led to reversed surface charge density leading to stable aqueous suspensions due to the presence of trimethylammonium groups [7]. In a recent study, the surface of CNC was cationically modified with 4-(1-bromoethyl/bromomethyl)benzoic acid, pyridine in organic media. A high degree of substitution was reported leading to a zeta potential of +59.0 mV [8].

Modification of the surface of CNC with primary amine groups not only introduces positive charge on the surface of CNC in acidic medium, but it can also be used for the conjugation of biomolecules to CNC for biomedical applications [9]. The importance of polysaccharides with amine functional groups in biological systems has led to an increase of research in this field [148, 149].

Different forms of cellulose have been modified with amine groups via several synthesis methods. In one study, a three-step procedure was used to prepare 6-deoxy-6-amino cellulose derivatives. First, cellulose was tosylated and reacted with sodium azide, where the azide was reduced to amine using a $CoBr_2$/2,2'-bypridine/NaBH4 system [150]. Amine cellulose esters were also prepared by reactions involving lactam ring opening in the presence of N-methyl-2-pyrolidone and p-toluenesulfonic acid chloride [151]. In another study, polyampholytic amino cellulose sulfates were prepared by the tosylation of C-6 carbon followed by the introduction of sulfate groups using a trioxide/pyridine complex. Further nucleophilic displacement of tosyl groups by different amines yielded various types of cellulose with different types of amine functional groups [152].

In recent years, amine functionalized CNCs have been produced via different synthesis routes. In one study, researchers decorated the surface of CNC with epoxide groups via reaction with epichlorohydrin (EPH) in sodium hydroxide at 60 °C. After dialyzing the reaction mixture, amine groups were introduced on the surface of CNC by opening the

epoxide rings using ammonium hydroxide at 60 °C. The final product was obtained after dialysis until the pH of 7 [10]. In another study, amine groups were introduced on the surface of CNC by esterification and consecutive thiol-ene click reaction [153]. Click-chemistry was also applied in another study to prepare amine functionalized CNC. Firstly, azide groups were introduced to the surface of CNC via etherification of 1-azido-2,3-epoxy-propane in a mixture of isopropanol/basic water at room temperature. In the next step, pH-responsive amine decorated CNC was achieved by reacting the azide groups with propargyl amine via copper catalyzed azide-alkyne cycloaddition [154]. In a recent study, amine functionalized CNC was obtained via a two-step procedure in aqueous media at ambient temperature. In the first step, the primary hydroxyl groups on the surface of CNC were converted to carboxylic acid via TEMPO-mediated oxidation. In the next step, peptidic coupling reaction between carboxylic acids and amines on bifunctional amines of small alkyl chain length was conducted [9]. Amine groups have also been introduced on the surface of CNC by grafting with chitosan oligosaccharide [155].

In the present study, we develop and optimize the functionalization of CNC with primary amines in aqueous solution in a simple reaction protocol. The synthesis protocols previously used for the synthesis of amine functionalized CNC was modified and different reaction parameters, such as time, temperature, ratios of CNC and reagents, and the effect of reflux were optimized leading to a higher content of surface amine groups. The pH-responsive properties of amine functionalized CNC was investigated by viscosity measurements.

3.2 Experimental Section

3.2.1 Materials

A freeze-dried cellulose nanocrystal (CNC) sample was supplied by FPInnovations. Epichlorohydrin (EPH), dimethylsulfoxide (DMSO), and tetrabutylammonium hydroxide (TBAH) were purchased from Sigma-Aldrich. Ammonium hydroxide ($28 - 30\%$) was purchased from Acros organics. Millipore de-ionized (D.I.) water was used for all experiments and sample preparations.

3.2.2 Synthesis and Optimization of Amine Functionalized Cellulose Nanocrystals

In the first step, epichlorohydrin (1.46 mL) was added to ammonium hydroxide (3.78 mL) and heated to 65 °C for 2 h. In the second step, CNC (1.00 g) was dispersed in DMSO (66.66 mL) and a different amount of TBAH was added to the mixture in a round bottom flask (molar ratio of TBAH/ AGU: 0.1-1.0). Contents from the reaction in step 1 was removed using a syringe and added to the second mixture in a dropwise manner. The reaction mixture was stirred for various time intervals (0.5-8 h) and heated at different temperatures (25-80 °C) for studies on the optimal reaction conditions. The reaction mixture was purified by dialysis against D.I. water (MW cut off: 12,000 Da) for at least a week until the conductivity of the dialysis medium remained constant. The final product was referred to as CNC-NH_2(T). Further purification of the reaction mixture was obtained by lowering the pH down to 3, which induced the agglomeration of amine CNC nanoparticles between positive NH_3^+ and negative OSO_3^- groups. The agglomerated amine CNC was separated by centrifugation at 10,000 rpm for 1 h. The sediment was redispersed in an alkaline aqueous solution, and the process was repeated once more, where the purified product comprised of the sediment (CNC-NH_2(P)) and supernatant (POLY-NH_2).

3.2.3 Potentiometric Titration

The amine content of the amine functionalized CNC was determined by potentiometric titration. A Metrohm 809 Titando automatic titrator was used and the pH and conductivity were measured simultaneously. The titrator is equipped with a Tiamo software that doses μL of titrants. All measurements were performed in a closed jacketed vessel at 25 °C and the stirrer was set at a medium rate. 50 mL of 0.1 wt% CNC suspensions were prepared in D.I. water. The pH of the suspensions was adjusted to approximately 3 using 1 M HCl. The suspensions were then degassed by bubbling argon gas into the solution and were then titrated using 0.1 M NaOH under argon blanket and stirring. The conductivity and pH of the suspensions were measured simultaneously until the pH of the samples approached 11. Finally, the pH and conductivity values were plotted against the volume of NaOH (in mL), which were used to determine the content of amine groups.

3.2.4 Fourier Transform Infrared (FT-IR) Spectroscopy

FT-IR spectra of the dried KBr pellets of pristine CNC, CNC-NH_2(T), CNC-NH_2(P), and POLY-NH_2 were determined using a Bruker Tensor 27 spectrometer with resolution of 4

cm^{-1} and a number of scans of 32 from 400 to 4000 cm^{-1}. KBr pellets were prepared by grinding approximately 2% of the samples in KBr and compressing the mixture into a pellet. The FT-IR spectra were monitored and analyzed using the OPUS software.

3.2.5 Elemental Analysis

The percent of carbon (C), hydrogen (H), nitrogen (N) and sulfur (S) contents (%) of pristine CNC, CNC-NH_2(T), CNC-NH_2(P) and POLY-NH_2 were determined by a CHNS, Vario Micro Cube, Elemental Analyzer. The freeze-dried samples were combusted at 1000 °C and the combustion products were detected by a thermal conductivity detector for quantitative analysis.

3.2.6 Transmission Electron Microscopy (TEM)

TEM images of pristine CNC, CNC-NH_2(T), and CNC-NH_2(P) were recorded using a Philips CM10 TEM with 60 keV acceleration voltages. Approximately 10 μL of 0.01 wt% aqueous suspensions of the samples were deposited on a carbon-formvar film on 200 mesh copper grids. In order to minimize possible agglomeration of the particles, excess solvent was removed from the grids placed on a filter paper. Then the grids were allowed to dry overnight.

3.2.7 Zeta Potential Measurements

Zeta Potential measurements for the various CNC systems at different pH values were measured using the ZetaPALS Analyzer (Brookhaven Instruments Corp., USA). The concentration of the samples was maintained at ∼0.01 wt% and the experiments were conducted at 25 °C. The reported values are an average of 10 measurements.

3.2.8 Viscosity Measurements

The relative viscosity of 0.1 wt% CNC-NH_2(P) suspension, at different pH values was determined using an automated kinematic viscometer, MiniPV (Cannon Instrument Company), at 25 °C. The sample was automatically drawn by a vacuum pump to the upper glass bulb, and the sensors placed at the top and bottom of the glass bulb measured the time taken for a known volume of liquid to flow through the capillary tube. Repeated tests

were performed and once the measured times were within 1% of each other, the relative viscosity was then calculated.

3.3 Results and Discussion

3.3.1 Two-step Synthesis of Amine Functionalized Cellulose Nanocrystals

Cellulose nanocrystals have previously been functionalized with amine groups by different research groups [9, 10]. However, in most of the studies, the amine content was found to be relatively low. Thus it would be desirable to increase the amine content by improving the synthesis protocol. In the synthesis method adopted by Dong et al. [10] and Mahmoud et al. [156] the low amine content could be attributed to the alkaline hydrolysis of the epoxide of epichlorohydrin [157] resulting in a lower grafting onto CNC. In the current study, a two-step synthesis protocol was developed to increase and enhance the grafting of amine functional groups onto CNC. In the first step, 2-hydroxy, 3-chloro propylamine was produced by opening the epoxide of epichlorohydrin with ammonium hydroxide. This reaction is highly explosive in a closed container and in order to prevent the risk of explosion and maximize the reaction yield, a reflux system with cooling water was used. In the next step, to minimize side reactions and undesirable hydrolytic reactions, we dispersed CNC in DMSO and TBAH was added gradually to deprotonate the hydroxyl groups on the surface of CNC. Finally, the dropwise addition of mixture 1 to 2 (Figure 3.1) resulted in the amine functionalized CNC.

3.3.2 Effect of Reaction Parameters

In our attempt to optimize the reaction, different parameters were varied and their effect was investigated. The amine content of the samples was determined by potentiometric titration. Optmization was carried out by first changing the time of the reaction and finding the optimum reaction time followed by optimizing the temperature. The optimized reaction time and temperature were used to find the optimum molar ratio of reagents. As shown in Figure 3.2a, the amine content of modified CNC increased with reaction time and reached an optimum at 3 hours. However, prolonging the reaction time resulted in a marginal reduction in amine content, and this could be attributed to the hydrolysis of ether bond in alkaline condition [158, 159]. The optimum temperature for reacting

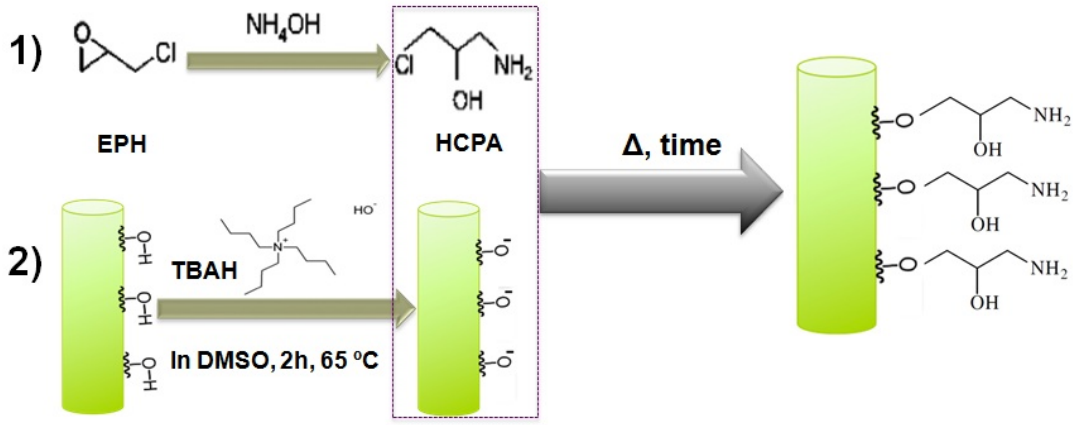

Figure 3.1: Two-step amine functionalization of CNC.

mixture 1 and 2 was found to be 50 °C (Figure 3.2b). The reduction in amine content at high temperature could be due to the enhanced hydrolysis of ether bonds in amine CNC under alkaline condition [160]. As shown in Figure 3.2c, the amine content of modified CNC increased with the molar ratio of TBAH to AGU due to the favorable activation of hydroxyl groups in the presence of TBAH. Figure 3.2d shows the effect of the EPH-to-CNC molar ratio on the amine content of CNC. At higher EPH content in the reaction system, a larger amounts of HCPA was available at the surface of the CNC (near the glucose molecules), therefore, favoring the etherification reaction [161]. However, beyond a critical EPH content, the amine content of modified CNC was found to decrease, and the optimum EPH to CNC molar ratio was found to be 3:1. In step 1 of the protocol, the amount of NH_4OH was also increased in proportion to EPH so as to maintain a constant molar ratio of epoxy to ammonium groups. This has led to a larger proportion of water in both reaction mixtures 1 and 2, which could have enhanced the undesirable hydrolytic reaction resulting in the reduction in the amine content above the EPH/CNC molar ratio of 3.5 [157]. Under refluxing in the first step, we were able to increase the total amine content from 0.45 to 2.2 mmol/g.

3.3.3 Purification

EPH has been used in the preparation of various kinds of polymers [162, 163] and hence we anticipated the possibility of side reactions forming polyfunctional amines that may necessitate additional purification of the reaction products. Initially, we purified the sam-

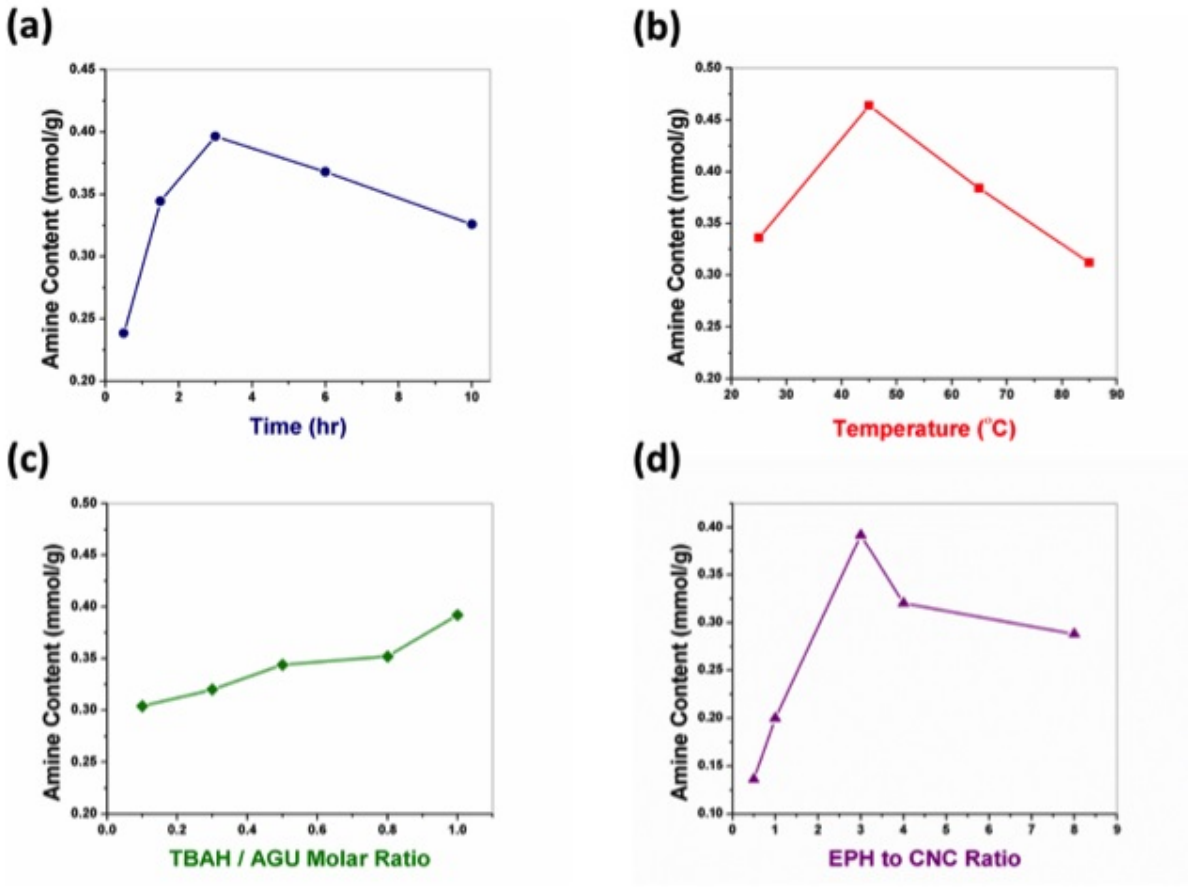

Figure 3.2: Optimization of amine-CNC synthesis by varying different reaction parameters (a) time, (b) temperature, (c) TBAH/AGU ratio, and (d) EPH/CNC ratio.

ple using a dialysis tube (MW cut off: 12,000 Da) against D.I. water. The dialysis was performed for more than a week until the conductivity of the dialysis medium remained constant. This purified sample was designated as CNC-NH_2(T), which we believed contained amine functionalized CNC (CNC-NH_2(P)) and polyfunctional amines (POLY-NH_2). In order to separate CNC-NH_2(P) from POLY-NH_2, the reaction mixture was subjected to centrifugation. First, the pH of CNC-NH_2(T) dispersion was adjusted to 3 to promote electrostatic interactions between positively charged amine groups and negatively charged sulfate ester groups on the surface of CNC, which induced the aggregation of the CNC nanoparticles. Next, centrifugation was performed at 10,000 rpm for 1 h. The supernatant was decanted and the sediment was redispersed in basic pH condition, and this step was repeated a second time. The sediment containing predominantly CNC-NH_2(P) dispersion was recovered and used in subsequent studies. Depending on the desired application either CNC-NH_2(T) with high amine content or CNC-NH_2(P) could be used.

3.3.4 Potentiometric Titration

The amine content of unmodified CNC, CNC-NH_2(T), CNC-NH_2(P) and POLY-NH_2 was determined by potentiometric and conductometric titrations and the results are shown in Figure 3.3. The suspensions were first treated with excess HCl and then titrated with 0.1 M NaOH. The titration curve for CNC did not reveal the presence of amine groups whereas the three samples after the modification reactions clearly showed the presence of amine groups. The potentiometric plots of the modified samples displayed three regions, namely (1) reaction of NaOH with excess HCl, (2) deprotonation of amine groups, and (3) titration of excess NaOH. The region between the two equivalent lines corresponded to the deprotonation of the amine groups. Based on Figure 3.3, the amine content of CNC-NH_2(T), CNC-NH_2(P) and POLY-NH_2 were determined to be 2.20, 0.62, 1.58 mmoles/g respectively. The amine content of our CNC-NH_2(P) has been noticeably enhanced compared to the majority of previously reported values in the literature. The amine content of CNC-NH_2(T) is also comparable to the amine content obtained from the peptidic coupling reaction which might be useful in applications in which direct grafting of amine groups to CNC surface is not required [9].

3.3.5 Elemental Analysis

The elemental composition of unmodified CNC, CNC-NH_2(T), CNC-NH_2(P) and POLY-NH_2 was evaluated from elemental analyses. As seen in Table 3.1, unmodified CNC con-

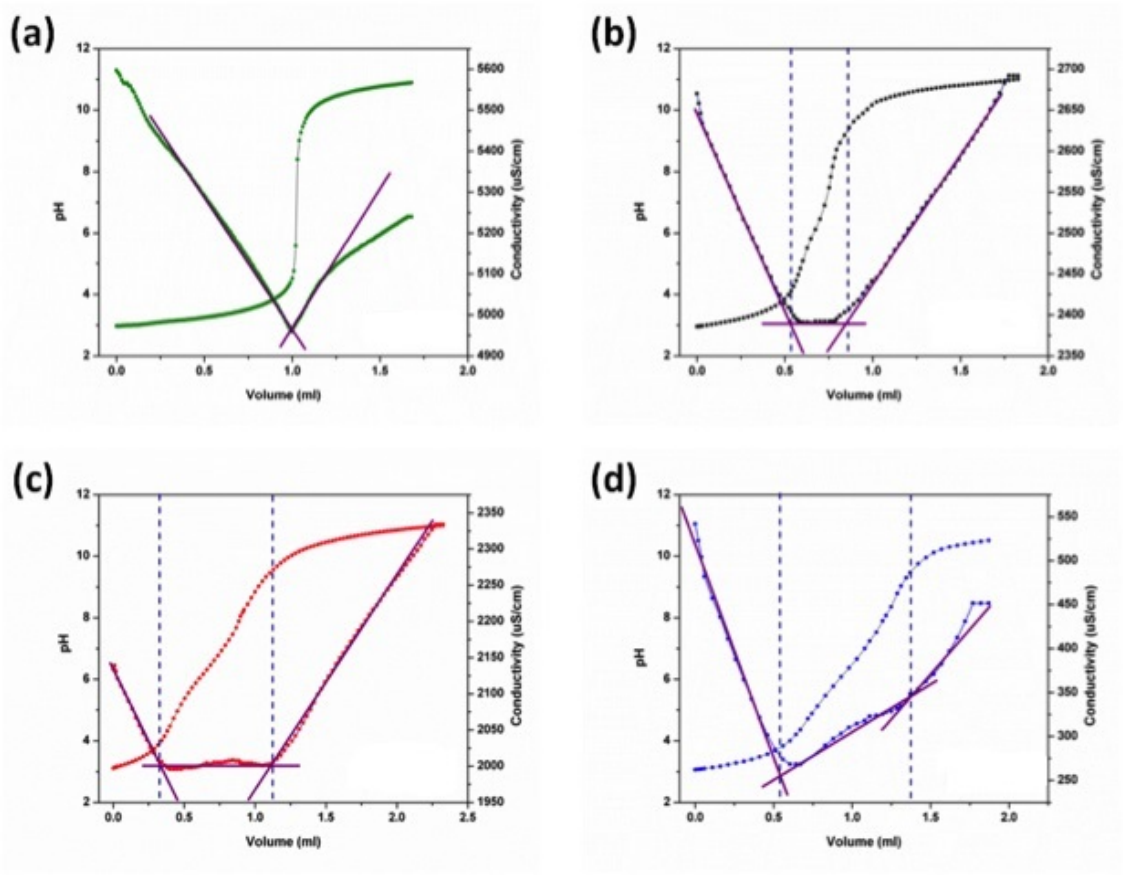

Figure 3.3: Potentiometric titration plots of (a) unmodified CNC, (b) CNC-NH_2(P), (c) POLY-NH_2, and (d) CNC-NH_2(T).

tained no nitrogen, whereas the amine CNC samples revealed the presence of atomic nitrogen confirming the successful surface modification of CNC with amines. The presence of atomic nitrogen in POLY-NH_2 suggested the presence of polyfunctional amines. The sulfur content of the amine CNC is lower than unmodified CNC, which is possibly attributed to the hydrolysis of sulfate ester groups at high pH during the purification step [164]. The degree of surface substitution (DS) was determined by the nitrogen content evaluated by elemental analysis based on Eq. 3.1 and the approach reported in the literature [165, 166]:

$$DS = \frac{162N\%}{1400 - 108.56N\%} \tag{3.1}$$

The DS of our CNC-NH_2(P) and CNC-NH_2(T) after reflux was calculated as 0.11 and 0.35, respectively. These results suggest that the amine functionalization protocol reported in this study yielded amine content that is significantly higher than previous reported studies Roman et al. 0.024 [10], Nielsen et al. 0.029 [153], and Pahimanolis et al. 0.02 [154].

Table 3.1: Elemental analysis of unmodified CNC, CNC-NH_2(P), POLY-NH_2, and CNC-NH_2(T)

Sample	**% C**	**% H**	**% N**	**% S**	**% O**
Unmodified CNC	40.98	5.53	0.00	0.86	52.63
CNC-NH_2(P)	18.85	2.99	0.90	0.59	76.66
POLY-NH_2	4.16	0.86	1.42	0.43	93.13
CNC-NH_2(T)	42.00	6.19	2.55	0.80	48.46

3.3.6 FT-IR

FT-IR spectra of unmodified CNC, CNC-NH_2(T), CNC-NH_2(P) and POLY-NH_2 are shown in Figure 3.4. The absence of characteristic peaks of the sample in the supernatant confirmed that no CNC was present in the supernatant. The new small absorption band in Figure 3.4.b and d, at 1550 cm^{-1} corresponded to N-H bending bands, which could be an indicator of surface functionalization with amine groups. The typical two weak bands for N-H of primary amines not observed in the FT-IR spectra as they overlapped with the strong O-H band in the region of 3500 cm^{-1} [9].

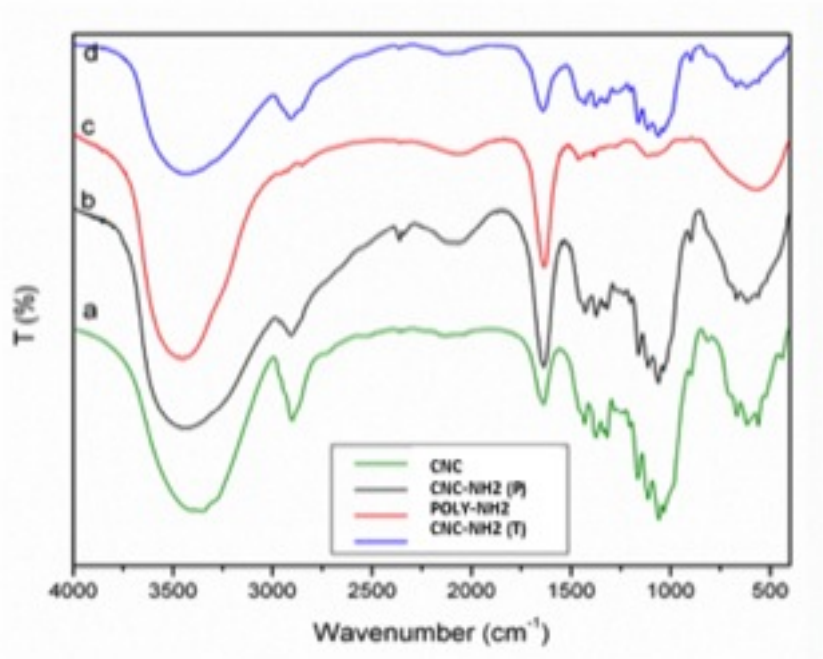

Figure 3.4: FT-IR spectra of (a) unmodified CNC, (b) CNC-NH_2(P), (c) POLY-NH_2, and (d) CNC-NH_2(T).

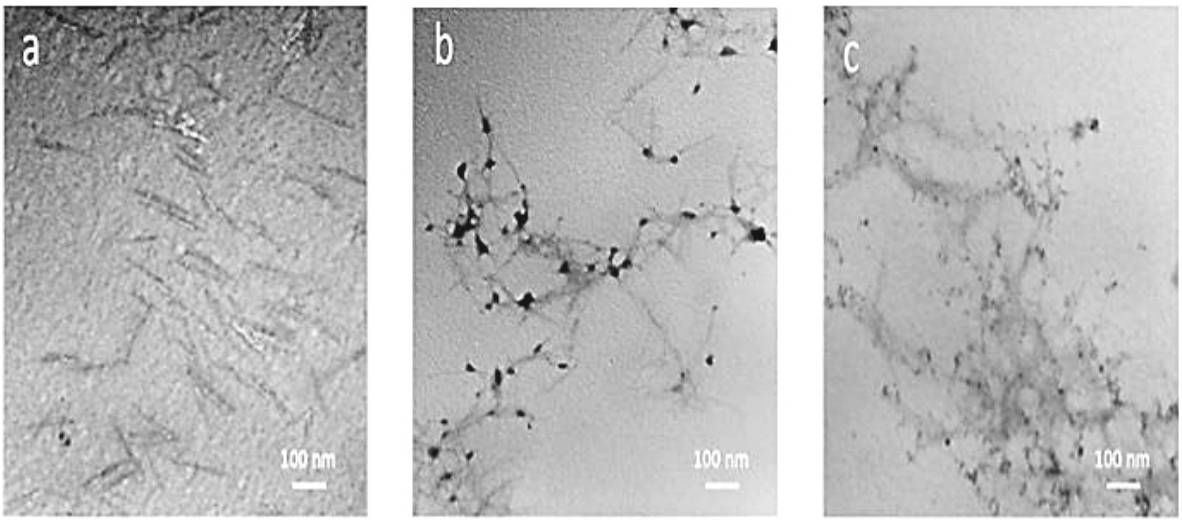

Figure 3.5: TEM images of (a) unmodified CNC, (b) CNC-NH_2(T), and (c) CNC-NH_2(P).

3.3.7 TEM

The TEM images of unmodified CNC, CNC-NH_2(T), and CNC-NH_2(P) are shown in Figure 3.5a, b and c respectively. As evident, surface functionalization did not alter the rod like structure of the nanocrystals. However, slight agglomeration was observed after surface amine functionalization due to the electrostatic interactions and drying process. Similar results were observed previously [9]. Figure 3.5b and c reveal that there are much less agglomerated polymer chains in CNC-NH_2(P) than in CNC-NH_2(T).

3.3.8 Zeta Potential Measurements

The zeta potential values of unmodified CNC, CNC-NH_2(T) and CNC-NH_2(P) at different pH values are shown in Figure 3.6A. At all pH values, unmodified CNC possessed negative zeta potentials. In acidic pH values, the negative charge is due to the presence of the sulfate ester groups (OSO_3^-) arising from the sulfuric acid hydrolysis. At high pH values, the negative OSO_3^- groups were hydrolyzed, leading to less negative zeta potential [164]. The successful amine surface modification of CNC could be confirmed by zeta potential measurements. As revealed by Figure 3.6 both CNC-NH_2(T) and CNC-NH_2(P) possessed positive zeta potentials at low pH due to the protonation of the amine groups. The more

positive zeta potential of CNC-NH_2(T) could be due to the presence of more amine groups. As the pH increased, the amine groups became deprotonated, and beyond a pH of 9, the amine groups were completely deprotonated resulting in a negative zeta potential. In addition, hydrolysis of the sulfate ester groups on the surface of CNC resulting in a less negative zeta potential, occurred at pH greater than 10.

The surface functionalization of CNC with amine groups and the enhanced grafting of amine groups by refluxing the reaction mixture was also proven indirectly by the zeta potential measurements shown in Figure 3.6B. In this figure unmodified CNC, CNC-NH_2(T) before and after reflux displayed negative zeta potentials at pH 12 due to the presence of sulfate ester groups. At low pH (pH 2), unmodified CNC was negatively charged whereas CNC-NH_2(T) possessed a substantial positive charge due to the presence of protonated amine groups. The higher zeta potential value observed for CNC-NH_2(T) after reflux illustrates the possibility of the presence of higher amine content leading to a more positive zeta potential value.

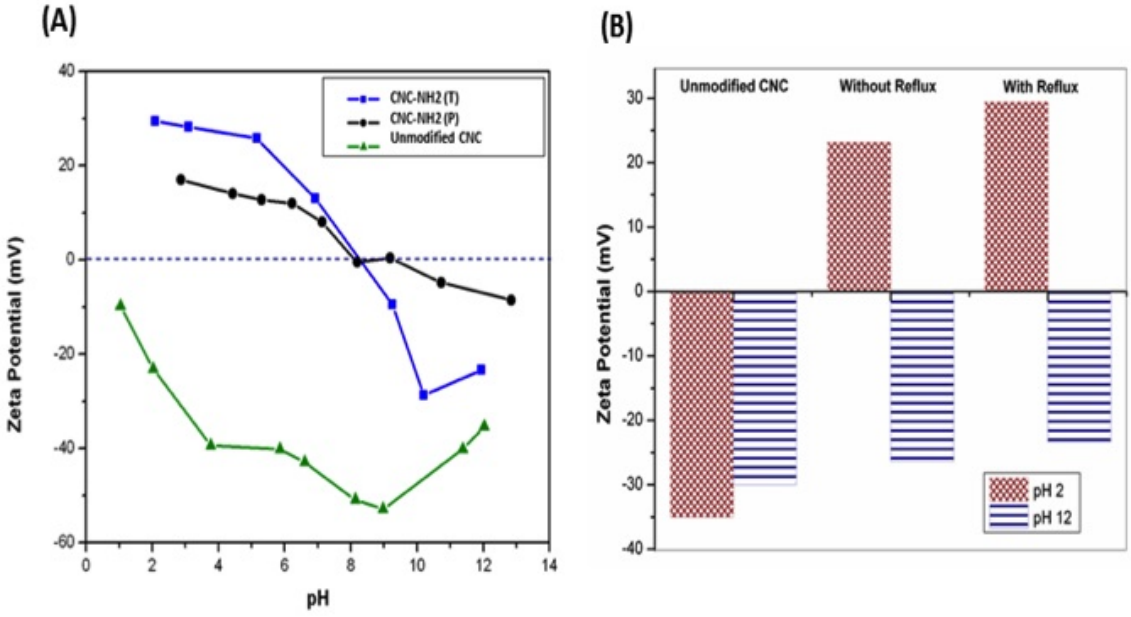

Figure 3.6: (A): Zeta potential values of unmodified CNC, CNC-NH_2(T) and CNC-NH_2(P) at different pH values, (B): Comparison of zeta potential values of unmodified CNC, CNC-NH_2(T) before reflux and after reflux at low and high pH.

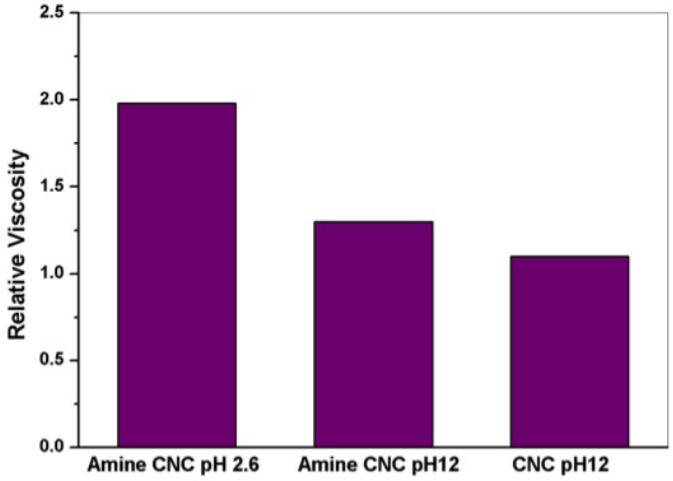

Figure 3.7: Relative viscosity of unmodified CNC and CNC-NH_2(T) before reflux at low and high pH.

3.3.9 Viscosity Measurements

The relative viscosity of unmodified CNC and CNC-NH_2(T) at low and high pH was measured (Figure 3.7). The higher relative viscosity at low pH for CNC-NH_2(T) is due to the formation of aggregates due to the electrostatic interaction between the positive charge of the protonated amine groups and the negatively charged sulfate ester groups. At high pH, the additional electrostatic interaction was removed due to the deprotonation of the amine groups leading to a reduction in the relative viscosity as reported previously [154].

3.4 Conclusions

In this chapter, a simple protocol for functionalizing the surface of CNC with amine groups is presented. The synthesis process was optimized by varying different parameters such as time, temperature and reactant ratios, and refluxing of the reaction mixture enhanced the grafting of amines onto CNC. The dialyzed final product contained amine functionalized CNC and aminated polymers that were formed during the side reactions. Further purification of the system was achieved through centrifugation. The sediment contained amine groups directly grafted on the surface of CNC through amide bonds. Potentiometric titration and elemental analysis confirmed the presence of high amine content in our modified

CNC samples. TEM microscopy showed similar structural properties of the nanocrystals along with some minor aggregation. Zeta potential and relative viscosity measurements also proved the presence of amine groups. The positive zeta potential values at low pH for the amine CNC particles resulted in higher relative viscosity due to electrostatic interactions. Both CNC-NH_2(T) and CNC-NH_2(P) can be further modified and used in different applications.

Chapter 4

Surface Modification and Characterization of Cellulose Nanocrystals with Chitosan Oligosaccharide *

A novel drug delivery system based on two of the most abundant natural biopolymers was developed by modifying the surface of oxidized cellulose nanocrystal (CNC) with chitosan oligosaccharide (CS_{OS}). First, the primary alcohol moieties of CNC were selectively oxidized to carboxyl groups using the 2,2,6,6-tetramethylpiperidine-1-oxyl radical (TEMPO) catalyst. The amino groups of CS_{OS} were then reacted with carboxylic acid groups on oxidized CNC (CNC-OX) via the carbodiimide reaction using N-hydroxysuccinimide (NHS) and 1-ethyl-3-(3-dimethylaminopropyl)-carbodiimide (EDC) as coupling agents. Successful grafting of CS_{OS} to CNC-OX was confirmed by infrared spectroscopy, solid state ^{13}C NMR, thermogravimetry, potentiometric titration, and zeta potential measurements. The grafting resulted in a conversion of $\sim 90\%$ carboxyl groups on CNC-OX and the degree of substitution (DS) was 0.26.

*This chapter is adapted from a paper "S.P. Akhlaghi, R.C. Berry, and K.C. Tam, Surface Modification of Cellulose Nanocrystal with Chitosan Oligosaccharide for Drug Delivery Applications, *Cellulose*, 2013, 20:1747-1764" and a patent "S.P. Akhlaghi, K.C. Tam and R.C. Berry, Surface Modified Nanocrystalline Cellulose and Uses Thereof, US patent 55596984-9USPR."

4.1 Introduction

The potentials of materials derived from natural sources are being extensively investigated, as they find many biomedical applications. The desire towards designing novel products for various applications from renewable resources has led to increased research activity on abundant, natural, biodegradable and biocompatible polymers over the last decade.

Cellulose fibre is the most abundant renewable material that contains amorphous and crystalline domains. The acid hydrolysis of cellulose fibre disrupts its amorphous domains and releases individual rod-like rigid crystallites called CNC. The treatment of native cellulose with sulfuric acid introduces negative charges to its surface due to the formation of sulfate ester groups [110]. Since the first discovery of CNC in 1949 by Ranby [95], interest in this system has risen over the last decade because of its availability, mechanical strength, high surface area and aspect ratio. CNC also possesses many benign properties, such as non-toxicity, biocompatibility and biodegradability, which make it an excellent candidate for pharmaceutical applications [5]. Large amounts of drugs can be bound to the surface of CNC due to negative charges and its very large surface area. It also provides the potential for high payloads and optimal control of dosage. Also, due to the presence of numerous hydroxyl groups, the surface of CNC can be modified with different functional groups that can be used to control the loading and release of drugs [6].

Chitosan (CS) is produced from partial deacetylation of chitin, the second most abundant biopolymer in nature. Two marine crustaceans (shrimps and crabs) are the main sources of chitin. CS is an amino polysaccharide that possesses positive charges in acidic media due to the protonation of its amino groups. CS possesses many interesting characteristics such as non-toxicity, biocompatibility and biodegradability. The positive charges on CS resulting from the presence of several amino groups allow the binding of different anionic drugs or polymeric systems. Thus, CS has a great potential for delivering drugs and allows the manipulation of their release profiles. In pharmaceutics, CS has been widely used as a coating material, disintegrant, tablet binder and a vehicle for peptide and gene delivery. In addition, CS has antimicrobial, hemostatic, wound healing, and mucoadhesive properties [89]. Due to its bioadhesive properties, it is known to increase the absorption of drugs from the mucosal membranes by increasing the residence time in the mucous and enhancing the permeability of drugs [167]. Despite the attractive functional properties of CS suitable for many uses, there are some problems associated with its *in-vivo* applications such as, high viscosity, high molecular weight, large aggregation formation and low solubility at physiological pHs (7.2-7.4) [15]. To overcome the solubility problems, CS was modified to produce water-soluble analogues, such as PEGylated chitosan and glycol chitosan [168, 169]. Another approach to address the solubility issues of CS

is the utilization of low molecular weight CS, known as chitosan oligosaccharides (CS_{OS}) [16]. One additional problem of CS in drug delivery is its limitations in the controlled release of encapsulated active ingredients due to its hydrophilic nature and its solubility in acidic medium. In order to improve drug delivery properties of CS, several modifications were studied, such as covalent attachment of polymeric chains to CS. These modifications change the physicochemical properties and make it more suitable for drug delivery [78].

Several systems have been established based on chitosan and cellulose derivatives for various applications. Films of chitosan and cellulose blends were prepared using trifluoroacetic acid [170, 171, 172] or N-methylmorpholine-N-oxide (NMMO) [173] as co-solvents. Most of these systems can be used as antimicrobial agents [174], in wound dressings [172, 175] or in electro-active papers [170]. Cellulose derivatives, such as carboxymethyl cellulose have been used together with chitosan to yield polyelectrolyte complexes (PEC) [176] or self assembled nanoparticles [177]. Composites of bacterial cellulose and chitosan have also been developed for medical applications [178]. Modified chitosans such as O-carboxymethylated chitosan [179] or quaternary ammonium derivative of chitosan oligosaccharide [174] have also been used in combination with cellulose. Microparticulate chitosan controlled release systems for buccal drug delivery using hydrophobic cellulosic polymers such as, cellulose acetate butyrate (CAB) or ethyl cellulose (EC) and hydrophilic chitosan microcores have also been produced [180].

However, there are limited studies on systems consisting of CNC and CS. Fernandes and coworkers made transparent nanocomposite films of nanofibrillated cellulose and chitosan by solution casting [181]. In another study, researchers used layer-by-layer (LBL) technique to create nanocomposite films of CNC and CS based on hydrogen bonds and electrostatic interactions. These biodegradable films have potential applications in biomedical sciences and food packaging [182]. The same group of researchers formed bio-based nanocomposites through covalent linkage of CS to CNC by producing reactive end groups on the surface of CNC with methyl adipoyl chloride (MAC) and reacting it with primary amino groups on CS [183]. In another study, Wang and coworkers studied the formation of polyelectrolyte macroion complex (PMC) between CNC and CS for oral drug delivery purposes. The particles were formed by electrostatic interactions due to the strong mismatch between the opposite charges of CNC and CS [184]. Researchers have previously used peptidic coupling reaction to form amide bonds between the carboxylic groups on oxidized CNC and different amine bearing compounds. Grafting compounds on CNC by an amide bond, provides greater stability against chemical conditions and heating [118, 127].

Due to the beneficial properties of CNC and CS, we embarked on a study to develop a novel, biocompatible, biodegradable and nontoxic system for the delivery of active compounds using peptidic coupling reaction. To the best of our knowledge, no attempts have

been made in exploiting the combined advantages of modifying the surface of CNC with CS_{OS} for potential biomedical applications. CNC-CS_{OS} particles could not only act as a carrier for active compounds, but also possess biological properties of CS, such as antibacterial, hemostatic and wound healing properties. This system can have potential applications, such as buccal drug delivery and addressing oral cavity problems. In our study, by using CS_{OS}, the insolubility problem of CS at physiological pH is addressed with the additional benefit of increased antibacterial properties.

4.2 Experimental Section

4.2.1 Materials

A freeze-dried CNC sample was supplied by FPInnovations. Chitosan oligosaccharide (average M_n 5000 Da, DD ~75%) was purchased from Sigma-Aldrich. For TEMPO-mediated oxidation, the following chemicals were purchased from Sigma-Aldrich: TEMPO (98%), sodium hypochlorite (NaOCl) (reagent grade, 10-15% available chlorine) solution, sodium bromide (NaBr) (99.0%), NaOH (1 N) standard solution, HCl (1 N) standard solution, and methanol. For the amide coupling reaction, crosslinkers EDC (1-ethyl-3-(3-dimethylaminopropyl) carbodiimide, commercial grade) and NHS (N-hydroxysuccinimide, 98%+) were purchased from Fluka and Acros Organics, respectively. As received MES (2-(N-morpholino) ethanesulfonic acid, >99%) purchased from Sigma was used as buffer for the EDC crosslinking reaction. Millipore de-ionized (D.I.) water was used for all experiments and sample preparations.

4.2.2 TEMPO Mediated Oxidation of CNC

In order to modify CNC with CS_{OS}, the surface hydroxyl groups of CNC was initially oxidized to carboxyl groups using NaClO assisted by 2,2,6,6,-tetramethyl-1-(pyperidinyloxy) radical (TEMPO). TEMPO is a stable and water-soluble nitroxyl radical and due to its steric hindrance, it can only oxidize the primary hydroxyl groups on CNC to convert them to carboxylic acids [128].

In order to disrupt the CNC bundles and obtain a homogenous dispersion, CNC (1.3 g, 8.02 mmol glycosyl units) was dispersed in D.I. water (100 mL) and sonicated in a Branson 1510 sonicator (Branson Ultrasonic Corporation, USA) for 10 min. Then, TEMPO (20 mg, 0.128 mmol) and NaBr (400 mg, 3.880 mmol) were added to the CNC suspension and

stirred for 30 min at room temperature. The pH of the solution was 5.8, and adjusted to 10 by adding 0.5 M NaOH. The oxidation was initiated by slowly adding NaClO 13% (9.8 mL, 17.1 mmol) over 30 min under gentle agitation. The pH was kept constant at 10, by the continuous addition of 0.5 M NaOH. The reaction was known to be complete when no additional reduction in pH was observed, which was determined to be approximately 4 hours. Once the reaction was complete, excess oxidant was quenched using methanol (10 mL) and the pH was adjusted to 7 using 0.5 M HCl. In order to purify the oxidized nanocrystals, the solution was dialyzed against distilled water using a dialysis tube (MW cut off: 12,000 Da) for at least 48 h [118].

4.2.3 Potentiometric Titration

Potentiometric titration was used to determine the composition of functional groups on the samples. From the titration curves, the carboxylic acid group densities of CNC, CNC-OX and CNC-CS_{OS} and amino group content of CS_{OS} and CNC-CS_{OS} were determined. A Metrohm 809 Titando autotitrator was used for simultaneous measurement of conductivity and pH. The titrator is equipped with a Tiamo software that doses μL of titrants. All measurements were performed in triplicate in a closed jacketed vessel at 25 °C while stirring at a medium rate. 50 mL of 0.1 wt% samples were prepared in 5 mM NaCl. The pH of the suspension was adjusted to ∼3 by adding 0.5 M HCl. The suspensions were titrated using 0.01 M NaOH under a nitrogen blanket and stirring. The conductivity and pH of the suspensions were measured simultaneously until the pH of the samples approached 11. Finally, the pH and conductivity values were plotted against the volume of NaOH (in mL), which were used to determine the composition of the functional groups [185].

4.2.4 Degree of Oxidation (DO)

The degree of oxidation (DO) is the number of primary hydroxyl groups that have been oxidized to carboxyl groups per anhydrous glucose unit (AGU) [164]. Using the information from the potentiometric titration curves, the DO of CNC-OX was calculated from Eq. 4.1 [124]:

$$\mathrm{DO} = \frac{162 \times (V_2 - V_1) \times c}{w - 36 \times (V_2 - V_1) \times c} \tag{4.1}$$

where, V_1 and V_2 are the amount of NaOH (in L), c is the NaOH concentration (mol/L), and w is the weight of the oven dried sample (g). Values of 162 and 36 correspond to

the molar mass of AGU and the weight difference between AGU and its sodium salt, respectively [126].

4.2.5 Grafting of Chitosan Oligosaccharide on CNC

Grafting of CS_{OS} onto CNC-OX was performed according to a method by Bulpitt and Aeschlimann [186] with some modification. Briefly, CNC-OX (0.2 g, 0.32 mmol COOH) was dissolved in 50 mL D.I. water. A 50 mL solution containing EDC (0.19 g, 1 mmol) and NHS (0.11 g, 1 mmol) was added to the CNC-OX suspension and stirred for 15 min. Another solution containing CS_{OS} (0.36 g, 1.3 mmol NH_2) was dissolved in 100 mL D.I. water and then added to the first solution resulting in a 200 mL reaction volume. MES buffer (1.95 g, 0.05 M) was added to the reaction medium and the pH was adjusted to 5 using 1 M NaOH or HCl. The reaction was stirred for 24 h at room temperature and purified using a dialysis tube (Mw cut off: 12,000 Da) against D.I. water for 4 days until the conductivity of the dialysis medium remained constant [164].

4.2.6 Degree of substitution (DS)

The degree of substitution of CS_{OS} on CNC-OX is defined as the number of amino groups grafted per 100 glucose units of CNC-OX and was determined by calculating the amounts of amino groups using potentiometric titration and considering the increased weight of CNC-CS_{OS} compared to the CNC-OX based on Eq. 4.2:

$$\mathrm{DS} = \frac{\text{Moles of COOH consumed}}{\text{Total moles of COOH}} \times \mathrm{DO} \times 100 \tag{4.2}$$

4.2.7 Fourier Transform Infrared (FT-IR) Spectroscopy

FT-IR spectra of the dried KBr pellets of CNC, CNC-OX, CS_{OS}, and CNC-CS_{OS} were obtained with a Bruker Tensor 27 spectrometer using a resolution of 4 cm^{-1} and acquiring 32 scans from 400 to 4000 cm^{-1}. In order to prevent the superposition of carbonyl band with the water peak, the samples were first acidified to pH=2 and then freeze dried [127]. KBr pellets were prepared by grinding approximately 2% of the samples in KBr and compressed into a pellet. In order to remove moisture, the pellets were dried in a vacuum oven prior to the measurements. The FT-IR spectra were monitored and analyzed using OPUS software.

4.2.8 Solid-state NMR

NMR experiments were performed with a Bruker Avance DSX 500 MHz spectrometer operating at 125.76 MHz for ^{13}C, using the combination of cross-polarization, high-power proton decoupling and magic angle spinning (CP/MAS) methods. The spinning speed was set at 4700 Hz for CNC and CNC-OX and 5600 Hz for CNC-CS_{OS}. The ^{1}H radio frequency field strength was set to give a 90° pulse duration at 4.5 s. The ^{13}C radio frequency field strength was obtained by matching the Hartman-Hahn conditions at 60 kHz. 15360, 10240 and 15000 transients were recorded for CNC, CNC-OX and CNC-CS_{OS}, respectively with a contact time of 2 ms and a recycle delay of 5 s. The acquisition time was set at 102 ms and the sweep width at 40000 Hz.

4.2.9 Thermogravimetric Analysis (TGA)

Thermogravimetric analyses were performed using a TGA Q500 of TA Instruments (Lukens Drive, Delaware, USA). TGA balance was calibrated and the freeze-dried samples were analyzed in platinum pans under dry nitrogen purge at a flow rate of 50 mL/min from ambient temperature to 800 °C at 10 °C/min. The experimental conditions for data acquisition and analysis were performed using the Universal Analysis 2000 V4.5A software (TA Instruments).

4.2.10 Zeta Potential Measurements

Zeta Potential measurements for samples at different pH values were measured using the ZetaPALS Analyzer (Brookhaven Instruments Corp., USA). The concentration of the samples was maintained at ∼0.1 wt% and the experiments were conducted at 25 °C. The reported values are an average of 5 measurements.

4.2.11 Transmission Electron Microscopy (TEM)

TEM images of CNC, CNC-OX and CNC-CS were recorded using a Philips CM10 TEM with 60 keV acceleration voltages. Approximately 10 μL of 0.01 wt% aqueous suspensions of the samples were deposited on a carbon-formvar film on 200 mesh copper grids. In order to minimize possible agglomeration of the particles, excess solvent was removed from the grids placed on top of a filter paper. Then the grids were allowed to dry overnight.

In order to increase the contrast of the image and improve the resolution, the grids were subsequently negatively stained with a 2% uranyl acetate solution.

4.2.12 Atomic Force Microscopy (AFM)

The surfaces of CNC, CNC-OX and CNC-CS_{OS} were investigated using a Bruker Dimension Icon AFM in air. To prepare the AFM samples, 20 μL of samples with a concentration of 0.1 mg/mL and an acidic pH (pH=4) was injected onto a freshly cleaved mica surface and incubated for 5 min to allow the particles to adhere to the surface. It was then washed 3 times with D.I. water. The extra moisture on the surface was removed using a tissue paper. The sample plate was then covered with Petri dish to avoid possible contamination and left to dry overnight. PeakForce QNM (Quantitative Nanomechanical Property Mapping) mode was used to scan the sample with a silicon tip on nitride lever (ScanAsyst-Air, Bruker) with a radius of 2 nm. The scan rate was set to 0.9 Hz.

4.2.13 Light Scattering

The microstructures of the samples were examined by a Brookhaven Laser Light Scattering system. The system has a BI200SMv2 goniometer, BI-9000AT digital correlator. A 636 nm vertically polarized helium-neon diode laser was used as the light source. For dynamic light scattering (DLS), the temporal intensity fluctuations for the samples were measured at 60°, 75°, 90°, 105°, 120°, 135°, and 150°. The data from the detector was transferred to the GENDIST (General Distribution) software package to perform the inverse Laplace transform technique to obtain the distribution of decay times, τ. GENDIST uses the regularized positive exponential sum (REPES) algorithm. The probability of reject was set to 0.5. This decay rate Γ $(1/\tau)$ is related to the translational diffusion coefficient D and the wave factor (vector), q according to Γ=Dq^2, where q =$(4\pi n/\lambda)\sin(\theta/2)$. Using the Stokes-Einstein equation, the hydrodynamic radius (R_h) was calculated.

For static light scattering (SLS), the time-averaged intensity of scattered light from CNC-CS_{OS} was measured at different scattering angles ranging from 60° to 110° in 5° intervals. The radius of gyration (R_g) can be determined by plotting I(q) versus q^2 using Berry plot.

4.3 Results and Discussion

4.3.1 TEMPO Mediated Oxidation of CNC

After 1 h of performing the TEMPO mediated oxidation of CNC to CNC-OX with the structure of $\beta - 1,4-$linked polyglucuronic acid sodium salt (cellouronic acid Na salt), the solution became clear. The cellulose molecules are packed in a crystalline unit cell in a manner where only half of the primary hydroxyl groups (hydroxymethyl) are extended out of the crystalline structure, which are then accessible for oxidation [125]. This is because some cellulose nanocrystals form aggregates due to defects such as twists, kinks and chain ends. The regioselective oxidation of hydroxyl groups on the surface of CNC to carboxylic acid is due to half of the cellulose chains on the surface being buried inside the crystalline domains of the nanocrystals whereas the other half on the exterior of the aggregates are available for oxidation. The 1-oxopiperidinium ions on the surface of CNC are accessible for oxidation [125]. The introduction of carboxylic acid groups on the surface of CNC without changing its crystalline structure provides a unique platform for further modification on CNC. By further manipulating these functional groups, one can create various novel compounds. The conversion of primary hydroxyl groups to carboxylic acids is known to be pH dependent. The pH of the reaction medium also affects the oxidation time, and a pH of 10 was shown to result in the shortest oxidation time [126]. At acidic pH values the secondary hydroxyl group might be oxidized [122] whereas, at pH values higher than 10, the cellulose could be degraded by β-elimination that decreases the molecular weight of the resulting cellulose fibers [127].

4.3.2 Potentiometric Titration

4.3.2.1 Determination of Carboxylic Acid Group Density

The density of the COOH moiety on CNC and CNC-OX was determined by potentiometric titration measurements and the titration curves are shown in Figure 4.1a and b, respectively. The suspensions were first treated with an excess of HCl to replace the sodium counter ions with protons. The acidified suspensions were then titrated with 0.01 M NaOH [164]. The titration curve for CNC-OX displays three regions, namely (i) excess HCl, (ii) carboxylic acid on the CNC-OX, and (iii) excess NaOH. The area between the two equivalent lines corresponds to the neutralization of the weak acid (COOH). However, according to Figure 4.1a, for CNC there was no weak acid detected and only strong acid and strong base were present. Based on Figure 4.1b, the COOH content of CNC-OX was determined

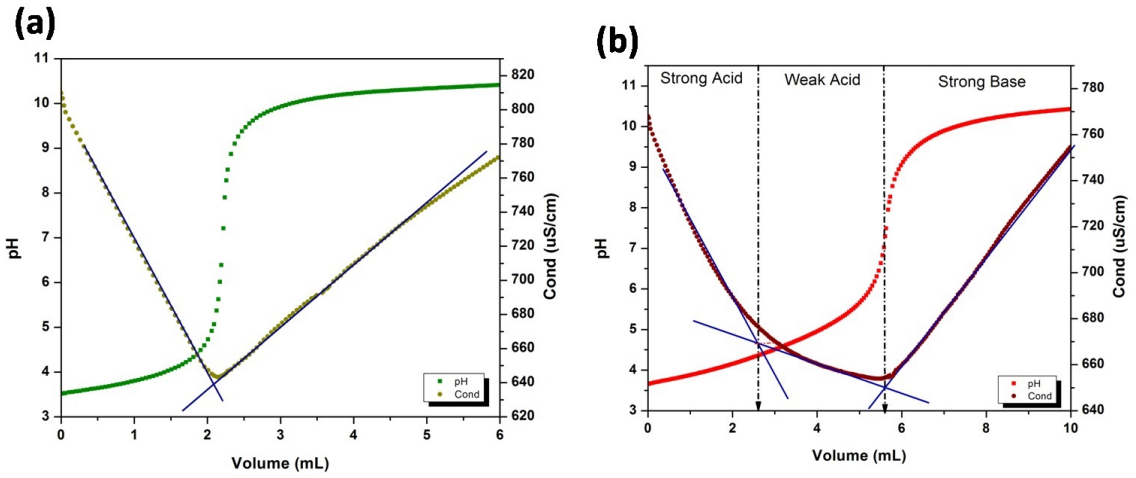

Figure 4.1: pH and conductivity titration curves of 0.1 wt% (a) CNC and (b) CNC-OX.

to be 1.63 mmoles of COOH/g of sample, determined from three consecutive measurements yielding an average value.

4.3.2.2 Degree of Oxidation (DO)

The degree of oxidation for CNC-OX was calculated to be 0.28. The calculated DO was reproducible and was in agreement with the results published in the literature [164]. The DO depends on the molar ratio of NaClO to AGU, and the optimum value depends on crystal size and the corresponding primary hydroxyl groups accessible to the reactants [125].

4.3.2.3 Determining Amino Group Density

Potentiometric titration was used to determine the moles of amino group on CS_{OS} that reacted with CNC-OX. As shown in Figure 4.2, the titration curve for CS_{OS} displayed three regions. The neutralization of excess HCl along with the lower mobility and molar conductivity of Na^+ with respect to H^+ resulted in the initial linear decrease in the conductivity. At the first equivalence point the rate of reduction in the conductivity decreased. The amines of CS_{OS} were deprotonated between the two equivalence points. With further addition of NaOH, the second equivalence point signaled the onset of excess amounts of

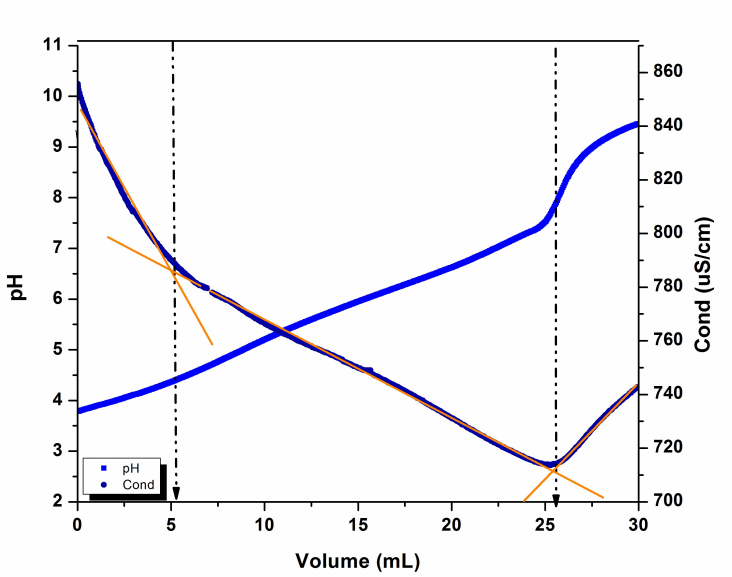

Figure 4.2: pH and conductivity titration curve of 0.1 wt% CS_{OS}.

Na^+ and OH^- titrated to the solution. The amino groups of CS_{OS} were calculated to be 3.62 mmoles of NH_2/g of CS_{OS} based on Figure 4.2, and the 100% acetylated chitin possesses 5 mmol/g of nitrogen [75]. Since the degree of deacetylation of our CS_{OS} was around 75%, the density of primary amine groups calculated is reasonable.

4.3.3 Grafting of Chitosan Oligosaccharide on CNC

CNC-CS_{OS} was synthesized via the carbodiimide coupling reaction also known as peptidic coupling reaction (Figure 4.3). This reaction involves the formation of an amide bond between amino groups of CS_{OS} and carboxyl groups on CNC-OX in the presence of EDC (1-ethyl-3-(3-dimethylaminopropyl) carbodiimide) an effective amidation reagent and NHS (N-hydroxysuccinimide), an esterification reagent in MES (2-(N-morpholino)ethanesulfonic acid) buffer. EDC is a water-soluble carbodiimide and forms amide bonds without a spacer molecule, hence it is known as a "zero-length" crosslinker [187]. EDC reacts with the carboxyl groups of CNC-OX forming an amine-reactive ester (O-acylisourea) intermediate. This active ester may further form an amide bond by reacting with primary amino group on CS_{OS}. However, this intermediate is susceptible to hydrolysis and thus, has a short lifetime in aqueous solutions. The addition of NHS stabilizes the amine-reactive intermediate by converting it into an amine-reactive NHS-ester. This increases the efficiency

of the EDC mediated coupling reaction. The purification of the sample was performed by dialysis against water, where unreacted CS_{OS}, EDC and by-product (isourea) were removed. Different parameters such as, reaction medium, reaction time, pH and molar ratios between reagents and crosslinker could be changed, resulting in variations of grafting behaviors [187]. In order to minimize the hydrolysis of EDC, crosslinking was conducted in 0.05 M MES buffer at pH 5. The choice of pH is important when using EDC as it affects the coupling efficiency of EDC to COOH groups. However, if the objective is to have well-dispersed particles and fully solubilized reagents, the pH should be chosen to satisfy these conditions. The commonly reported optimal pH range for EDC is 4-6 [188]. In our approach, we adjusted the pH to 5, where EDC is not only at its optimal pH range but also CS_{OS} is fully soluble. Different ratios of COOH, NH_2, EDC and NHS have been reported in the literature. In this study, the ratios used were as follows: (COOH, 1 mmol):(NH_2, 4 mmol):(EDC, 3 mmol):(NHS, 3 mmol). The reason for choosing a 4:1 molar ratio of NH_2 on CS_{OS} COOH on CNC-OX was to ensure that all the possible carboxyl groups had sufficient amino groups for the grafting reaction [164], and the unreacted CS_{OS} could be removed by dialysis. The choice of a 1:1 molar ratio of EDC to NHS was based on the work of Sam and co-workers who found that the optimum coupling reaction was obtained with [EDC]=[NHS]=5 mM [189].

4.3.4 Determination of Amino Group Density

The amino groups on CNC-CS_{OS} were calculated to be 1.60 mmoles of NH_2/g of CNC-CS_{OS} based on the analysis of Figure 4.4. By comparing the amino groups on CS_{OS} (3.62 mmol/g), it could be concluded that 44.2% of amino groups on CS_{OS} have either reacted with the COOH groups on CNC-OX or have been removed during dialysis. Due to the similarities and overlap in the titration regions of COOH and NH_2, unreacted COOH was not detectable. However, based on the stoichiometric reaction of COOH and NH_2, the amount of COOH moieties substituted with CS_{OS} can be calculated based on the consumption of NH_2. The amounts of COOH consumed during the surface modification were determined from the differences between the experimentally determined moles of NH_2 in CS_{OS} added and CNC-CS_{OS} recovered.

4.3.5 Degree of Substitution (DS)

The reaction between COOH groups of CNC-OX and NH_2 of CS_{OS} was confirmed by comparing the values of DS and DO. In the preparation of CNC-CS_{OS}, we added 0.20 g

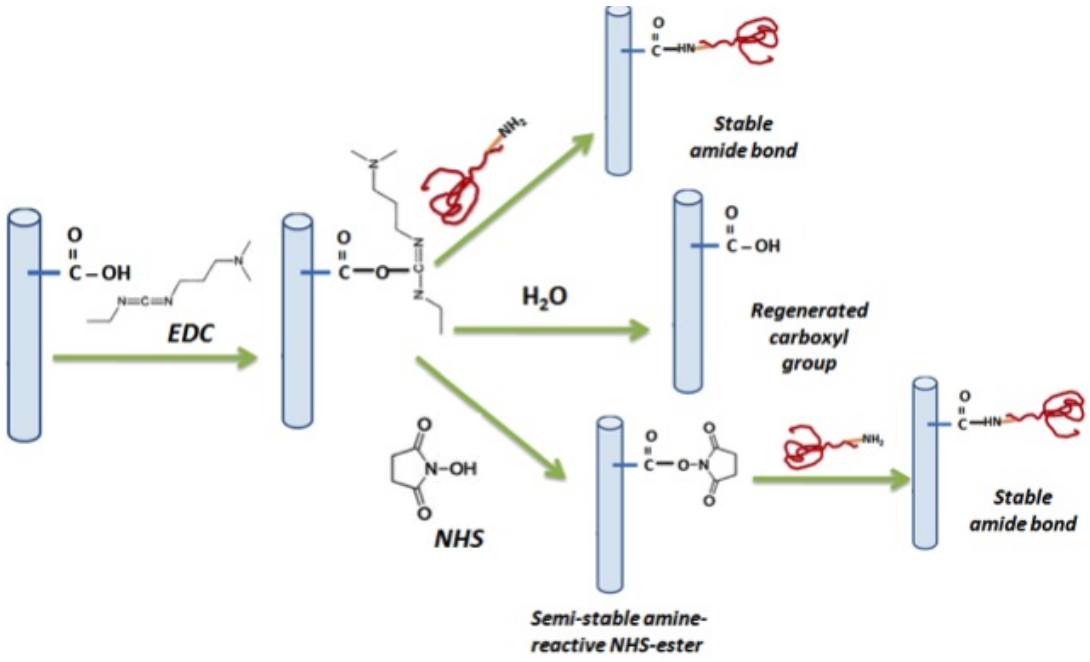

Figure 4.3: Mechanism of carbodiimide coupling reaction.

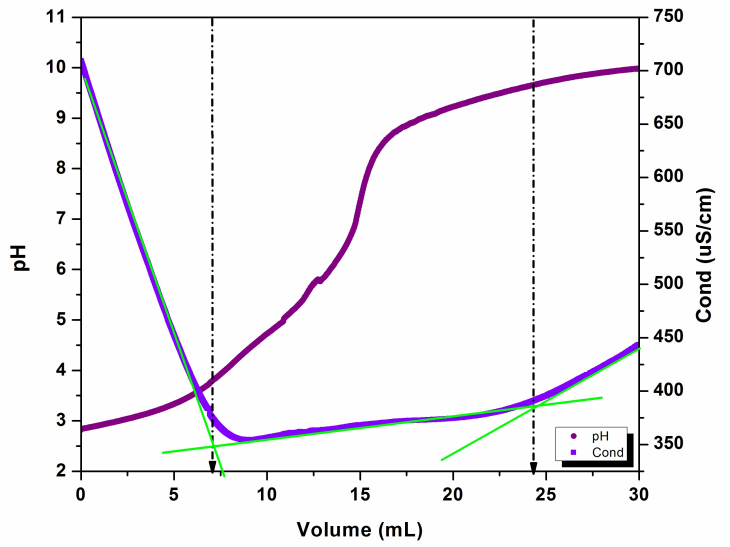

Figure 4.4: pH and conductivity titration curve of 0.1 wt% CNC-CS_{OS}.

(0.32 mmoles of COOH) of CNC-OX and 0.36 g (1.29 mmoles of NH_2) of CS_{OS}. After the reaction and dialysis, 0.51 g solid was recovered. We calculated the amino groups on CNC-CS_{OS} to be 1.60 mmoles of NH_2/g (0.81 mmoles of NH_2). By subtracting the detected NH_2 from the primary amine groups added to the reaction medium, we concluded that 0.48 mmoles of NH_2 have either reacted with COOH or been removed during dialysis. Based on the weight loss after dialysis, we assumed that 0.05 g (0.18 mmoles of NH_2) of CS_{OS} was removed, thus 0.30 mmoles of NH_2 and COOH have reacted. Hence, 0.02 mmoles of COOH remained, which is equal to a DO of 1.75. Thus, the degree of substitution was calculated to be 0.26. Similar degrees of substitution have been reported in the literature [190]. Since the DO was determined to be 0.28, we concluded that most of the COOHs on CNC-OX have been substituted by CS_{OS} via the formation of amide bonds. The DO of 0.28 means that 28% of the hydroxyl methyl groups on CNC have been oxidized to the corresponding carboxylic acid groups and are thus susceptible for subsequent grafting reactions. Therefore, the maximum grafting density corresponds to the condition where approximately one out of every three and a half anhydroglucose units in CNC contained a grafted CS_{OS} segment. Since the molar ratio of NH_2 in CS_{OS} was 4 times greater than COOH on CNC-OX, this result was not unexpected and similar results have been reported previously [191]. Also, small hydrophilic amino groups (CS_{OS}) are known to display higher degrees of substitution due to a lower steric hindrance [127]. It should be noted that the measurement of degree of substitution by conductometry, which is based on the reduction in the number of amino groups after reacting with carboxyl groups is an indirect proof of grafting [164]. Therefore, to further confirm the covalent nature of the grafting, FT-IR spectroscopy was used.

4.3.6 Fourier Transform Infrared (FT-IR) Spectroscopy

The FT-IR spectra of CNC, CNC-OX, CS_{OS} and CNC-CS_{OS} are shown in Figure 4.5. In the spectrum of CNC (Figure 4.5 curve a), the broad band between 3600 and 3000 cm^{-1} is attributed to O-H stretching vibration [170]. The stretching vibrations of aliphatic C-H and bending vibrations of CH_2 are related to the bands between 3000 and 2800 cm^{-1} and 1500 and 1250 cm^{-1}, respectively. The peaks at 1160 cm^{-1} and 1070 cm^{-1} are attributed to the saccharide structure [182]. The bands in the finger-print region are due to the C-O bonds in the glucose ring and the asymmetrical C-O-C stretching vibration that yielded a sharp and steep band at 1070 cm^{-1} [184]. Finally, the O-H out-of-plane vibrations appeared between 800 and 450 cm^{-1}. The spectrum of CNC-OX (Figure 4.5 curve b) is similar to CNC. When the hydroxyl group on C6 was selectively oxidized to carboxyl group, some changes occurred in the FT-IR spectrum. Most importantly, a strong C=O

band appeared at 1730 cm^{-1} which is characteristic of the carboxyl group in their acid form. The appearance of this peak validated the oxidation process [164], which is shown by the dash line in Figure 4.5. Due to the similarities in the chemical structures of cellulose and chitosan, the FT-IR spectra of CNC and CS_{OS} are similar, which was previously reported in the literature [182]. CS_{OS} FT-IR spectrum (Figure 4.5 curve c) shows a broad band between 3450 and 3200 cm^{-1}, which is due to O-H and N-H stretching vibrations. The C-H stretching peaks were observed between 3000 and 2800 cm^{-1}, and the spectrum showed some additional peaks between 1700 and 1500 cm^{-1}. In CS_{OS} FT-IR spectrum the C=O stretching vibrations of the acetyl groups (amide I bands) appeared around 1640 cm^{-1}. Peaks at 1506 and 1616 cm^{-1} represent NH_3^+. However in our results, these peaks were not clearly observed and they were overwhelmed by stronger peaks from the amide-I and amide-II at 1620 and 1510 cm^{-1}, respectively. Similar to CNC, the C-O stretching vibrations of the saccharide ring were observed at 1070 and 1030 cm^{-1}. The CH_3 and the CH_2 groups of the N-acetylglucosamine residue can be observed at 1375 and 1450 cm^{-1}, respectively. The spectrum of CNC-CS_{OS} is shown in Figure 4.5, curve d. As expected, the spectrum is identical to those of CNC and CS_{OS} and shows characteristic bands of both materials. However, some changes were apparent in the grafted compound as indicated by the arrow. In the grafted compound, the peak corresponding to C=O group at 1730 cm^{-1} has significantly reduced in comparison with CNC-OX which reveals the consumption of most of the carboxyl groups in the reaction with amines. Due to the formation of new amide bonds, the C=O group shifted to lower frequencies and were buried under the water peak. It should be noted that since some C=O groups are found on the acetyl groups of CS_{OS} chains, this peak was not significantly reduced. The saccharide, C-H stretching bands and N-H bending bands were evident, where the bands observed at 1647, 1555 and 1375 cm^{-1} corresponds to the amide-I, amide-II and amide-III, respectively. The peak around 1650 cm^{-1} can be attributed to either residual water or amide-I absorption, thus the amide-I peak overlapped with the water absorption peak. However, when this peak was compared to CNC-OX, it displayed a significant increase that can be partly related to the formation of amide bond. Moreover, the small new peak shown by the arrow at 1555 cm^{-1} represents the N-H stretching of amide-II [164]. The N-H bending vibration of the amide group in CNC-CS_{OS} resulted in a weak peak on the right of the carbonyl group of around 1640-1150 cm^{-1}. The new peaks shown by the arrow observed at 1231 and 1465 cm^{-1} could be related to this peak. The displacement of this peak to lower frequencies indicated the successful grafting of CS_{OS} onto CNC. It is important to note that the characteristic bonds of CS_{OS} are amide bands I and II that appeared at 1620 cm^{-1} and 1510 cm^{-1}, respectively. After the formation of amide bonds, the new amide bands shifted to higher frequencies [50]. Therefore, the new peak observed at 1696 cm^{-1} is an indicator of the new amide bonds. Despite the fact that NH_3^+ cannot be clearly observed in CNC-CS_{OS} due to

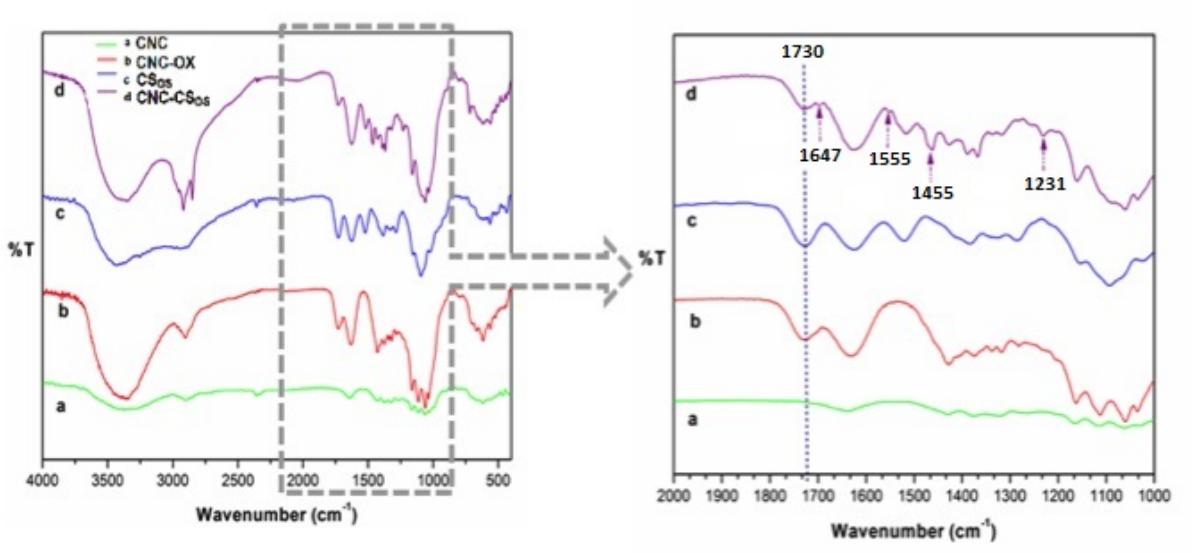

Figure 4.5: FT-IR spectra of (a) CNC, (b) CNC-OX, (c) CS_{OS}, and (d) CNC-CS_{OS}.

overlapping with amide peaks, the reduction in the peak at 1510 cm^{-1} compared with CS_{OS} was related to the decrease in NH_3^+ on CNC-CS_{OS}, which suggested that most of the NH_2 groups underwent amidation reaction with CNC-OX. Apart from the formation of amide bonds between CNC-OX and CS_{OS}, other interactions can also occur. The broad band between 3600 and 3250 cm^{-1} is due to the overlapping N-H and O-H stretching vibrations. Compared to the starting materials, this broad band was slightly shifted to the left due the hydrogen bonding between amino groups of CS_{OS} and hydroxyl and carboxyl groups of CNC-OX and ionic interactions between the sulfate groups on CNC-OX and the NH_3^+ groups on CS_{OS}. Moreover, because of the interactions between CS_{OS} segments, the O-H band in CS_{OS} spectrum is broader than the O-H band in CNC-CS_{OS} due the interactions between CNC and CS_{OS}, such as hydrogen bonding and amide formation [54].

4.3.7 Solid-state NMR

The ^{13}C NMR spectra of CNC and oxidized CNC have been previously reported in the literature and the signals have been assigned [164]. ^{13}C NMR spectra of samples are shown in Figure 4.6. The NMR spectrum of CNC-OX displays a small peak at 175 ppm, which is due to the carbonyl group of the carboxylic acids. The significant reduction of the carbonyl

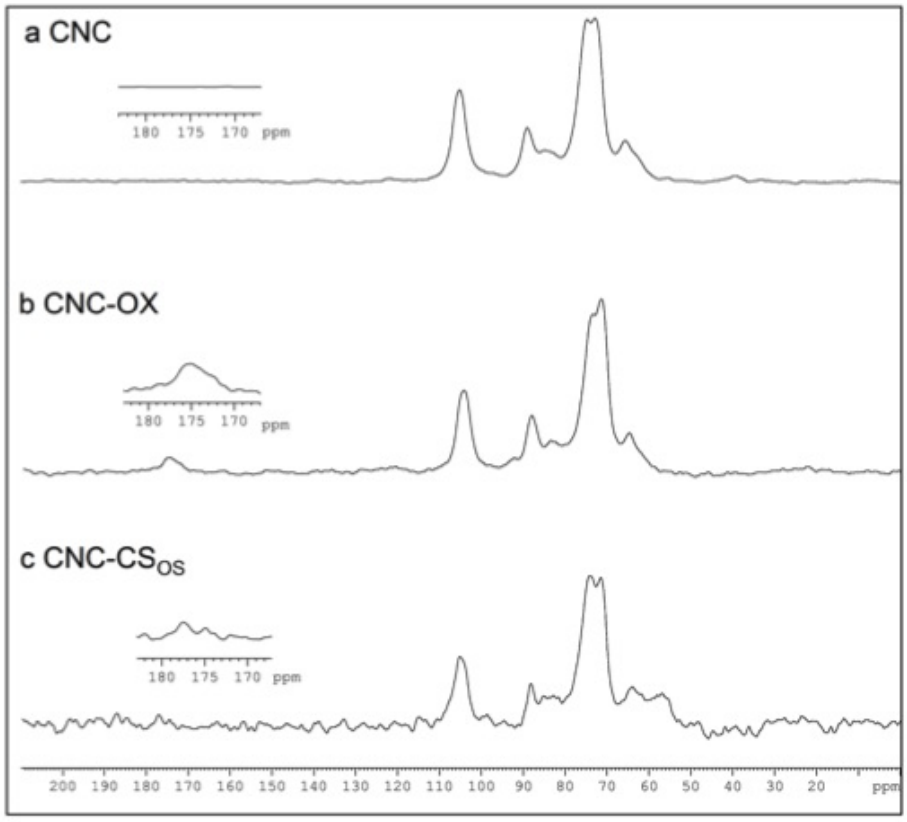

Figure 4.6: ^{13}C solid-state NMR spectra of (a) CNC, (b) CNC-OX, and (c) CNC-CS_{OS}.

peak in the spectra of CNC-CS_{OS} proves the grafting of CS_{OS} on CNC-OX and formation of amide bonds and is consistent with other techniques.

4.3.8 Thermogravimetric Analysis (TGA)

The thermal decomposition and thermal stability of CNC, CNC-OX, CS_{OS} and CNC-CS_{OS} were investigated using the TGA. TGA analysis of the starting materials and modified CNCs showed significant changes in the thermal profiles. Figure 4.7a and b show the thermogravimetric curves of the samples. All samples displayed a three-stage weight loss. The small weight loss at the low temperature range is due to the evaporation of absorbed water, whereas the two other weight losses are due to pyrolysis of hydrocarbon chains [192]. The

dehydration and depolymerization of the samples produced the first dominant transition of the flammable and volatile degradation products. The oxidation of charred residues yielded the second transition [193, 194]. In CNC-OX the main decomposition temperatures were shifted to lower temperatures due to the decarbonation of anhydroglucoronic acid groups. As shown in Figure 4.7, the pyrolysis of CNC displayed a two-step degradation, which can be attributed to trace amounts of sulfuric acid in the CNC causing a reduction in the degradation temperature of CNC. The first stage corresponds to the primary pyrolysis of CNC catalyzed by sulfate groups, and the second stage is related to the slow charring process of the solid residue. It is reported that during char decomposition of celluloses, the char residue ignites and undergoes a self-sustained exothermic process termed the region of glowing combustion. This two step pyrolysis of CNC is similar to the thermal decomposition of spherical cellulose nanocrystals with sulfate groups [194]. Sulfuric acid is a dehydration catalyst and facilitates the formation of char. Comparison of the residual mass of the samples revealed that the pyrolysis of CNC leads to the highest amount of residual mass (19.87 wt%) which is mainly due to the formation of levoglucosan [195]. However, the pyrolysis of CNC-CS_{OS} produced the minimum amount of residual mass with 7.9 wt% char residue at 800 $^{\circ}C$. The initial decomposition temperature (IDT) and decomposition temperature at 50% weight loss (T50) are indicatives of thermal stability. CNC-CS_{OS} possessed a higher thermal stability than its precursors CNC-OX and CS_{OS}. It decomposed at a higher temperature that can be attributed to the formation of new covalent bonds in this material. Due to the similarities in the structure of CNC-OX and CS_{OS}, the decomposition temperature of these biopolymers were fairly similar, 300.4 $^{\circ}C$ and 278.2 $^{\circ}C$, respectively. Therefore, it is difficult to measure the amount of grafting via TGA analyses. However, the fact that the first thermal degradation of CS_{OS} was not present in CNC-CS_{OS} together with the difference in the thermal behavior of these compounds, confirmed the successful grafting of CS_{OS} onto CNC. The high melting temperature of CNC benefits the thermal transition properties of covalently attached polymers on them and increases the overall thermal stability of their composites [64]. However, in a physical blend of CS_{OS} and cellulose, Kim and coworkers reported a reduction in the decomposition temperature with increasing CS_{OS} content. They concluded that blending CNC with CS_{OS} weakens the intra-and intermolecular bonds and causes them to decompose more easily [170].

4.3.9 Zeta Potential Measurements

The zeta potential values of the four samples at different pHs are shown in Figure 4.8, where CNC and CNC-OX displayed identical trends. Also, CS_{OS} and CNC-CS_{OS} showed a similar trend with slightly different zeta potential values. Figure 4.8 shows that at all

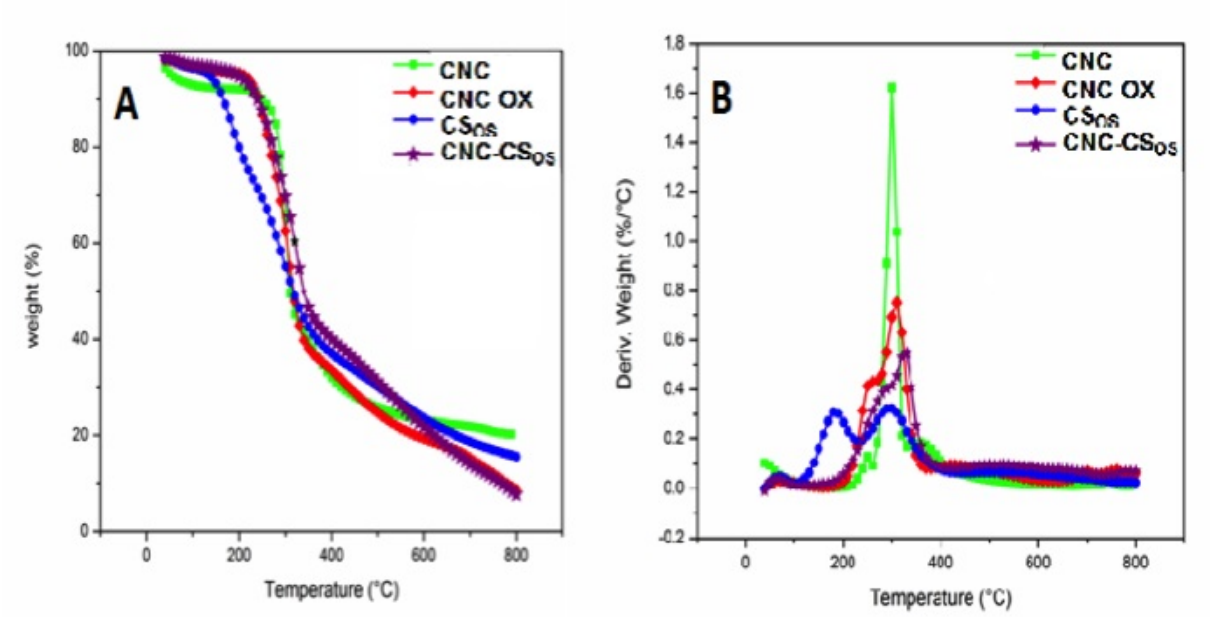

Figure 4.7: (a) Thermogravimetric and (b) differential gravimetric curves of samples.

pH values, CNC and CNC-OX possessed a large negative charge. In acidic pH values, the negative charge on both samples is due to the presence of the sulfate ester groups (OSO_3^-) after sulfuric acid hydrolysis. The zeta potential of a stable suspension of CNC was reported to be equal or larger than -27 mV [182]. By increasing the pH, the ionization of acid groups increases the net value of the zeta potential resulting in more negative charges. Due to the presence of more carboxylic acid groups on the surface of CNC-OX, the net surface charge of CNC-OX was more negative. Azzam and coworkers reported a reduction in the net surface charge of CNC after TEMPO oxidation, and they attributed this to the hydrolysis of sulfate ester groups at basic conditions during the reaction. At high pH values, the negatively charged OSO_3^- groups are hydrolyzed, leading to a smaller zeta potential [164]. This phenomenon was more evident for CNC-OX leading to a less negative zeta potential compared to CNC at high pH.

The successful grafting of CS_{OS} on CNC can also be verified by zeta potential measurements. The variation in the zeta potential of CNC-CS_{OS} at different pH values showed a similar trend to CS_{OS} (Figure 4.8). However, CNC-CS_{OS} exhibited larger zeta potential values at lower pH values due the more extended chain conformation of CS_{OS} when they were grafted onto CNC. The zeta potential of CNC-CS_{OS} was positive at pH$<$6, almost zero at pH$\sim$6 and negative at pH$>$6. The positive charge at acidic medium is due to the

protonation of amino groups on CS_{OS}. In strong acidic medium, CNC-CS_{OS} possessed a smaller positive charge compared to moderate acidic medium. This is because in strong acidic medium (pH=2.1), the high density of the positive charge on CS_{OS} shielded the negative charge of sulfate ester groups on CNC. However, when the pH was increased, the amounts of positive charges decreased, and the corresponding lower charge shielding resulted in a higher net charge. At around neutral pH (pH$\sim$6), the total charge is almost zero due to the neutralization of NH_3^+ on CS_{OS} with COO^- and OSO_3^- groups, yielding the isoelectric point. At pH above 6, the negative charge is due to the remaining COO^- and OSO_3^- groups on CNC. The zeta potential of almost zero at neutral pH on CNC-CS_{OS} can be an indirect proof of successful grafting of CS_{OS} on CNC and the formation of amide bonds. The zeta potential of CS_{OS} and CNC-OX at the neutral pH is +20 and -70 mV, respectively. If CS_{OS} and CNC-OX were physically mixed together, the zeta potential of their mixture would have been somewhere around -50 mV. However, at this pH the zeta potential of CNC-CS_{OS} is almost zero. This dramatic increase in the zeta potential is due to the depletion of COOH groups on CNC-OX as a result of the reaction with the NH_2 groups on CS_{OS} [57].

4.3.10 TEM Analyses

The TEM images of CNC and CNC-OX on the individual nanocrystals and some aggregates are shown in Figure 4.9a and b, respectively. The aggregates are formed because of the high aspect ratio of nano-whiskers and strong hydrogen bonding between them. It is important to note that these aggregates can form during the drying process when the solvent was removed [182]. During the sample preparation, the evaporation of water can intensify the agglomeration of nanocrystals inducing more nanocrystals to agglomerate [196]. As shown in Figure 4.9, the oxidation of CNC to CNC-OX did not alter their morphology. However, because of electrostatic repulsion induced by increased negative charge on the surface of CNC-OX, they tended to be more dispersed and displayed less aggregates [125]. TEM micrographs of CNC-CS_{OS} are shown in Figure 4.9c. As expected, larger particles for CNC-CS_{OS} were observed compared to CNC or the precursor CNC-OX. CNC-CS_{OS} particles showed loose crosslinked structures. This could either be due to CS_{OS} chains forming amide bonds with CNC-OX resulting in the crosslinking of several CNC particles or the alignment of particles due to the drying process. The grafted CS_{OS} polymer chains were not visible in TEM micrographs due to their relatively low surface density, which could not generate a detectable contrast [164]. For TEM studies, at least 3 samples were examined and more than 15 TEM images were obtained confirming the reproducibility of the images.

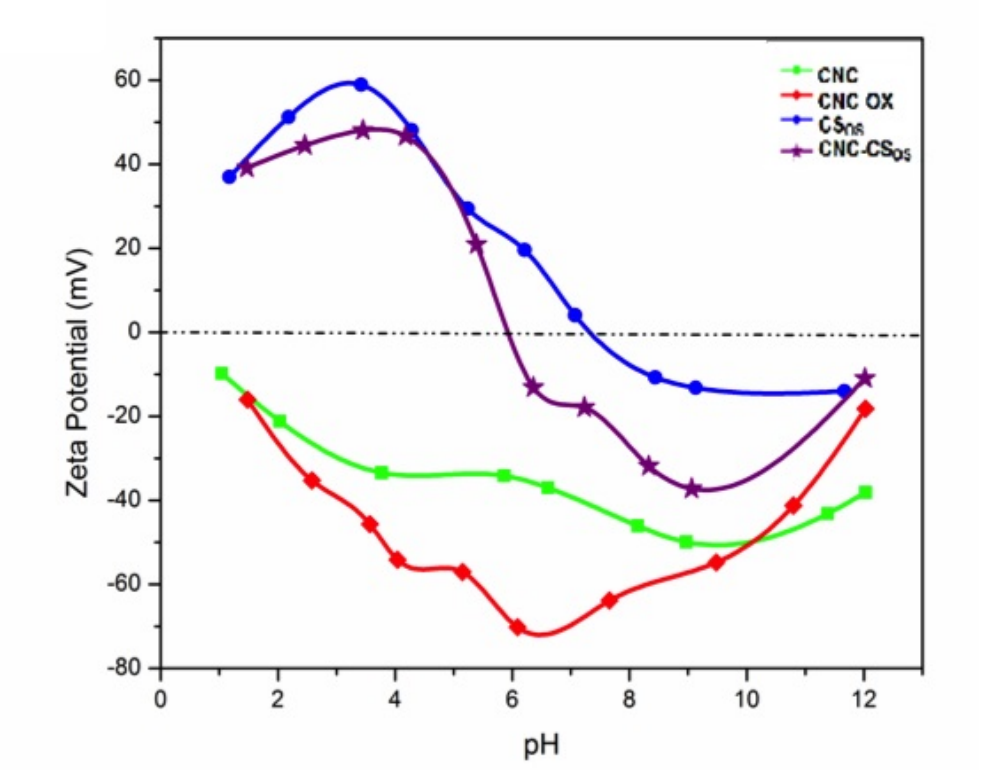

Figure 4.8: Zeta potential versus pH for 0.1 wt% samples.

4.3.11 AFM Analyses

The samples used for AFM imaging were produced by placing 20 μL of samples with a concentration of 0.1 mg/mL onto freshly cleaved mica surface and incubated for 5 min to allow the particles to adhere to the surface. It was then washed 3 times with D.I. water. The extra moisture on the surface was removed with a tissue paper. This method resulted in well-dispersed particles that strongly adhered to the mica substrate. The rinsing was implemented for two reasons: first, to lower the concentration of samples on the mica surface; second, to ensure that the remaining particles would be the ones that adhered to the mica surface [98]. As seen in Figure 4.10a and b, CNC and CNC-OX possessed rod-like structures and oxidation did not alter the morphology of the particles. In the drying process, the extra intermolecular hydrogen bonding between crystallites may lead to irreversible aggregation, which may also be responsible for the change in the shape of the particles [197]. Figure 4.10c shows the AFM image of CNC-CS_{OS}. As can be

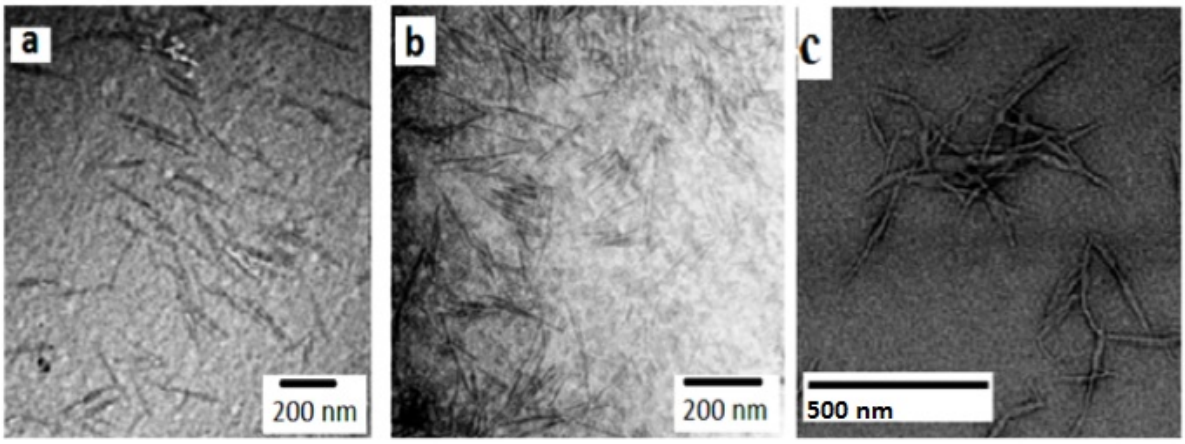

Figure 4.9: TEM images of 0.01 wt% (a) CNC, (b) CNC-OX, and (c) CNC-CS_{OS}.

seen, small network structures were formed due to the grafting of CS_{OS}. Mica is a layered aluminosilicate mineral, and each layer has a strong negative charge due to the isomorphous substitution of silicon by aluminum [198]. CNC-CS_{OS} sample had a pH of 4 and therefore possessed positive charges, therefore at this pH there was attractive interactions between CS_{OS} and mica that enhanced the adsorption of the particles onto mica and prevented the rinsing of the particles [7].

4.3.12 Light Scattering

Hydrodynamic Radii of CNC, CNC-OX and CNC-CS_{OS} were measured as 43.8, 42.6 and 78.6 nm, respectively. Based on the SLS studies, the R_g of CNC-CS_{OS} was calculated as 120 nm. Therefore, R_g/R_h is 1.52, which indicates a Gaussian chain morphology. Based on R_g/R_h value, TEM and AFM images, we believe that the alignment of the chitosan chains on the surface of CNC is random with some chains orienting on the surface of the crystals and some sticking out crosslinking some CNC.

4.4 Conclusions

A new chemical modification procedure to produce chemically grafted CS_{OS} on CNC was developed. In the first step, primary hydroxyl groups on the surface of CNC were selectively

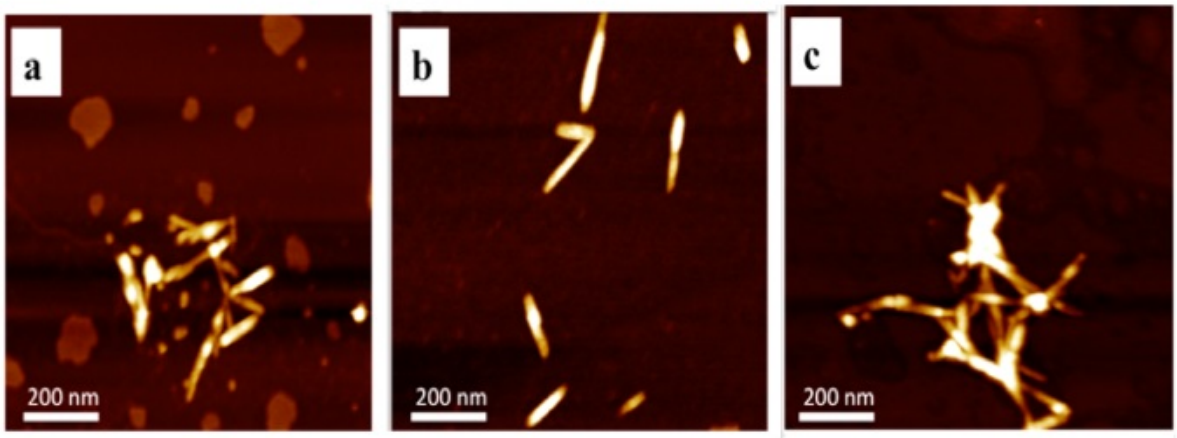

Figure 4.10: AFM images of 0.01 wt% (Scale: 1μm $\times$ 1μm) of (a) CNC, (b) CNC-OX, and (c) CNC-CS_{OS}.

oxidized to carboxylic acid groups using TEMPO-mediated oxidation. The amino groups of CS_{OS} were then reacted with carboxylic acid groups on oxidized CNC via carbodiimide reaction. The appearance of C=O peak in FT-IR spectrum accompanied with calculations based on potentiometric titration revealed that CNC was successfully oxidized with a degree of oxidation (DO) of 0.28. The grafting of CS_{OS} on oxidized CNC was confirmed by (i) the reduction of C=O bond in FT-IR of CNC-CS_{OS} and appearance of new amide peaks, (ii) higher decomposition temperature in TGA of CNC-CS_{OS}, (iii) positive zeta potential of CNC-CS_{OS} at acidic pH (iv) degree of substitution of 0.26 that is close to the DO (0.28) indicating that most COOH on CNC-OX groups were involved in formation of amide bond with CS_{OS}. TEM and AFM studies revealed a completely different morphology of CNC and CNC-OX with CNC-CS_{OS}.

Chapter 5

Comparative Release Studies of Two Cationic Model Drugs from Different Cellulose Nanocrystal Derivatives *

Native CNC, oxidized CNC (CNC-OX) and chitosan oligosaccharide grafted CNC (CNC-CS_{OS}) were evaluated as potential drug delivery carriers for two model drug compounds, procaine hydrochloride (PrHy) and imipramine hydrochloride (IMI). The loading of PrHy and IMI was performed at pH 8 and 7, respectively. IMI displayed higher binding to CNC derivatives than PrHy. Drug selective membranes were prepared for each model drug and a drug selective electrode system was used to measure the drug concentration in the filtrate and release medium. Isothermal titration calorimetry (ITC) was used to elucidate the types of interactions between model drugs and CNC and its derivatives. The complexation between model drugs and CNC derivatives was further studied by zeta potential and transmittance measurements. The binding and release of these drugs correlated with the nature and types of interactions that exist between the CNC and drug molecules.

5.1 Introduction

Polymers have been widely used in the pharmaceutical industry. Examples are in rubber closures, plastic tubing for injection and polyvinylchloride bags for intravenous solutions.

*This chapter is adapted from a paper "S.P. Akhlaghi, D. Tiong, R. Berry, and K.C. Tam, Comparative Release Studies of Two Cationic Model Drugs from Cellulose Nanocrystal Derivatives, *European Journal of Pharmaceutics and Biopharmaceutics, In Press.*"

In recent years, they are being used for the design and development of novel pharmaceutical carriers that allow the slow or fast release of drugs. Polysaccharides are natural carbohydrate polymers that possess many advantages such as, abundance, low cost, sustainability, biocompatibility, biodegradability, non-toxicity and surface functionalities making them excellent candidates as drug carriers. Cellulose and its derivatives are often used as emulsifiers, thickeners, and tablet binders. These derivatives can modify the drug release by film formation, water retention, adhesion enhancement and control of rheology [63]. Effective delivery and release of drugs, enzymes and proteins at their target site can be achieved by nanoparticle delivery systems. Cellulose nanocrystals (CNC) are obtained by the removal of the amorphous regions in cellulose chains via acid hydrolysis leading to rigid, rod-like, nanoscale materials [95]. In recent years, CNC and its derivatives have been studied extensively in the biomedical field due to their desirable properties including high aspect ratio, large surface area, high mechanical strength, and hydrophilicity [117]. The hydrophilic nature of CNC is due to the presence of several hydroxyl groups on its surface that lead to low protein adsorption, which delays initial clearance from the blood stream and prolongs circulation in blood [199]. The surface hydroxyl groups on CNC provide a platform for surface modification with different chemicals by different methods. Surface modification of CNC can allow the binding and release of drugs that do not bind to CNC in its native form [14]. The non-toxicity of CNC has been confirmed by its interactions with rainbow trout hepatocytes and microvascular endothelial cells [200].

Different acidic or basic drugs have been loaded onto charged particles as observed in ion-exchange resins [21]. The drug release from the drug-loaded resins is rapid due to the displacement of drug molecules bound to the resins by counter ions present in body fluids. The release from the resins can be sustained using different cellulose derivatives, such as carboxymethyl or epoxy cellulose and chitosan. The high charges on these biopolymers allow a strong binding between the drug and its carrier leading to a slower release [22]. Ion-exchange mechanisms have been explored in the binding and controlled release of drugs from nanocrystalline clays in pharmaceutical formulations [201].

CNC was first reported as a drug excipient by Jackson and coworkers [14]. Unmodified and surfactant modified CNC was used for the loading of hydrophobic and hydrophilic drugs, respectively. The hydrophobic drugs displayed a 2-day release compared to a 1-day release for hydrophilic drugs. Lin and coworkers incorporated different polysaccharide nanocrystals including CNC into sodium alginate nanocomposite microspheres resulting in higher encapsulation efficiency and desirable release profiles [146]. CNC hindered the diffusion of the model drug, theophylline and reduced the collapse and dissolution of microgels. Dash and Ragauskas developed a novel nanocarrier based on functionalized CNC for the delivery of amine-containing drugs. CNC was grafted with gamma aminobutyric acid, a

spacer molecule, by using periodate oxidation and a Schiff's base condensation reaction. Syringyl alcohol was then attached to the functionalized CNC as a releasable linker to induce the controlled and fast release of the targeting agent [202].

In several studies, Kolakovic and coworkers have investigated the potential applications of CNC for sustained drug delivery. In one study, they prepared drug-loaded CNC microparticles using a spray drying method. The particles were spherical with diameters of about 5 microns, and the controlled release profiles were associated to the limited drug diffusion from the system due to the tight fibre network. The release kinetics depended on the solubility of the drug in the medium and its affinity to CNC. In their study, the unbound drug fraction was relatively high, and they attributed it to the fraction that was weakly bound and accessible to water [18]. In another study, water insoluble drugs were encapsulated into tight fibre networks of CNC by filtration to produce drug-loaded CNC films. Their results showed that drugs could be released from the CNC films over prolonged durations due to the presence of a tight fibre network around the drug molecules that inhibit the drug dissolution and act as a barrier for drug diffusion [19]. Recently, Kolakovic and coworkers used isothermal titration calorimetry (ITC) to study the interactions between CNC and various model drugs of different molecular weights and charge characteristics. The ITC studies showed that the drugs bind to CNC in a pH dependent manner induced mainly by electrostatic interactions. The diffusion of drugs through the dry, porous, thin CNC films was investigated by permeation studies that revealed the size dependent diffusion rate of the model drugs through the films [20].

CNC has also been used to enhance the storage stability of drug nanoparticles by immobilizing them. Valo and coworkers coupled an engineered hydrophobin infusion protein with two cellulose binding domains to enhance the binding of drug nanoparticles to CNC. Their results demonstrated that once itraconazole (a model drug) was coated with protein and fused to CNC, nanoparticles with a size of 100 nm could be stored for more than 10 months. Furthermore, they observed that the nanodispersion increased the dissolution rate of itraconazole leading to more desirable *in vivo* profiles of the drug [203]. In another study, Valo et al. prepared CNC aerogels by freeze-drying method. Hydrogels produced using CNC obtained from different sources and microcrystalline cellulose (MCC) were used as reservoirs for oral drug delivery studies [204]. They coated beclomethasone dipropionate nanoparticles with hydrophobin proteins and incorporated them into the nanogels. They observed fast and sustained release of the drug depending on the type of cellulose matrix formed during the freeze-drying of the CNC and the types of interactions involved. They concluded that despite the fairly similar chemical structures of CNC, very different release profiles were obtained, and this should be taken into consideration in formulation studies [204]. In a recent study, Yildir et al. prepared porous cellulose beads and studied the

potentials of the spherical matrices as drug carriers. The beads were prepared by three different methods and three drugs were used as models. They loaded the cellulose beads by immersing them in the drug solution, and the drug loading and release from the cellulose beads displayed a controlled release profile [205].

In this study we aim to examine the potential of CNC and two CNC derivatives as nanocarriers for drug release applications. In recent years, there has been an increasing interest in investigating different CNC systems for pharmaceutical applications and researchers have shown that drugs can be loaded onto the CNC surface through different types of interactions [14]. However, to the best of our knowledge no studies have examined the pH dependent drug binding to CNC and the characterization of the CNC-drug complex. Understanding the types of interactions between drug molecules and CNC at various pH is beneficial to optimize drug loading that leads to a more desirable *in vivo* release profile. Surface modified CNC with chitosan oligosaccharide (CNC-CS_{OS}) has many notable biological properties making it an excellent nanocarrier for drugs. The chitosan chains grafted on the surface of CNC can hinder the drug release from CNC while acting as a pH responsive drug carrier. The antioxidant, antibacterial and mucoadhesive properties of chitosan provide a platform for the design of nanocarriers with potential applications in buccal drug delivery and addressing complications in the oral cavity. The two model drugs used in this study are procaine hydrochloride (PrHy), a local anesthetic used in dental surgery, and imipramine hydrochloride (IMI), a tri-cyclic antidepressant with local analgesic activity. CNC samples loaded with these model drugs can be applied in topical formulations to alleviate pain.

5.2 Experimental Section

5.2.1 Materials

A freeze-dried CNC sample was supplied by FPInnovations. For preparation of CNC-OX, the following chemicals were purchased from Sigma-Aldrich: TEMPO (98 %), NaOCl (reagent grade, $10-15\%$ available chlorine), NaBr (99.0 %), NaOH (1 N), HCl (1 N), and methanol. For surface modification of CNC with CS_{OS} and preparation of CNC-CS_{OS}, CS_{OS} (average Mn 5,000 Da) was purchased from Sigma-Aldrich. EDC (1-ethyl-3-(3- dimethylaminopropyl) carbodiimide, commercial grade) and NHS (N-hydroxysuccinimide, 98 %) were purchased from Fluka and Acros Organics, respectively. MES (2-(N-morpholino) ethanesulfonic acid, 99 %) purchased from Sigma was used as the buffer for the amide coupling crosslinking reaction. For drug selective membrane preparation, poly(vinyl chloride)

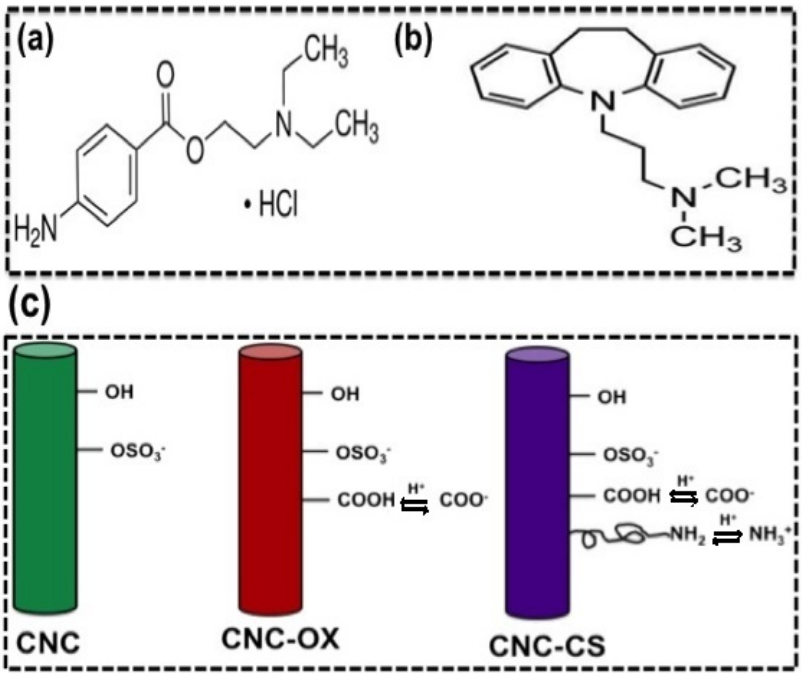

Figure 5.1: Structure of (a): PrHy, (b): IMI, (c): CNC and its derivatives.

carboxylated (PVC), poly(ethylene-co-vinyl acetate-co-carbonmonoxide) (PE-co-PVA-co-CO) were purchased from Sigma. Sodium tetraphenylborate (NaTPB) was obtained from Fluka. The model drugs used procaine hydrochloride (PrHy) (Figure 5.1a) a local anesthetic used in dental surgery, and imipramine hydrochloride (IMI) (Figure 5.1b) an antidepressant, were purchased from Sigma. Millipore de-ionized (D.I.) water was used for all experiments and sample preparations.

5.2.2 Synthesis of CNC-OX and CNC-CS_{OS}

The synthesis and characterization of CNC-OX and CNC-CS_{OS} were described in detail in Chapter 4. A schematic of CNC, CNC-OX and CNC-CS_{OS} denoting their functional groups is shown in Figure 5.1c.

5.2.3 Preparation of Drug-Selective Membranes

The drug-selective membranes were prepared using a procedure previously described by Tan and Tam [206]. The first step was the preparation of the carboxylate PVC-drug complex by an ion-exchange process. Carboxylated PVC (0.5 g) was dissolved in 30 mL THF. For preparation of drug selective membranes, the drugs were dissolved in a mixture of 90 mL of THF and 10 mL of distilled D.I. water. For PrHy membranes, 0.955 g PrHy and for IMI membranes 1.100 g IMI was added. The carboxylated PVC solution was then slowly added to the rapidly stirring drug solution and mixed for 2 days. In order to precipitate the carboxylated PVC-Drug complex, the mixtures were slowly added to 900 mL of cold distilled D.I. water using a glass pipette. The precipitate was concentrated using a rotary evaporator until the complex aggregated into a visible white dispersion. The complex was filtered using a 20-25 μm filter paper and washed several times with distilled D.I. water, and left to dry at room temperature. In the next step of the membrane preparation, 0.18 g of the plasticizer (Elvaloy 742 resin (i.e. PE-co-PVA-co-CO), 0.114 g of the carboxylated PVC-Drug complex, and 6 mg of the ion-exchanger (i.e. NaTPB) were dissolved in 30 mL of THF. The solutions were then poured into a 55 mm diameter Petri dish and the solvent was left to slowly evaporate at room temperature for 1 to 2 days. Finally, the membrane was removed from the Petri dish and a 12 mm disk was cut and attached onto a PVC cap using THF.

5.2.4 Electro-Motive Force Measurement (EMF) System

The EMF system consisted of a measuring drug membrane electrode (DME) and an Ag/AgCl reference electrode purchased from VWR. The electrochemical system arrangement was: AgBr/Ag/internal solution/membrane/test solution/Ag/AgCl reference electrode. The interior of the Teflon electrode casing was filled with a 1 mM solution of drugs in 10 mM NaCl. The sensor membrane was conditioned for half an hour prior to use [206]. The electrodes were attached to an ELIT 4-Channel Ion-Analyzer (ELIT 9804), and the electromotive force was recorded using the software ELIT 4-Channel Ion-Analyzer version 7.1.44sa.

5.2.5 DSE Calibration and Concentration Determination

Prior to each measurement, the EMF system was calibrated using drug standard solutions. For drug release studies, standard solutions with concentrations of 0.1, 1, 10 and 100

mM PrHy and 0.01, 0.1, 1 and 10 mM IMI in 10 mM NaCl were prepared. Calibration curves were plotted and the logarithmic line of best fit was determined, which was used to calculate the concentration of PrHy and IMI in subsequent measurements (Figure 5.2a and c). To obtain a graph of concentration versus time, the electrodes were placed in the test solution and EMF readings were automatically acquired by the 4-channel ion-analyzer at precise time intervals (20 s) for the duration of the experiment. The EMF values were then converted to concentration values using the calibration curve. The stability of membranes over time and their fast response to drug concentration change was also evaluated (Figure 5.2b and d).

5.2.6 Drug Loading

The drug loading of PrHy and IMI was performed in a similar way resulting in a final concentration of 0.05 wt% sample (CNC, CNC-OX, CNC-CS_{OS}), 18.3 mM drug (PrHy or IMI) in 10 mM NaCl solution. The loading was achieved by dropwise addition of a fixed volume of 36.6 mM of drug to the same volume 0.1 wt% sample in a 20 mM NaCl solution. The pH of the drug-loaded solution was then adjusted to 8 and 7 for PrHy and IMI, respectively. The solutions were stirred for 30 mins at room temperature and equilibrated for at least 1 h. In order to remove the unbound drug, the drug-loaded solutions were passed through a stirred ultrafiltration cell (Millipore Corporation, Bedford, USA) with filters having cut-off pore sizes of 25 nm (Millipore, VSWP, Ireland). The concentration of free drug in the filtrate was measured using a DSE and, the EMF measurements were recorded using a built-in micro-voltammeter.

5.2.7 Isothermal Titration Calorimetry (ITC)

The Microcal VP-ITC instrument was used to study the interactions between PrHy and CNC-CS_{OS} at 3 different pH values and the model drugs (PrHy and IMI) and cellulose nanocrystal samples (CNC, CNC-OX and CNC-CS_{OS}). Once the thermal equilibrium was reached, the titrations were carried out at a constant temperature by injecting the titrant (drug) solution in NaCl from a $\sim$282 μL injection syringe into a 1.4551 mL sample cell filled with 0.05 wt% cellulose nanocrystal solution prepared at the same pH and ionic strength. An injection schedule was automatically performed using an interactive software after setting the number of injections, volume of each injection, and time between each injection. For studying the interactions between PrHy and CNC-CS_{OS} at 3 different pHs, the ΔH values for the dynamic interactions were reported as kcal/mol of injectant and

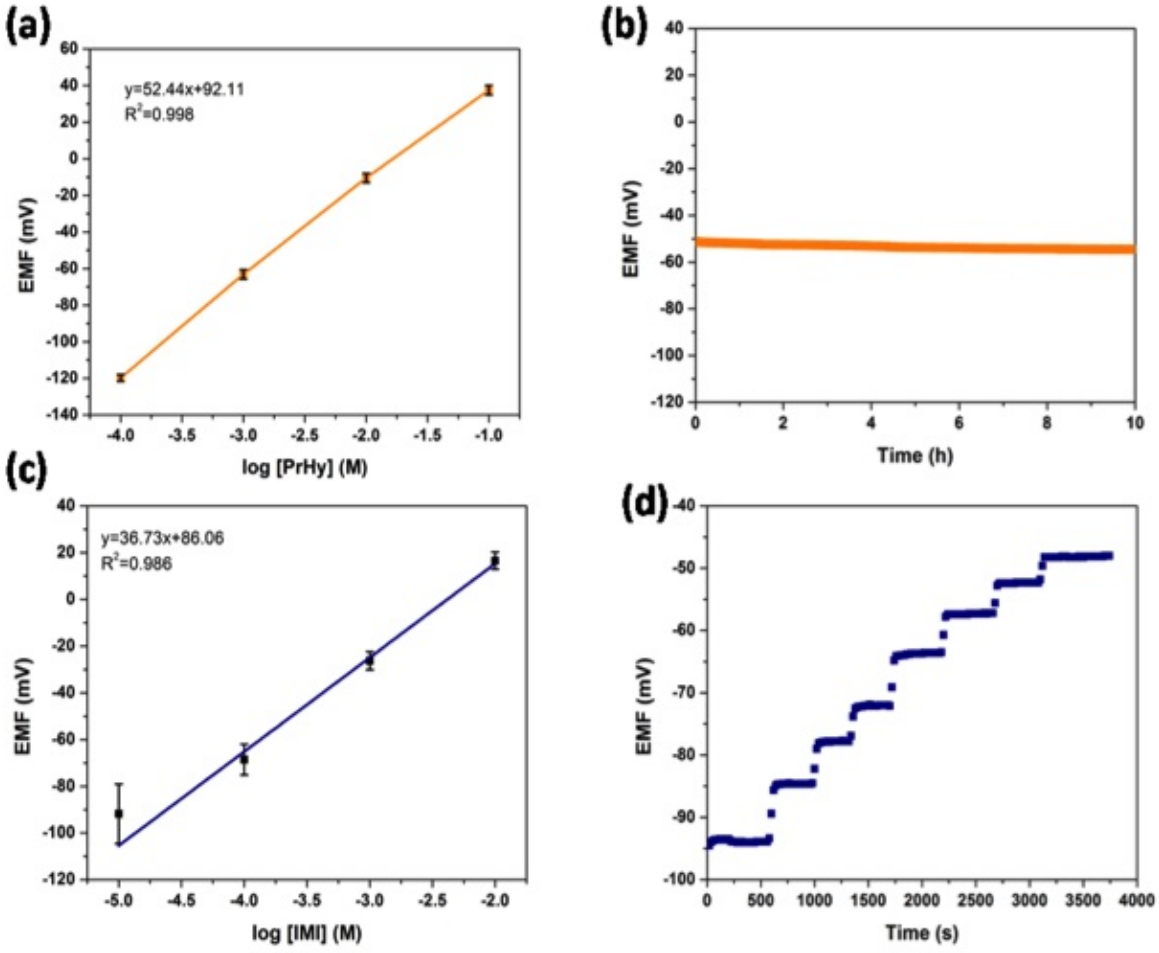

Figure 5.2: Calibration curves of (a): PrHy and (c): IMI. (b): stability of PrHy membrane over time, and (d): fast response of IMI membrane to change in concentration.

were plotted against the molar ratio. Control experiments were performed by injecting the same aliquot of PrHy into 0.01 M NaCl at pH of 6, 7 and 8.

For studying the interactions between model drugs and CNC samples, the ΔH values for the dynamic interactions were reported as kJ/mol of injectant and were plotted against drug concentration. The interactions between PrHy and cellulose nanocrystals were studied by injecting 100 mM or 10 mM PrHy into sample cells with an ionic strength of 10 mM NaCl at pH 8 and at 25 °C. For IMI, the interactions were studied by first titrating 100 mM IMI into sample cell containing cellulose nanocrystals in 10 mM NaCl at pH 7 at 25 °C. In order to further elucidate the interactions between IMI and CNC-OX, three additional titrations were performed, keeping the other titration parameters constant: (1) at high temperature (50 °C), (2) at high ionic strength (200 mM NaCl), and (3) high urea concentration (200 mM). Blank titrations were performed by injecting the same aliquot of drugs into water at the same pH, temperature and ionic strength to obtain the heat of dilution. The differential enthalpy curves of heat of dilution were subtracted from the enthalpy curves of titrating drugs into cellulose nanocrystal solutions.

5.2.8 UV Transmittance

The transmittance of solutions containing 0.05 wt% cellulose nanocrystal samples with different drug concentrations was measured using a HP 8453 UV-visible spectrophotometer (Hewlett-Packard Company, Palo Alto, CA) equipped with a 1 cm quartz cell, at a wavelength of 600 nm. The pH and ionic strength of the solutions were chosen to match the conditions in the ITC cell.

5.2.9 Zeta Potential Measurements

The zeta potential of the complexes prepared by mixing 0.05 wt% cellulose nanocrystals with different drug concentrations were measured using the Malvern Nano-ZS 90 (Malvern, Nano ZS, UK). The measurements were performed at room temperature at pH 7 for IMI and pH 8 for PrHy. The Smuloschowski model was used to convert electrophoresis mobility to zeta-potential, where the reported values are an average of 10 measurements.

5.2.10 *In vitro* Drug Release Studies

The *in-vitro* drug release studies were performed at room temperature using the DSE. For the release studies, ∼3 mL of drug-loaded samples were added to 25 mL phosphate buffer

saline (PBS) medium at a specific pH with gentle stirring. The EMF of the bulk solution was recorded by the ELIT 4-Channel Ion-Analyzer at a regular interval of 20 s and the values were later converted to concentration values. A cumulative release profile of drug concentration vs. time was then obtained.

5.3 Results and Discussion

5.3.1 Drug Loading Capacity

The binding efficiency (BE%) of samples was determined indirectly by measuring the free drug in the filtrate using the following expression:

$$\text{Binding Efficiency (\%)} = \frac{[\text{Drug}]_{\text{total}} - [\text{Drug}]_{\text{filtrate}}}{[\text{Drug}]_{\text{total}}} \times 100 \tag{5.1}$$

In order to compare the loading of PrHy and IMI into the samples, all conditions were kept constant except the pH. As discussed in the following section, ITC studies confirmed that the optimal interaction between CNC-CS_{OS} and PrHy was observed at pH 8 leading to the highest BE%. At lower pH values, the amine groups of CNC-CS_{OS} are protonated and the surface charge is positive. The repulsion between the positively charged drugs and CNC-CS_{OS} limits the BE%. Therefore, PrHy was loaded in the CNC samples at pH 8 to maximize the drug loading. As IMI is not fully soluble at pH 8, IMI was loaded into the samples at pH 7.

Figure 5.3 shows the BE% of IMI and PrHy with different cellulose nanocrystal samples. Previous studies showed that hydrophilic drugs could directly bind to the CNC surface through various types of interactions, ionic interaction being the most dominant as it is long range [14]. The BE% of IMI was higher than PrHy. The higher BE% of IMI compared to PrHy was attributed to the structural differences of the two drugs leading to more favorable interactions between cellulose derivatives and drug molecules [46]. Moreover, the differences in the solubility of the drugs and CNC samples at pH 7 and 8 could lead to different affinities to CNC samples [19]. For PrHy, CNC-OX had the highest BE% and CNC and CNC-CS_{OS} had similar BE% values. For IMI, CNC displayed the highest BE% while, the BE% of CNC-OX and CNC-CS_{OS} were lower but similar to each other. The differences between the BE% on different CNC samples can be further explained through the results of ITC, zeta potential and transmittance studies to be discussed later.

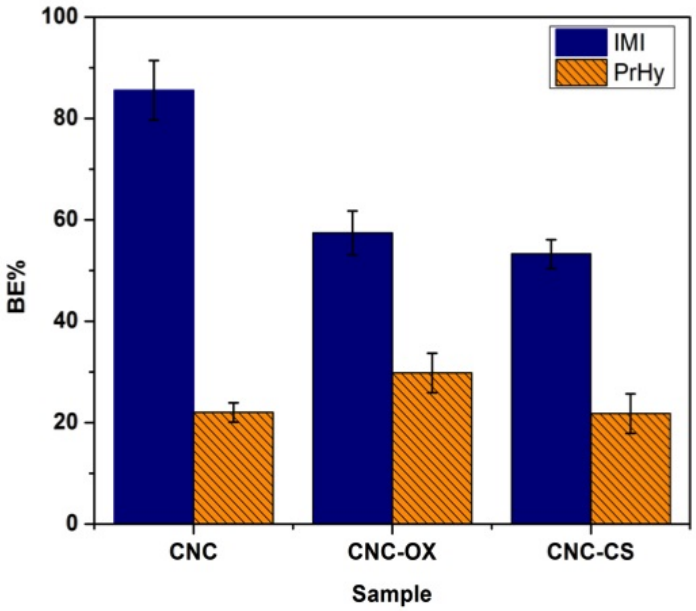

Figure 5.3: Binding Efficiency (BE%) of IMI at pH 7 and PrHy at pH 8 to different CNC samples.

5.3.2 Isothermal Titration Calorimetry (ITC)

Evaluating the interactions between drugs and carriers and determining the mechanisms involved is an important factor for establishing the optimum conditions for drug uptake and to understand their release behavior. In the first step, ITC was used to determine the optimum pH for loading PrHy into CNC-CS_{OS}. The thermodynamics of CNC-CS_{OS}-PrHy interaction at different pH values was studied by ITC and the results are shown in Figure 5.4a. Insignificant interaction between CNC-CS_{OS} and PrHy was observed at pH 6 due to the electrostatic repulsion between the positively charged samples. At pH 7, CNC-CS_{OS} possessed an initial endothermic interaction, followed by almost no interaction. CNC-CS_{OS} displayed the most interaction with PrHy at pH 8, therefore, this pH was chosen for drug loading experiments. The equilibrium binding parameters at pH 8 was determined by fitting the experimental calorimetric data with a two-site model. The binding constants K_1 (3.45×10^5) and K_2 (1.83×10^4) possessed large values, suggesting that PrHy has a good affinity to CNC-CS_{OS} at pH 8 and can be incorporated with high efficiencies onto CNC-CS_{OS} particles. The thermodynamic signatures are shown in Figure 5.4b, and by comparing the thermodynamic signatures with previously reported results, we conclude that the binding at pH 6 and pH 8 for the second site is dominated by hydrophobic interactions whereas at pH 7 and pH 8 first site are due to hydrophobic interactions and favorable hydrogen binding [207].

ITC was also used to determine the types and nature of interactions between CNC samples and the two model drugs. The ITC results from titrating 100 mM PrHy into CNC samples at pH 8 (Figure 5.5) revealed an exothermic reaction with the largest enthalpy change for CNC-OX. CNC and CNC-CS_{OS} displayed similar enthalpy values, where an endothermic and exothermic reaction was observed for the CNC and CNC-CS_{OS} respectively. Exothermic reactions usually signify an enthalpically driven process [208] while endothermic reactions are generally entropically driven; this could be related to the release of counter-ions or dehydration of samples. Figure 5.5 indicated that the saturation was reached at higher PrHy concentrations for CNC-OX ($\sim$4 mM) followed by CNC-CS_{OS} ($\sim$3 mM) and CNC ($\sim$2 mM). In order to identify the interactions between PrHy and CNC samples at lower concentrations, the CNC samples were titrated with 10 mM PrHy (Figure 5.5-inset). It can be observed that the titration resulted in similar trends to 100 mM PrHy with CNC-OX showing the maximum enthalpy change. The small heat change after titrating CNC samples with PrHy signified the low binding of PrHy to the three CNC samples compared to IMI. Similarly, low endothermic heat release values were observed when titrating PrHy into polyaspartic acid [209]. As discussed previously, fitting a two site model to the ITC plot of 10 mM PrHy to CNC-CS_{OS} at pH 8 suggested that the in-

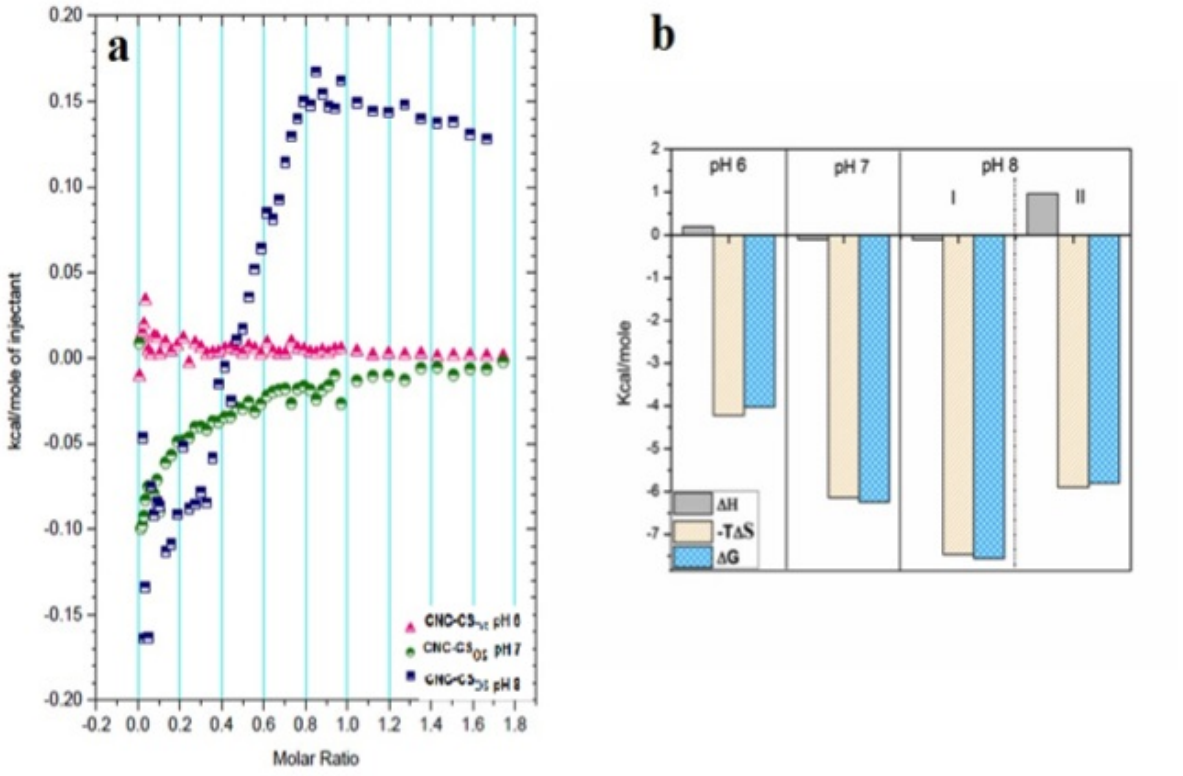

Figure 5.4: (a) Heats of reaction as obtained from the integration of the calorimetric traces of titrating 10 mM PrHy into 0.05 wt% CNC-CS_{OS} at pH 8. (b) Thermodynamic signatures of 0.05 wt% CNC-CS_{OS} and 10 mM PrHy at pH 6, 7 and 8.

teractions between CNC-CS_{OS} and PrHy was mainly due to hydrophobic interactions and hydrogen bonds [155]. Govender et al. had previously stated that the interaction between polyacrylic acid and PrHy at pH∼5 was mainly due to non-electrostatic interactions [46]. Tan et al. proposed that the ethyl groups in the structure of PrHy would cause steric hindrance limiting the electrostatic interactions between the positive charge on the nitrogen atom of PrHy and negative charges of their nanogels [206]. Aromatic residues of proteins have been shown to bind to the glucopyranose units of crystalline segments of cellulose via hydrophobic interactions, which were then enhanced by hydrogen bonding [210].

Figure 5.6a shows the ITC plots of titrating CNC samples with 100 mM IMI. The heat change after titrating CNC samples with IMI was much larger than in PrHy. This might explain the higher BE% observed for IMI-CNC systems. The order of the maximum heat change was similar to that of PrHy with CNC-OX displaying the most heat. The high heat release when titrating CNC-OX with IMI signified strong binding that yielded white precipitates recovered from the ITC cell at the end of the experiment (Figure 5.7). Similar to PrHy, the reaction between CNC and IMI was endothermic, however the concentration at which the enthalpy approached zero was not identical. The saturation IMI concentration for CNC-OX (∼7 mM) was the largest followed by CNC-CS_{OS} (∼4 mM) and CNC (∼3 mM). This result suggested that the differences between the saturation concentrations of the CNC samples could be attributed to the differences in the strength of electrostatic interactions [206]. The presence of carboxylic acid groups on CNC-OX and the deprotonation of COOH groups to COO^- at pH 7 together with the sulfate ester groups (OSO_3^-) on the surface of the CNC, resulted in the largest negative zeta potential compared to CNC-CS_{OS} and CNC. For CNC-CS_{OS}, most COOH groups participated in the carbodiimide reaction, while the negative zeta potential on pristine CNC was solely due to OSO_3^- groups. In order to elucidate the interactions between CNC-OX and IMI, ITC measurements were performed at different conditions (Figure 5.6b). When the temperature was increased from 25 to 50 °C, the heat release was significantly larger, confirming the presence of hydrophobic interactions [206]. At 50 °C, the IMI concentration at which enthalpy equaled zero occurred at a lower concentration (∼3 mM) compared to ∼7 mM for 25 °C. By increasing the temperature, Brownian motion of the drug molecules and CNC is enhanced, resulting in a higher probability of collisions that promotes the interactions between drug molecules and CNC. Urea was added to minimize or reduce the hydrogen bond interaction, and at high urea concentration, the exothermic peak was reduced. However, since hydrogen bonding interaction is not present, the addition of urea could have altered the polar-π interactions between water molecules and the aromatic structures of the IMI molecules. Moreover, urea could form hydrogen bonds with the protonated carboxylic acid groups on the surface of CNC-OX as well as the hydroxyl groups that lower the dispersibility

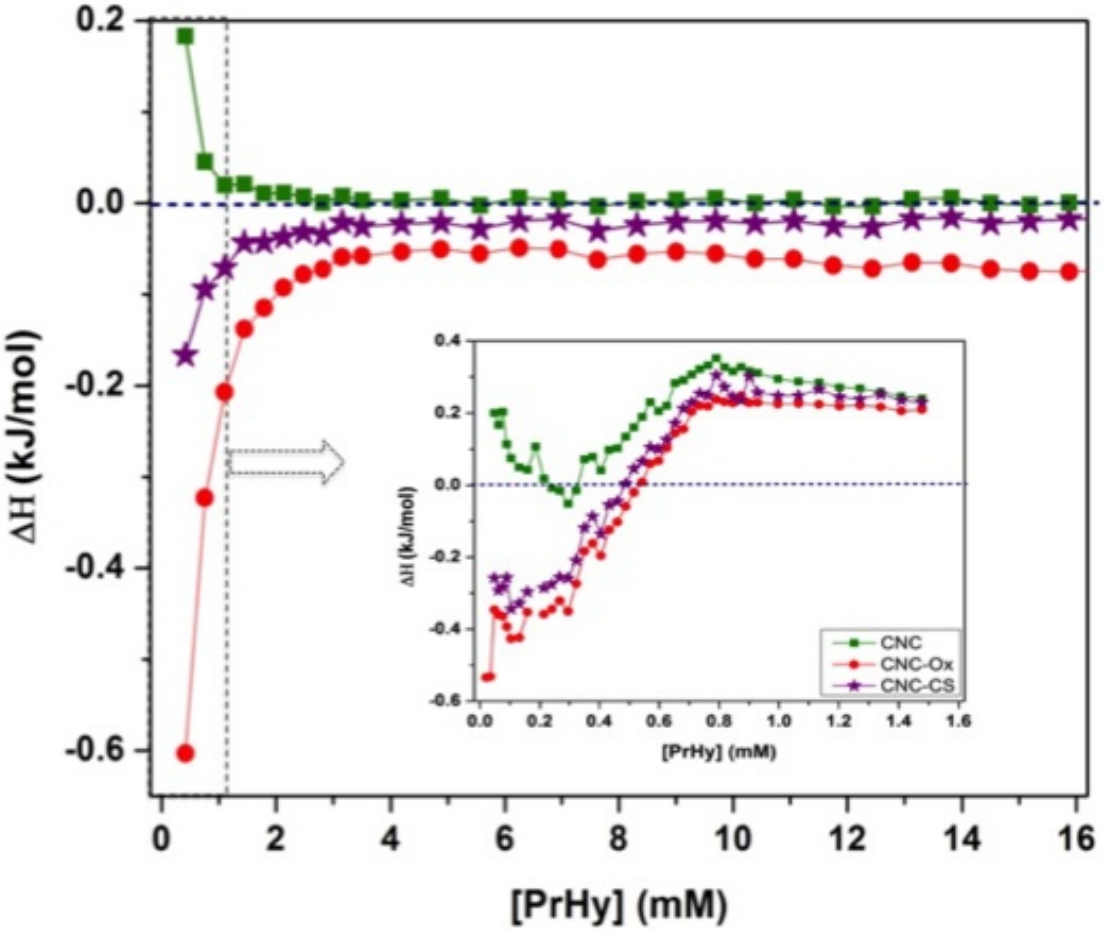

Figure 5.5: Heats of reaction as obtained from the integration of the calorimetric traces of titrating 100 mM PrHy into 0.05 wt% CNC samples at pH 8. (Inset plot titrating 10 mM PrHy).

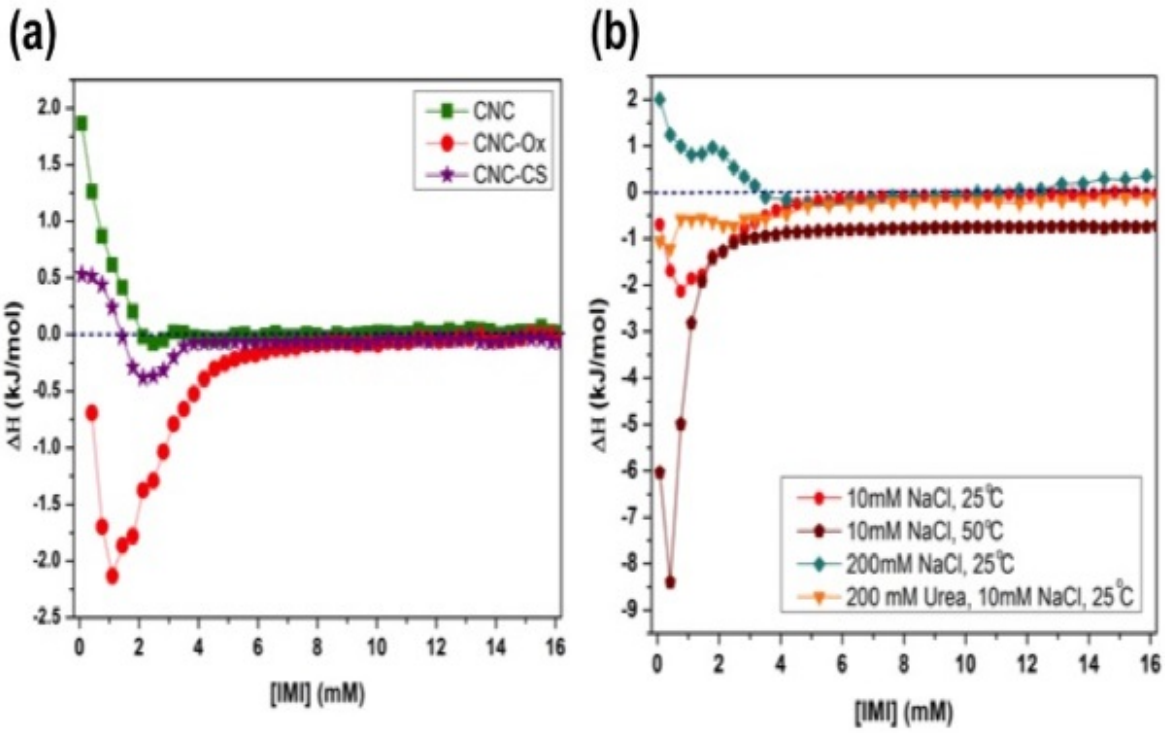

Figure 5.6: Heats of reaction as obtained from the integration of the calorimetric traces for titrating 100 mM IMI into (a) 0.05 wt% CNC samples at pH 7, (b): 0.05 wt% CNC-OX under different conditions at pH 7.

of CNC-OX in aqueous solution, and reduce the interaction between IMI and CNC-OX. Performing the titration in high salt concentration led to an interesting result, where heat was absorbed (endothermic reaction). This could be due to the shielding of charge on the surface of CNC-OX in high salt conditions. However, the saturation concentration remained unchanged ($\sim$7 mM), which suggests that other interactions (in addition to electrostatic) were present. If the interaction was dominated by electrostatic forces, the saturation concentration would be lowered in a high ionic strength environment. This is in contrast to other ITC results obtained by previous researchers, where they had observed a reduction in the exothermic peak due to the charge screening leading to a lower saturation concentration [211]. The observed difference between the different CNC samples is most probably due to the differences in the surface charge of the CNC systems.

5.3.3 Studying Complexation: UV Transmittance and Zeta Potential Measurements

In order to shed light on the complexation mechanisms of CNC samples and the two model drugs, six CNC samples containing different drug concentrations were prepared. The pH and ionic strength of all solutions were monitored closely to resemble the conditions in the ITC cell at the end of titration and after drug loading. Table 5.1 summarizes the results of the zeta potential and % transmittance results from samples with different drug concentrations prepared that represented the different stages of the interactions between drug molecules and CNC when the drugs were titrated into the CNC samples. Figure 5.7 shows the solutions of CNC samples containing 16 mM of each drug; the condition at the completion of the ITC experiments. For all CNC samples with increasing concentration of PrHy, the surface charge increased gradually due to the binding of positively charged PrHy onto the surface of CNC leading to a reduction in the transmittance. However, for CNC-OX the zeta potential of the final solution was negative. This could be due to the disruption of the complexes to produce individual CNC particles as reflected by the clear solution shown in Figure 5.7. The higher loading and more rapid release of PrHy observed for CNC-OX compared to CNC and CNC-CS_{OS} could be explained by the enhanced binding sites available in CNC-OX. Compared to PrHy, a much more dominant reduction in the transmittance was observed as shown in Figure 5.7. This could be due to the more favorable complex formation for IMI as indicated from ITC binding isotherms, which led to a higher drug loading. CNC-OX containing 16 mM IMI formed larger particles that precipitated from solution. It should also be noted that the differences in the values reported for pure CNC samples for PrHy and IMI is due to the difference in pH values.

Based on ITC, zeta potential and transmittance data, we have postulated a mechanism for the complexation between the cationic model drugs and the three types of CNC samples. For PrHy, due to the weak ionic interactions between PrHy and CNC nanoparticles (note: the ethyl groups on the tertiary amine reduces the electrostatic interaction, Figure 5.1a), the Columbic attractive forces draw the PrHy molecules closer to CNC particles allowing the planar surface alignment facilitating the hydrogen bonding between the primary amine groups of PrHy and hydroxyl groups on the CNC surface. For CNC-OX and CNC-CS_{OS}, the tertiary amine groups form hydrogen bonds with the carboxylic acid groups. Similarly for IMI, the stronger electrostatic attractions (since the tertiary amine groups are surrounded by methyl groups for IMI, Figure 5.1b) draw the positively charged IMI molecules to the CNC surface that facilitates the hydrophobic interactions between the drug and the surface of CNC. Similar mechanisms were proposed from studies on the complexation between doxorubicin and dextran [212]. The ionic interactions between pos-

Table 5.1: Transmittance (T%) at 600 nm and zeta potential (ZP) measurements of CNC samples at different concentrations of PrHy and IMI

		CNC		**CNC-OX**		**CNC-CS_{OS}**	
Conc. (mM)		T (%)	ZP (mV)	T (%)	ZP (mV)	T (%)	ZP (mV)
PrHy	0	93.4	-35.7	94.6	-38.5	58.1	-22.3
	0.756	91.8	-35.7	92.9	-36.5	60.6	-20.0
	1.099	90.2	-34.8	89.9	-26.2	56.9	-21.9
	1.474	91.3	-34.4	76.4	-17.5	56.6	-19.1
	16	65.7	-15.8	58.0	-37.6	51.5	3.5
IMI	0	92.2	-33.1	97.3	-36.5	86.1	-15.5
	0.756	90.9	-33.3	43.0	-34.5	47.2	-10.9
	1.099	86.9	-34.7	44.6	-39.4	51.4	-14.8
	1.474	80.8	-33.2	40.0	-37.2	49.6	-11.8
	16	4.0	-12.3	42.2	-4.73	27.7	2.6

itively charged doxorubicin and negatively charged dextran resulted in the formation of polymer-drug complexes, which were strengthened by hydrogen bonding and $\pi - \pi$ stacking of the aromatic groups on doxorubicin [212]. Our results are in agreement with the findings of Govender et al., where they had concluded that the interactions between PrHy and polyacrylic acid were entropically driven and dependent on the release of counter-ions. Despite the presence of large electrostatic driving forces for the initiation of complex formation, non-electrostatic charges were the dominant forces for the complex formation [46].

5.3.4 *In vitro* Drug Release Studies

The *in vitro* release profiles of PrHy and IMI from CNC samples at different pHs are shown in Figure 5.8 and Figure 5.9, respectively. Figure 5.8a shows the release profile of PrHy from CNC samples at pH 7.4. The total amount of PrHy released was the highest for CNC (∼80 %) followed by CNC-OX (∼60 %). CNC-CS_{OS} displayed the lowest amount of total PrHy released (∼40 %), and this could be due to the presence of chitosan chains on the surface of CNC that inhibited the release and diffusion of the drug molecules. The maximum release time for CNC-CS_{OS} was also the highest (∼ 12 min) compared to CNC (∼ 6 min) and CNC-OX (∼ 3 min). The sustained release profile of PrHy from CNC-CS_{OS} offers the possibility of drug release carriers for applications where more controlled release profiles are desirable. Figure 5.8b shows the *in vitro* release profile of PrHy from CNC-CS_{OS}

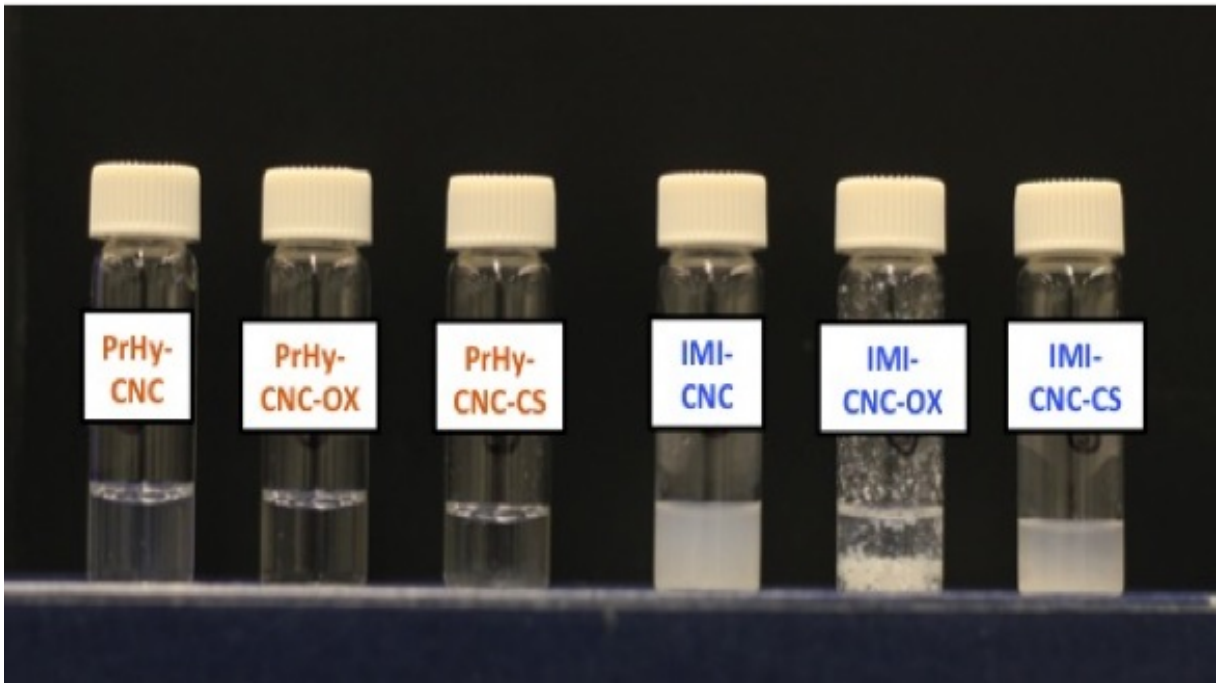

Figure 5.7: Complexes of 0.05 wt % CNC samples at 16 mM drug concentration.

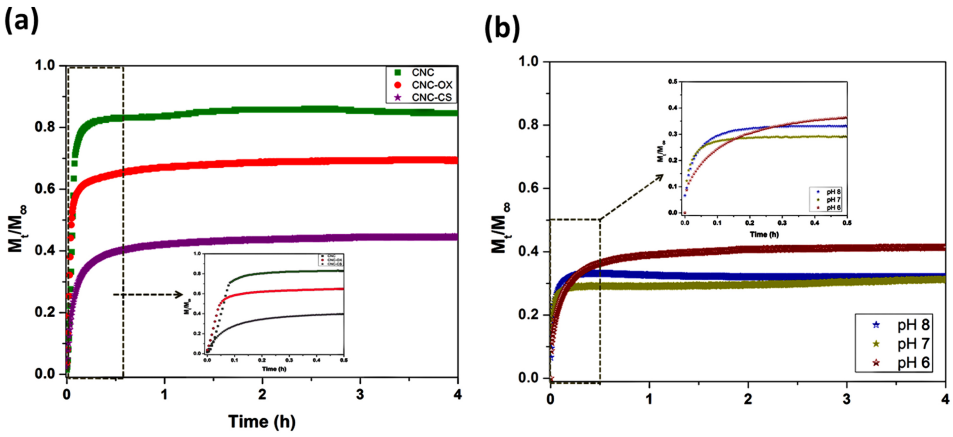

Figure 5.8: Cumulative *in vitro* release of PrHy from (a): CNC samples in PBS pH 7.4, (b): CNC-CS_{OS} in PBS pH 6, 7 and 8.

at different pHs. At pH 6 where both CNC-CS_{OS} and PrHy are positively charged, the electrostatic repulsion led to the release of the maximum amounts of PrHy from the drug-particle complexes.

The *in vitro* release profile of IMI from CNC samples at pH 7.4 and 5.7 is shown in Figure 5.9a and b, respectively. pH 7.4 is the physiological pH of blood and pH 5.7 is the pH of most wounds. The higher amount released at pH 5.7 was attributed to the higher solubility of IMI at lower pH due to the greater degree of protonation of amine groups. Similar results have been reported previously [213]. Moreover, the differences in the counter ions present in PBS at different pH values could lead to larger ion-exchange at pH 5.7 leading to a faster and more complete release of IMI molecules. IMI is released almost immediately but incompletely from CNC at both pH values. The release of IMI from CNC-OX at both pH values occurred in a relatively controlled manner. At pH 5.7, electrostatic interactions between the positively charged IMI and negatively charged CNC-OX dominate (because of the deprotonation of carboxylic acid groups), a more sustained release profile was observed compared to pH 7.4. At both pH values, CNC-CS_{OS} exhibited the highest total amount released followed by CNC-OX and CNC. This is in contrast to the release observed for PrHy where CNC-CS_{OS} displayed the least amount of drugs released. As seen in Figure 5.9a, CNC-CS_{OS} displayed a desirable release profile for IMI at pH 7.4, where ~80 % of IMI was released in a controlled manner over 2 hours. However at pH 5.7, due to electrostatic repulsion, IMI was expelled and released immediately. This pH responsive behavior of CNC-CS_{OS} makes it an excellent candidate for the triggered drug

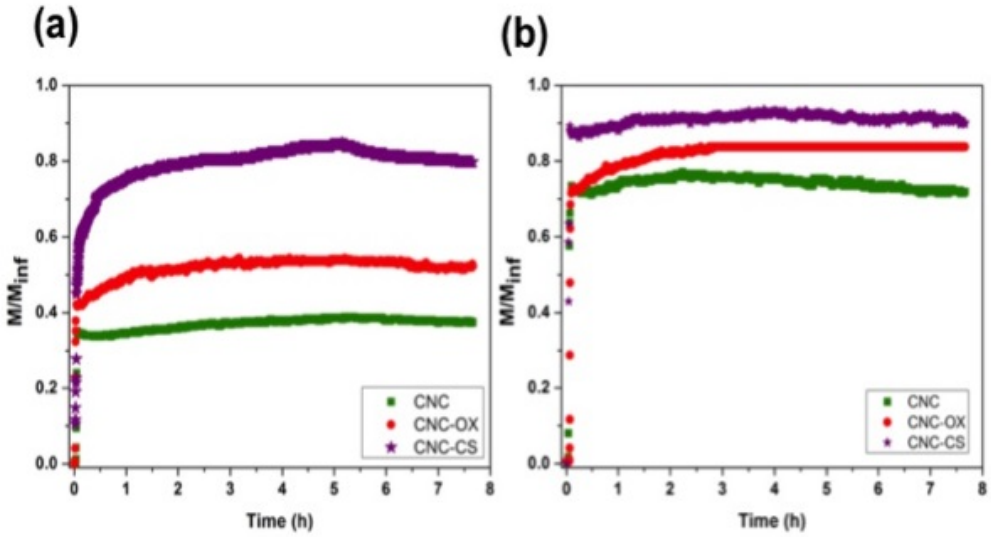

Figure 5.9: Cumulative *in vitro* release of IMI from CNC samples in PBS (a): at pH 7.4 and (b): at pH 5.7.

release that is desirable in some applications.

In general, the release of drug molecules from CNC samples was rapid, which could be due to the ion-exchange between the ions in the release medium and the surface of CNC [14]. The rapid release profile was observed for acidic or basic drugs bound to ion-exchange resins [21]. Immediate release delivery systems provide the instantaneous availability of drugs for pharmacological action or absorption. The drugs are dissolved rapidly without the need to prolong the dissolution and absorption of drug molecules [63]. Rapid release systems can have potential applications in areas where rapid action is required such as in the delivery of local anesthetics and analgesics, wound-dressing materials and addressing issues in periodontal cavities. Despite the general fast release of drugs from CNC and CNC-OX, both drugs were released from CNC-CS_{OS} in a sustained manner.

5.4 Conclusions

In this chapter the drug loading and *in vitro* release profiles of two cationic drugs (i.e. procaine hydrochloride (PrHy) and imipramine hydrochloride (IMI)) from native cellulose nanocrystals (CNC) and two derivatives; oxidized CNC (CNC-OX) and surface modified

CNC with chitosan oligosaccharide (CNC-CS_{OS}) were studied. Isothermal calorimetry (ITC), transmittance and zeta potential measurements were used to elucidate the complexation between the drugs and CNC samples. It was seen that the higher binding of IMI to CNC samples could be explained by the more dominant exothermic peak observed in the ITC isotherms leading to the formation of larger particle-drug complexes. Drug selective electrodes that displayed good stability and fast response were used to quantify the release profiles. Different release profiles at varying pH conditions were observed due to the pH responsive properties of the systems and changes in the solubility of drugs. Both drugs were released rapidly from CNC samples due to the ion-exchange effect, and CNC-CS_{OS} displayed a more sustained release profile. These immediate drug release systems can have potential applications in the delivery of local anesthetics and treatment of periodontal cavities.

Chapter 6

Cellulose Nanocrystal Grafted Chitosan Oligosaccharide: A Novel Antioxidant for Vitamin C Delivery *

Cellulose nanocrystal grafted with chitosan oligosaccharide (CNC-CS_{OS}) was used to encapsulate vitamin C and prepare CNCS/VC complexes using sodium tripolyphosphate (TPP) via ionic complexation. The stability of vitamin C and the antioxidant activity of CNCS/VC complexes were elucidated. The formation of the complex was confirmed using DSC and UV-Vis spectrophotometry and TEM was used to study the morphology of the complexes. The encapsulation efficiency of vitamin C at pH 3 and pH 5 was $71.6\% \pm 6.8$ and $91.0\% \pm 1.0$, respectively. Strong exothermic peaks observed in ITC studies at pH 5 could be attributed to additional electrostatic interactions between CNC-CS_{OS} and vitamin C at pH 5. The *in vitro* release of vitamin C from CNCS/VC complexes showed a sustained release of up to 20 days. The vitamin C released from CNCS/VC complex displayed a higher stability compared to the controlled vitamin C solution, and this was also confirmed from the ITC thermograms. The antioxidant activity of various samples was studied using the DPPH method and reported in terms of scavenging activity. CNC-CS_{OS} possessed a higher scavenging activity and faster antioxidant activity compared to its precursors, i. e. oxidized CNC and CS_{OS}, and their physical mixture. Complexing vitamin C into CNC-CS_{OS} particles yielded a dynamic antioxidant agent, where the vitamin C is

*This chapter is adapted from a paper "S.P. Akhlaghi, R. Berry, and K.C. Tam, Cellulose Nanocrystal Grafted Chitosan Oligosaccharide: A Novel Antioxidant for Vitamin C Delivery, submitted to *AAPS PharmSciTech*."

released over time and displayed sustained antioxidant properties. Therefore, CNCS/VC can potentially be used in cosmeceutical applications as topical formulations.

6.1 Introduction

Antioxidants protect our body from the damage caused by free radicals. Environmental factors such as air pollution, cigarette smoke, and sunlight produce free radicals that damage the skin. An effective antioxidant in biological systems is vitamin C (L-ascorbic acid) that serves as a cofactor in hydroxylation reactions and scavenges reactive oxygen species [23]. Similar to other important antioxidants, vitamin C is only provided exogenously, therefore, the topical application of vitamin C is beneficial as a protector for the skin [24]. Vitamin C has also been used in different cosmetic and pharmaceutical formulations because of its beneficial effects for the skin [25, 214]. Vitamin C topical formulations are also applied due to their depigmenting activity [215] and anti-wrinkle activity through collagen synthesis promotion [216]. Despite the several cosmeceutical formulations containing vitamin C on the market, very few are topically effective. The major drawbacks in the design of these formulations are: (1) low concentration of vitamin C in the formulations; (2) incomplete absorption and metabolism of different forms of vitamin C (mixture of isomers or ester) of vitamin C by the skin; and (3) chemical instability of vitamin C once the product is opened [24, 26]. Vitamin C is easily oxidized to dehydroascorbic acid (DHA) due to its exposure to air, light and high temperature, which results in a short shelf time for formulations containing vitamin C. The bioactivity of DHA is reported as 80% of the activity of vitamin C [217]. In basic conditions, these reactions occur rapidly and result in the irreversible hydrolyzation of vitamin C into 2,3-L-diketogulonic acid (2,3-KDG), which is a biologically inactive form [218]. The degradation pathway of vitamin C is shown in Figure 6.1 [26].

There are several requirements for cosmeceuticals containing vitamin C to be topically effective: (1) they must contain vitamin C in the form of L-ascorbic acid; (2) the concentration of vitamin C must be sufficiently high ($\sim$10%); (3) vitamin C must be stable; and (4) the pH of the formulation must be less than the pKa of vitamin C (i.e. 4.2). The optimum pH of the formulations is $\sim$3.5 [24]. In order to attain an effective vitamin C topical formulation with the aforementioned requirements, developing formulations that enhance the stability of vitamin C is required. One way to increase the stability of vitamin C is to chemically modify its structure by esterifying the hydroxyl groups with organic or inorganic long chain acids [219]. Another method is to encapsulate vitamin C within nanoparticles that have the potential to protect the sensitive bioactive compound from

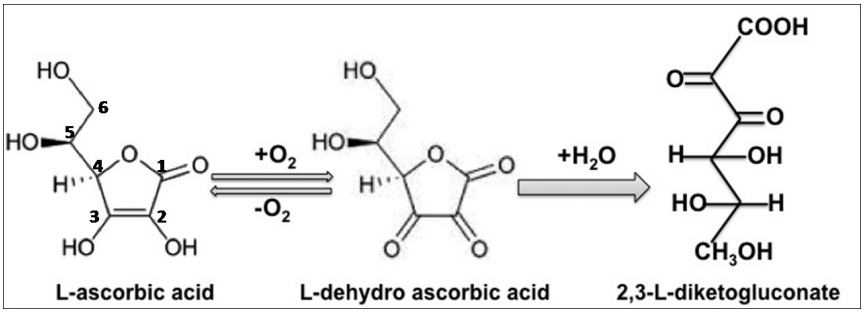

Figure 6.1: Degradation pathway of vitamin C in aqueous solutions.

chemical and enzymatic degradation during storage [27].

Recently there has been interest in using renewable resources for the design of various novel products. The abundance and biodegradability of natural polymers has led to extensive research in this field. There is an ever-increasing desire to design novel carriers for the delivery of bioactive compounds to increase their stability and improve their properties for enhanced patient compliance. CNC is practically non-toxic, biocompatible, and biodegradable, which makes it an excellent candidate for biomedical applications [5]. CS is an amino polysaccharide with interesting biological properties such as biocompatibility, biodegradability, antimicrobial, and wound healing properties [89]. The protonation of amine groups in acidic media imparts positive charges onto CS, allowing the binding of different anionic compounds. CS has a great potential for manipulating the loading and release profiles of bioactive compounds. The antioxidant activity of CS and its derivatives has also been studied by researchers over the past several years [220, 221]. Low molecular weight CS (CS_{OS}) is known to have better water solubility and higher antioxidant properties [16, 222]. Due to the beneficial properties of CNC and CS_{OS} and the numerous advantages of designing novel carrier systems based on abundant natural polymers, we discussed the chemical grafting of CS_{OS} onto the surface of CNC via a peptidic coupling reaction in Chapter 4.

Several studies reported in the literature on the applications of CS nanoparticles for the delivery of vitamins [28]. Modified CS nanoparticles have been reported as carriers for vitamin C. N-acyl CS modified with different acyl chain lengths has been used to load vitamin C via a sonication method [223]. CS nanoparticles have also been prepared by ionic gelation of CS with tripolyphosphate (TPP). In one study, Jang and coworkers studied the characteristics and stability of vitamin C-loaded CS nanoparticles in aqueous solutions during heat processing. Their results showed an increase in the stability of vitamin C during heat processing and suggested the potential applications of vitamin C loaded CS

nanoparticles as enhanced antioxidants due to the continuous release of vitamin C in food processing [29]. CS nanoparticles have also been prepared by similar methods by Alishahi and coworkers to encapsulate vitamin C and to increase its stability [224].

In this study, we aim to increase the stability of vitamin C via the formation of complexes between vitamin C and CS_{OS} grafted CNC via ionic gelation resulting in CNCS/VC complexes. The potential benefits of these complexes in topical applications would be the following: (i) CNC-CS_{OS} particles will both act as a carrier for vitamin C and increase its stability; (ii) CNC interfaces will reduce the oxidation-induced degradation of vitamin C by acting as barriers for oxygen reaching encapsulated vitamin C in the complexes [26]; (iii) CS has interesting biological properties such as antioxidant, antibacterial, hemostatic and wound healing properties suitable for topical cosmeceutical applications; (iv) CNC-CS_{OS} has high antioxidant activity, pertaining to a dual antioxidant activity of CNCS/VC i.e. after the release of vitamin C from the complex as a fast and potent antioxidant, the carrier CNC-CS_{OS} also possesses antioxidant properties leading to a synergic and stable antioxidant effect.

6.2 Experimental Section

6.2.1 Materials

A freeze-dried CNC sample was supplied by FPInnovations. CS_{OS} (average Mn 5000 Da, DD ∼75%) was purchased from Sigma-Aldrich. For TEMPO-mediated oxidation, the following chemicals were purchased from Sigma-Aldrich: TEMPO (98%), NaOCl (reagent grade, 10-15% available chlorine), NaBr (99.0%), NaOH (1 N) standard solution, HCl (1 N) standard solution, and methanol. For the amide coupling reaction, crosslinkers EDC (commercial grade) and NHS (98%+) were purchased from Fluka and Acros Organics, respectively. As received MES (2-(N-morpholino) ethanesulfonic acid, >99%) purchased from Sigma was used as a buffer for the EDC crosslinking reaction. For antioxidant studies, stable free radical 1,1-diphenyl-2-picryl hydrazyl (DPPH) was purchased from Aldrich. Alcohol reagent consisting of 90% ethanol, 4.6% methanol and 5.1% isopropyl alcohol was purchased from Fisher Scientific. Vitamin C (L-Ascorbic Acid) was obtained from Sigma-Aldrich. For the complexation, acetic acid (>99.7%) and sodium tripolyphosphate (TPP, technical grade 85%) were purchased from Sigma-Aldrich. Millipore de-ionized (D.I.) water was used for all experiments and sample preparations.

6.2.2 Synthesis of CNC-CS_{OS}/Vitamin C Complex (CNCS/VC)

The synthesis and characterization of CNC-OX and CNC-CS_{OS} were described in detail in Chapter 4. To 10 mL 0.1 wt% CNC-CS_{OS} in acetic acid (6 v/v %), 4 mL of freshly prepared vitamin C in D.I. water (1 mg/mL) was added while stirring. After 5 minutes, 6 mL of sodium TPP (5 mg/mL) was added dropwise to the solution using a syringe. The pH of the mixture was kept at ∼3, while in some experiments the pH was adjusted to ∼5. The mixture was then vortexed for 5 minutes and sonicated for 10 minutes. Oxygen in the system was removed by bubbling argon into the vessel for 10 minutes. The vessel was then covered in aluminum foil and the mixture was left to stir overnight in darkness.

6.2.3 Transmission Electron Microscopy (TEM)

TEM images of CNC-CS_{OS} and CNCS/VC were recorded using a Philips CM10 TEM with 60 keV acceleration voltages. A few drops of 0.01 wt% aqueous samples were deposited on a carbon-formvar film on 200 mesh copper grids. Excess solvent was removed from the grids placed on top of a filter paper to minimize the agglomeration of particles and the grids were dried overnight.

6.2.4 Vitamin C Encapsulation Efficiency and Drug Loading

In order to remove the unbound vitamin C and calculate the encapsulation efficiency and loading of vitamin C, CNCS/VC solution was passed through an ultrafiltration stirred cell (Millipore Corporation, Bedford, USA) with filters having a cut-off pore size of 25 nm (Millipore, VSWP, Ireland). The concentration of free vitamin C in the filtrate was measured at 265 nm using an Agilent 8453 UV-visible spectrophotometer and based on the vitamin C calibration curve. A fresh stock solution containing 100 μg/mL of vitamin C was prepared by dissolving 1.5 mg of vitamin C in 15 mL of D.I. water. The solution was stored in a glass-stoppered bottle, which was covered in an aluminum foil. Standard solutions of different concentrations (50, 25, 18.75, 12.5, 10, 7.5, 5 and 1 μg/mL) were prepared by diluting the stock solution in D.I. water and the absorbance of these solutions was recorded at a wavelength of 265 nm by an Agilent 8453 UV-visible spectrophotometer. The encapsulation efficiency and drug loading were determined indirectly by measuring the free vitamin C in the filtrate using the following expressions:

$$\text{Encapsulation Efficiency (\%)} = \frac{[\text{Vitamin C}]_{\text{total}} - [\text{Vitamin C}]_{\text{filtrate}}}{[\text{Vitamin C}]_{\text{total}}} \times 100 \qquad (6.1)$$

$$\text{Drug Loading (\%)} = \frac{\text{Weight of Vitamin C loaded}}{\text{Weight of CNC-CS}_{\text{OS}}} \times 100 \tag{6.2}$$

6.2.5 Differential Scanning Calorimetry (DSC)

Calorimetric analyses were performed using a Q2000 calorimeter (TA Instruments Inc., USA). Approximately 2 mg of the samples (vitamin C, CNC-CS_{OS}, and $CNCS/VC_{pH=5}$) were placed in standard aluminum pans and sealed by a hermetic aluminum lid. The samples were heated from 20 $^{\circ}C$ to 300 $^{\circ}C$ with a heating rate of 10 $^{\circ}C$/min under nitrogen atmosphere.

6.2.6 UV Spectrophotometry For Proving the Complex Formation

Spectra of 0.1 wt% vitamin C, CNC-CS_{OS}, and CNCS/VC in quartz cuvettes (Hellma Analytics) were recorded at 265 nm using an Agilent 8453 UV-visible spectrophotometer.

6.2.7 Vitamin C *In Vitro* Release Studies

2 mL of CNCS/VC complex was placed in a SnakeSkin dialysis tube (Pierce Biotechnology Inc., Mw cut off: 3500 Da) and immersed in 20 mL of phosphate buffer saline (PBS, pH=7.4) while being gently stirred in the dark in a closed container. At given time intervals, 1 mL aliquots were removed for analysis and replaced with the same volume of fresh release medium. Based on the vitamin C calibration curve, the samples were assayed for vitamin C content. In order to compare the stability of vitamin C loaded in the CNCS/VC complex, a known solution of vitamin C with the same amount of vitamin C loaded in the complexes was placed in a SnakeSkin dialysis tube and immersed in 20 mL PBS buffer as a control.

6.2.8 Isothermal Titration Calorimetry (ITC)

The Microcal VP-ITC instrument was used to study the interactions between vitamin C and CNC-CS_{OS} at pH 3 and pH 5. Once the thermal equilibrium was reached, the titrations were performed at a constant temperature by injecting the titrant (vitamin C 100 mM) from a $\sim$282 μL injection syringe into a 1.4551 ml sample cell filled with 0.1 wt%

CNC-CS_{OS} solution prepared at the same pH. An injection schedule was automatically performed using an interactive software after setting the number of injections, volume of each injection, and time between each injection. Blank titrations were performed by injecting the same aliquot of vitamin C into water at the same pH to obtain the heat of dilution.

6.2.9 DPPH Radical Scavenging Activity

The antioxidant activity of the samples was measured by a slightly modified DPPH scavenging activity method [225]. To study the scavenging activity of samples, 1 mL test samples at different concentrations were diluted with 1.85 mL of alcoholic reagent and the absorbance was measured as blank. CNC-CS_{OS} samples were prepared in acetic acid (6% v/v) to ensure complete solubility. 150 μL of freshly prepared methanolic solution of DPPH (1 mg/mL) was then added to the solutions. The reaction mixture was shaken well and incubated for 30 minutes at room temperature in darkness. The absorbance of the resulting solutions was determined at 517 nm against a blank using the Agilent 8453 UV-visible spectrophotometer. Solvents with DPPH were used as a control. Each sample was run in triplicate, and the values were averaged. The radical scavenging activity was measured by the reduction in the absorbance of DPPH and it was calculated using the following equation:

$$\text{DPPH Scavenging Activity (\%)} = \frac{\mathrm{A_{Control}} - \mathrm{A_{Sample}}}{\mathrm{A_{Control}}} \times 100 \tag{6.3}$$

6.2.10 Antioxidant Activity Kinetics

Antioxidant kinetics of CNC samples were studied by measuring the rate constant (k) of each scavenging activity reaction using the same DPPH protocol [226]. 1 mL sample solutions (0.1 wt%) were diluted with 1.85 mL of alcoholic reagent and then 150 μL of freshly prepared methanolic solution of DPPH (1 mg/mL) was added to the solutions. The solution was fully mixed and the reduction in absorbance was determined at 517 nm at time 0, and different time intervals over a period of 200 minutes using a Cary 100 Bio UV-visible spectrometer. All experiments were repeated in triplicate. The antioxidant rate constant (k) was calculated using the following equation:

$$-kt = \ln \frac{\mathrm{A}_\infty - \mathrm{A}_t}{\mathrm{A}_\infty - \mathrm{A}_0} \tag{6.4}$$

where, t is time and A_∞, A_t, A_0 are the absorbances at infinite time, time t, and at time zero, respectively.

6.3 Results and Discussion

6.3.1 Synthesis of CNC-CS_{OS}/Vitamin C Complex (CNCS/VC)

The structure of CNC-CS_{OS} and vitamin C along with a schematic representing the mechanism of formation of CNCS/VC is shown in Figure 6.2. The CNCS/VC complexes were produced spontaneously by the ionotropic gelation between vitamin C, TPP and positively charged amino groups on CS_{OS} [224]. Unlike other crosslinking agents (formaldehyde or gluteraldehyde), TPP is non-toxic [227, 228]. CS has protonable amine groups, which possess positive charges at a pH below 6, and vitamin C possesses many electrophilic groups. Four hydroxyl groups with different acidities are present in the structure of vitamin C in positions 2, 3, 5, and 6 giving rise to varying pKa values for each hydroxyl group. The strongest acidity belongs to the hydroxyl group in position 3 (pKa=4.2). Hydroxyl groups in position 2 possess a pKa value of 11.6. Hydroxyl groups in positions 5 and 6 act as secondary and primary alcoholic residues, respectively [229]. CNCS/VC complexes are formed through non-covalent bonds such as H-bonds and hydrophobic interactions [230]. Based on the Lewis acid-base theory, the acidic hydroxyl group in position 3 of vitamin C is expected to react with the amino groups of chitosan [231]. At pH 5, additional electrostatic interactions between the amino groups of CS_{OS} in CNC-CS_{OS} and deprotonated hydroxyl groups in vitamin C are expected.

6.3.2 TEM Analyses

The TEM images of CNC-CS_{OS} and CNCS/VC complex are shown in Figure 6.3A and B, respectively. It can be seen that CNCS/VC complexes were larger compared to the loose network structures of CNC-CS_{OS} due to ionic gelation.

6.3.3 Vitamin C Encapsulation Efficiency and Drug Loading

The encapsulation efficiency (EE%) and drug loading (DL%) of vitamin C in CNCS/VC complexes were calculated indirectly by measuring the vitamin C in the filtrate using a vitamin C calibration curve (Figure 6.4). The results based on three measurements are

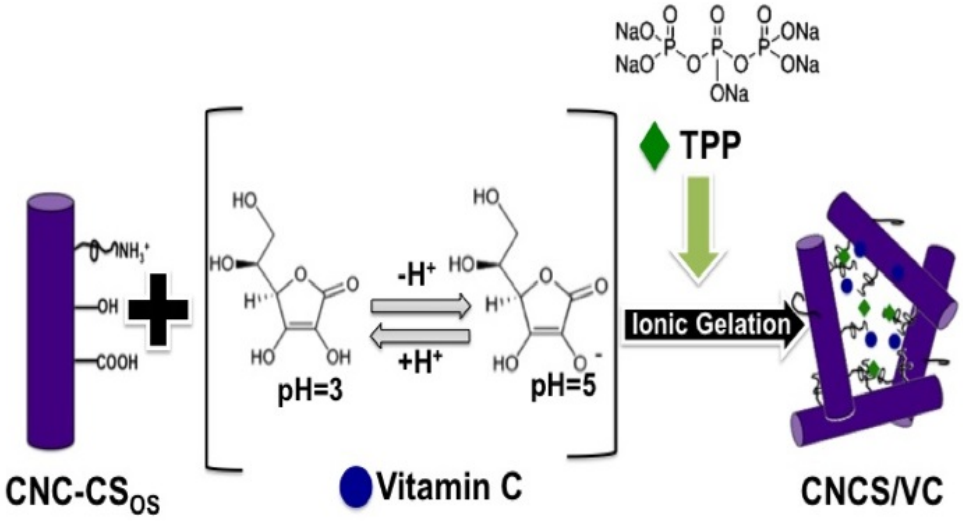

Figure 6.2: Illustration of formation of CNCS-VC complex by ionic gelation

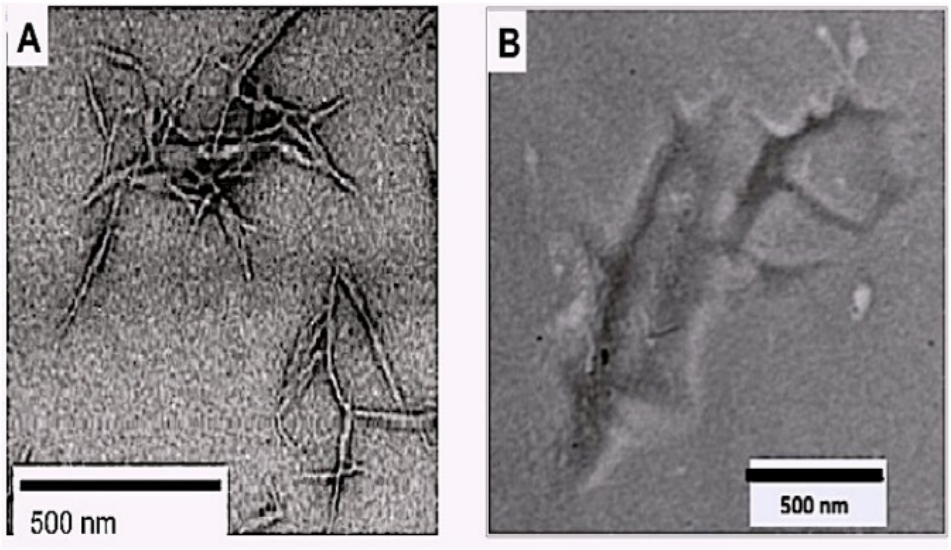

Figure 6.3: TEM images of CNC-CS_{OS} and CNCS/VC complex.

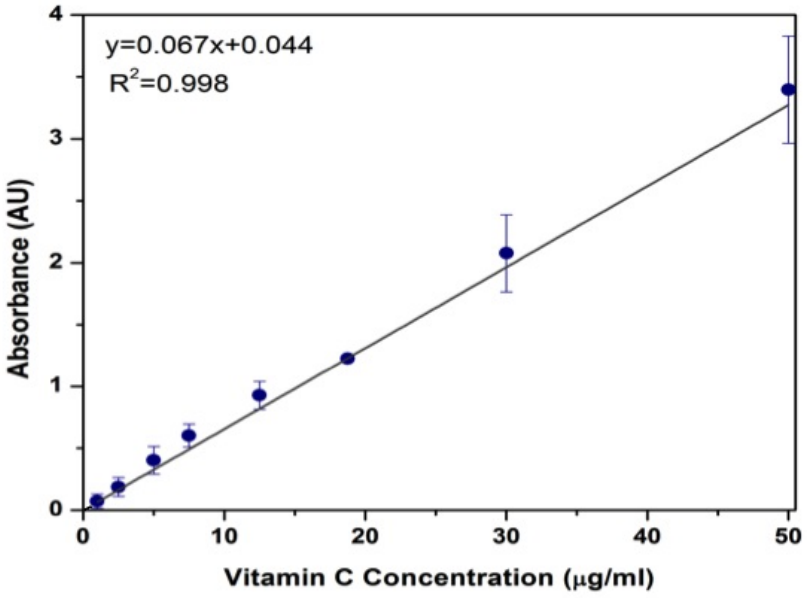

Figure 6.4: Calibration curve of vitamin C.

Table 6.1: Encapsulation Efficiency and Drug Loading of vitamin C in CNCS/VC complexes at pH 3 and pH 5 (n=3)

pH	**EE%SD**	**DL%SD**
3	71.6 ± 6.8	28.6 ± 2.7
5	91.0 ± 1.0	38.4 ± 2.5

summarized in Table 6.1. It can be seen that a higher EE% and DL% of vitamin C was observed at pH 5. The first pKa of vitamin C is at pH 4.2. At pH 3 the hydroxyl groups of vitamin C are protonated and the loading is probably due to the physical entrapment of vitamin C and hydrogen bonding with CNC-CS_{OS}. At pH 5, vitamin C is partially deprotonated, resulting in an additional electrostatic interaction between positively charged CNC-CS_{OS} and the negative charge on vitamin C, leading to a higher encapsulation and loading.

6.3.4 Differential Scanning Calorimetry (DSC)

In order to study the physical state of the materials, DSC analyses of pure vitamin C, CNC-CS_{OS}, and CNCS/VC were performed (Figure 6.5). The calorimetric analysis of

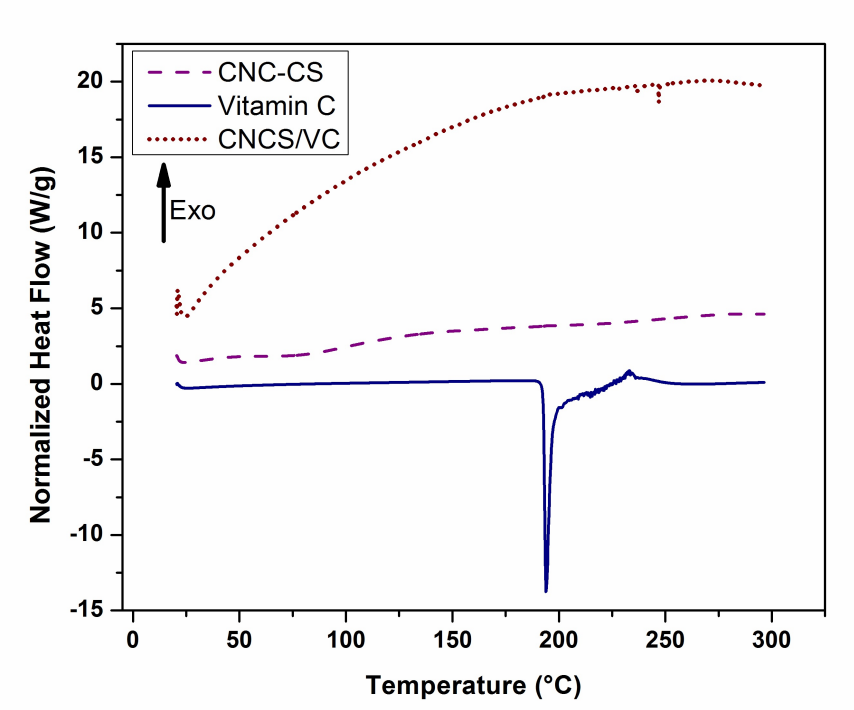

Figure 6.5: DSC thermograms of CNC-CS_{OS}, vitamin C, and CNCS/VC complex.

pure vitamin C displayed a sharp endothermic peak due to the melting point of vitamin C molecules at 190 °C. The absence of the endothermic peak of vitamin C in the CNCS/VC complex indicated the ionic interactions between vitamin C and CNC-CS_{OS} and the complex formation [232]. This phenomenon can also be attributed to the miscibility of vitamin C complexed with CNC-CS_{OS} [233].

6.3.5 UV Spectrophotometry for Proving the Complex Formation

Further confirmation of the insertion of vitamin C in CNC-CS_{OS} was obtained by comparing UV spectra of pure vitamin C, CNC-CS_{OS}, and CNCS/VC (Figure 6.6). It can be seen that vitamin C displayed an absorption peak at 265 nm. The CNCS/VC UV spectrum clearly showed the absorption peak of vitamin C, which is indicative of the presence of vitamin C in its native form. In the presence of amine moieties, the lactone ring in the structure of vitamin C can be subjected to ring opening. The presence of the vitamin C absorption peak in the CNCS/VC complex suggested that vitamin C was not subject to ring opening during the complex formation [231]. The shift in the absorption peak of vitamin C to lower wavelengths in the complex and its broadening could be attributed to

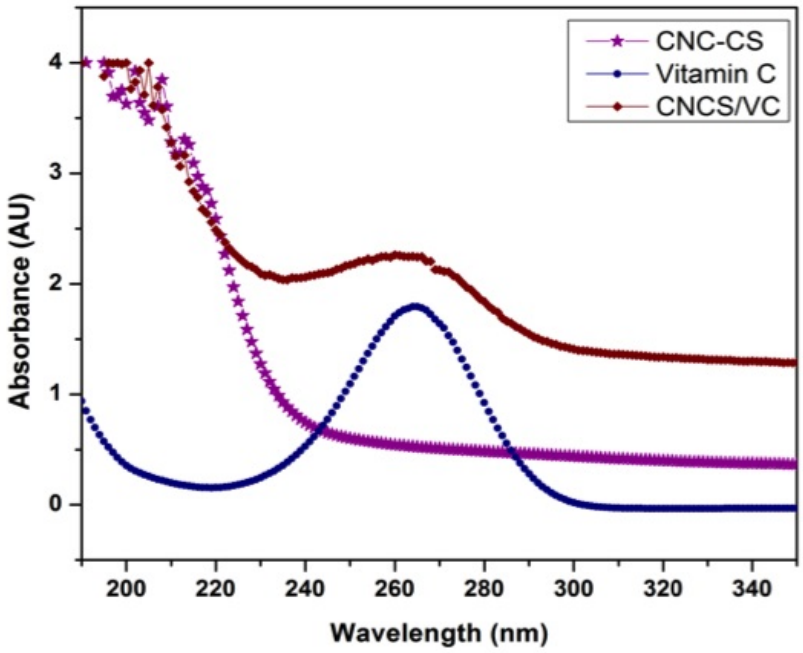

Figure 6.6: UV spectrum of CNC-CS_{OS}, vitamin C and CNCS/VC.

the complexation between vitamin C and reactive groups of CNC-CS_{OS}. Similar results were reported in the literature [234].

6.3.6 Vitamin C *In Vitro* Release Studies

The cumulative *in vitro* vitamin C release from CNCS/VC loaded at pH 3 and 5 is shown in Figure 6.7. The *in vitro* release profile of vitamin C loaded at pH 5 showed a more controlled release profile and a higher percentage of vitamin C was released. This could be attributed to the higher loading of vitamin C in the complex at pH 5, which resulted in a higher concentration gradient and faster diffusion. The size of vitamin C is significantly smaller than CNC-CS_{OS} and vitamin C molecules can easily diffuse through the pores and from the surface of the carrier [29]. A control solution of vitamin C containing the same amount of vitamin C loaded at pH 3 in CNCS/VC complexes was placed in a dialysis tube and immersed in PBS solution. The controlled vitamin C solution diffused rapidly from inside the dialysis tube to the release medium and degraded over time; however, based on Figure 6.7, vitamin C loaded in CNCS/VC was released gradually over 20 days from the complex and was more stable. Our results are in accordance with the results reported by Alishahi and coworkers, where they compared the shelf life of free vitamin C with

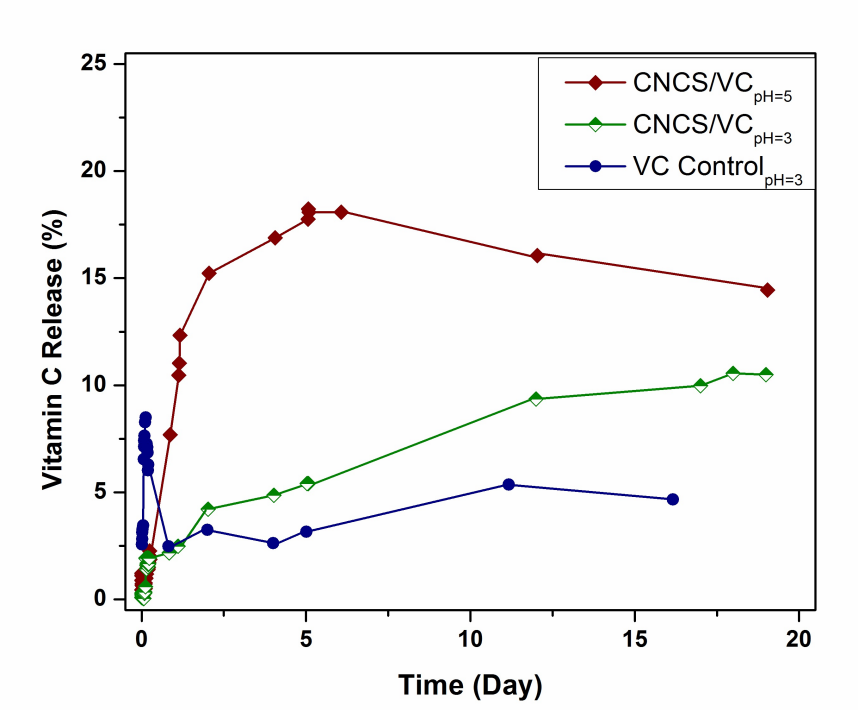

Figure 6.7: Vitamin C *in vitro* release profile from CNCS/VC (prepared at pH 5 and 3) and control vitamin C (pH 3) in PBS pH=7.4.

encapsulated vitamin C in CS nanoparticles. Encapsulated vitamin C was more stable where a $\sim$ 70% reduction in free vitamin C concentration was observed over a period of 20 days [235].

6.3.7 Thermodynamics of CNC-CS_{OS} and Vitamin C Interaction

ITC was used to investigate the binding thermodynamics between vitamin C and CNC-CS_{OS} at pH 3 and 5. Figure 6.8 shows the raw ITC data of titrating 100 mM vitamin C into CNC-CS_{OS} at pH 3 and 5 as well as the blanks containing the same concentration of vitamin C titrated into water. The pH of the titrant and CNC-CS_{OS} solutions were adjusted to the same pH values. Our results were reproducible and displayed an unusual behavior. At pH 3, titrating vitamin C into water resulted in an exothermic heat of dilution plot (plot a). However, when titrating vitamin C into CNC-CS_{OS} at pH 3, we observed small exothermic peaks with a shift in the baseline (plot b). At pH 5, raw ITC plot of titrating vitamin C into water displayed a significant baseline drift with the first titration points being exothermic and the final points being endothermic (plot c). This could be due to the instability of vitamin C at pH 5, leading to a continuous change in the characteristics

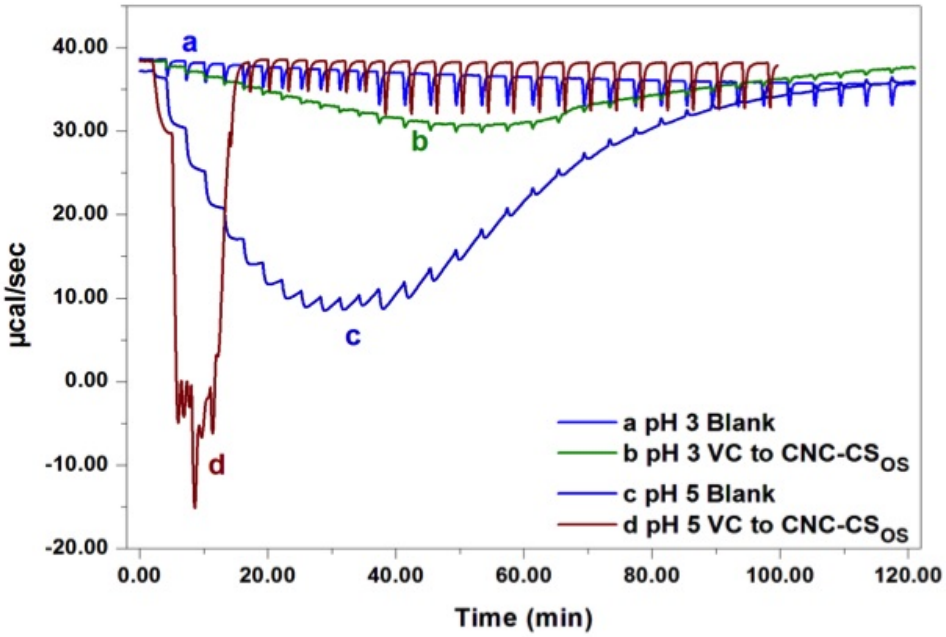

Figure 6.8: Raw ITC data for titrating 100 mM vitamin C (VC) into (a) water at pH 3, (b) water at pH 5, (c) CNC-CS_{OS} at pH 5 and (d) CNC-CS_{OS} at pH 3.

of the titrant, i.e. vitamin C. Titrating vitamin C into CNC-CS_{OS} at pH 5 resulted in an interesting and reproducible thermogram (plot d). The few first titrations resulted in large exothermic peaks with a drastic baseline drift. The fact that the equilibrium was not re-established after the first few injections could indicate that the binding of vitamin C to CNC-CS_{OS} at pH 5 was affected by a slow aggregation-like process [236]. However, as seen in Figure 6.8d, after a fixed number of injections, and once the complex between vitamin C and CNC-CS_{OS} was formed, the equilibrium was re-established and there was no drift in the baseline. The large exothermic peaks when titrating vitamin C into CNC-CS_{OS} at pH 5 compared to pH 3 could be attributed to ionic interactions between negatively charged vitamin C and positively charged CNC-CS_{OS}. This result could explain the higher binding efficiency for vitamin C at pH 5 reported in Table 6.1.

6.3.8 DPPH Radical Scavenging Activity

An important antioxidant mechanism involves the scavenging of hydrogen radicals. DPPH possesses a hydrogen radical with a characteristic absorbance of 517 nm. As antioxidants react with DPPH radical, the absorbance at 517 nm decreases and the purple color of the

DPPH solution changes to yellow [225]. Therefore, by measuring the absorbance using a spectrophotometer, the progress of the reaction can be analyzed [237]. In this study, DPPH was used to deduce the antioxidant activity of samples. The scavenging activity (SA%) of the samples on DPPH at various concentrations is shown in Figure 6.9. Our results showed that oxidizing the CNC enhanced its antioxidant activity. Also, the SA% of CNC-CS_{OS} was much higher than the SA% of the physical mixture of its precursors (CNC-OX + CS_{OS}). The scavenging activity of samples depends on their capacity to donate an electron to DPPH. This property is a function of different sizes of electron-cloud density and its accessibility to DPPH [238]. The higher SA% of CNC-CS_{OS} compared to its precursors could be due to the orientation of the functional groups of CS chain after the chemical conjugation on the CNC surface leading to increased accessibility of the functional groups to react with the DPPH radical. The decrease in the SA% of CNC-CS_{OS} at 1 wt% concentration might be attributed to the slight reduction in the solubility of CNC-CS_{OS}, leading to a lower antioxidant activity. Moreover, the lower mobility of CNC-CS_{OS} at high concentrations might increase the possibility of inter- and intramolecular bonding that minimized the exposure of active functional groups that were responsible for the scavenging activity.

The SA% of 0.1 wt% CNCS/$VC_{pH=5}$ and 0.1 wt% vitamin C was measured over 4 consecutive days (Figure 6.10). It can be seen that the SA% of the vitamin C solution slightly decreased over the course of 4 days due to the instability of vitamin C. The SA% of CNCS/$VC_{pH=5}$ increased over time as vitamin C was being released from the complex. The results are in accordance with the vitamin C release profile observed in Figure 6.7. The low SA% of CNCS/$VC_{pH=5}$ on day 1 might be due to the involvement of the functional groups of CNC-CS_{OS} with vitamin C in the complex preventing the functional groups from reacting with the DPPH radical.

6.3.9 Antioxidant Kinetics Studies

The antioxidant kinetics of CNC samples were studied by monitoring the decay of the absorbance peak of DPPH at 517 nm over time and calculating the rate constants (k). The antioxidant reaction rate has been proposed as another parameter to elucidate the antioxidant activity of various of compounds [239]. As seen in Figure 6.11, CNC-CS_{OS} possessed the largest slope leading to the highest rate constant, and the slope of the first-order kinetic plot of CNC-OX was larger than CNC. DPPH was added in excess and sample concentration determined the rate therefore a first-order plot was applied. The high antioxidant rate constant leading to the fastest antioxidant activity observed for CNC-CS_{OS} might be attributed to the presence of several functional groups (OH, COOH and NH_2) on

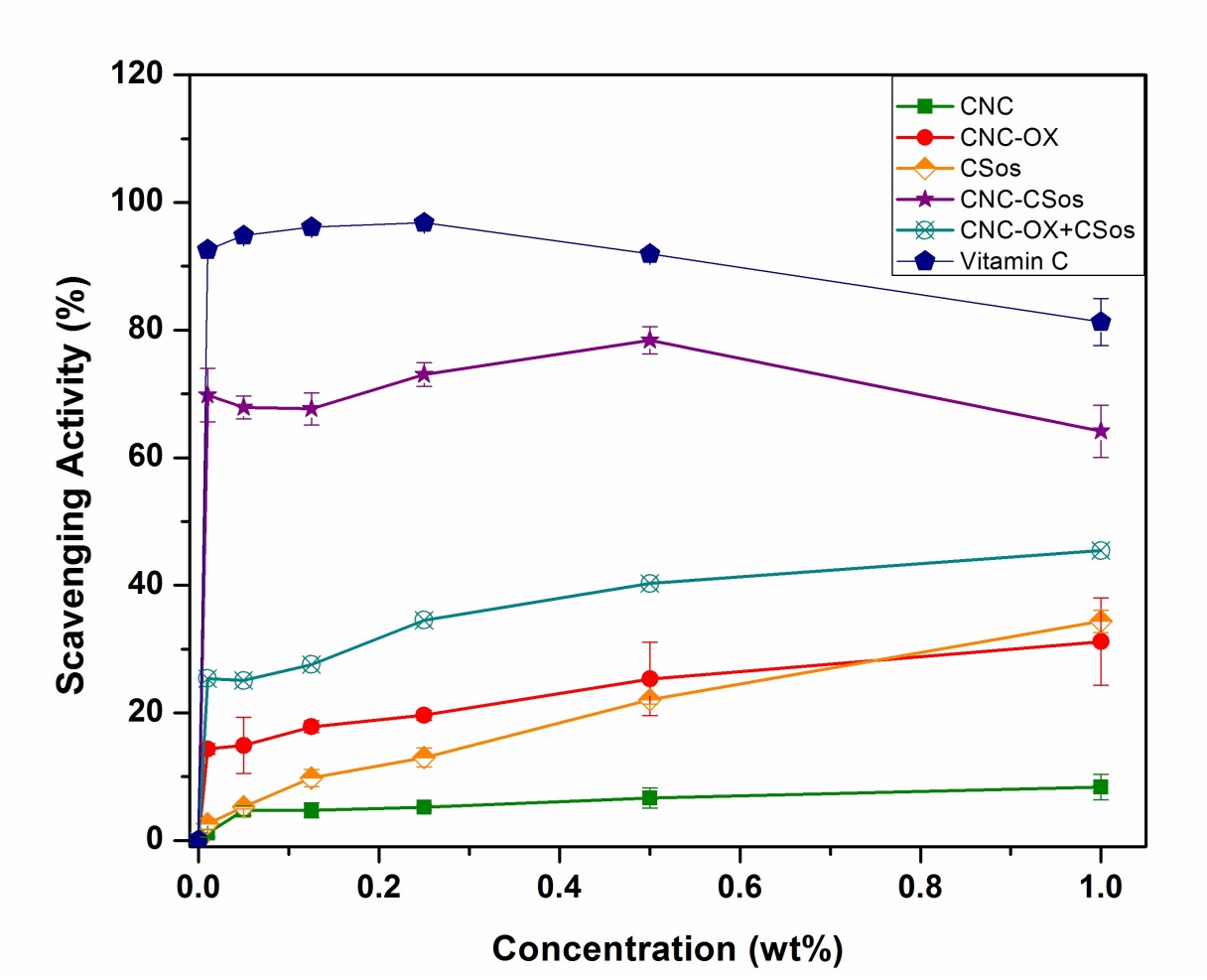

Figure 6.9: Scavenging activity of different samples at different concentrations on DPPH radical (n=3).

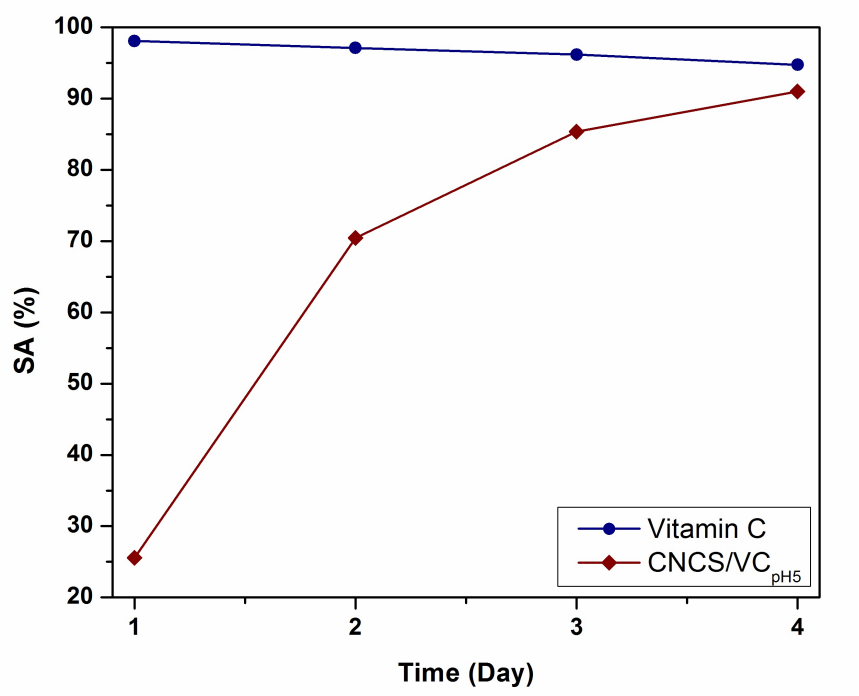

Figure 6.10: Scavenging activity of CNCS/$VC_{pH=5}$ and vitamin C over time.

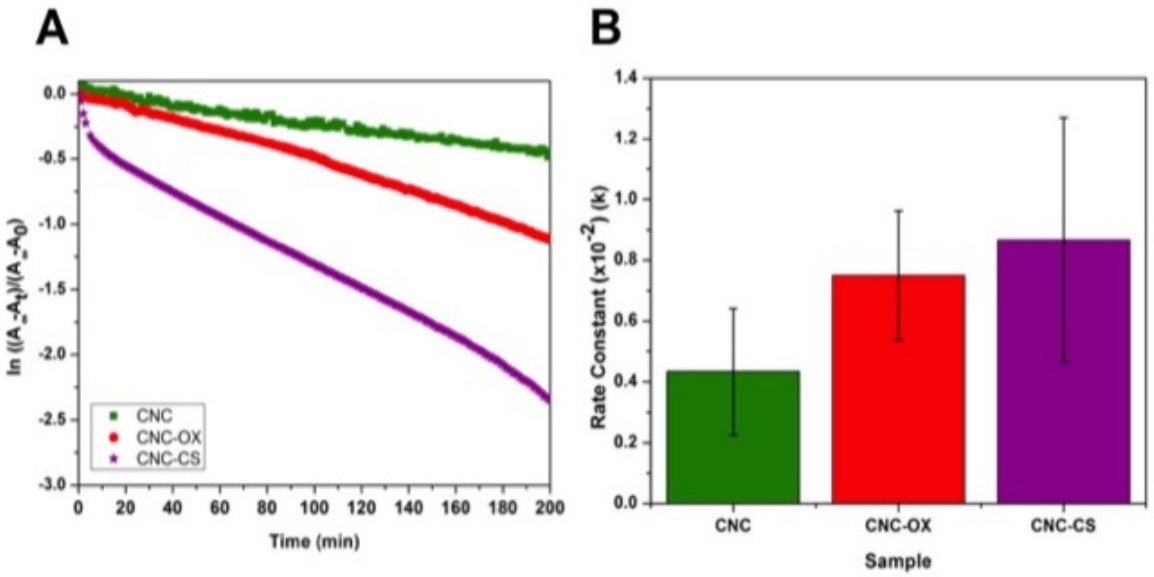

Figure 6.11: (A) Decay of the visible absorbance (517 nm) of a DPPH solution following addition of CNC samples. (B) Estimation of antioxidant rate constant for first H atom abstraction (k) for CNC samples using Eq. 6-4).

the surface of CNC and their synergistic effect in increasing the speed of the scavenging activity.

6.4 Conclusions

An effective and novel antioxidant system was developed by forming complexes between vitamin C and cellulose nanocrystals grafted with chitosan oligosaccharide (CNC-CS_{OS}). CNC-CS_{OS} was first prepared via peptidic coupling by reacting the carboxylic acid groups on oxidized CNC with the amino groups on CS_{OS}. CNCS/VC complexes were then prepared using TPP through the ionic complexation of CNC-CS_{OS} and addition of vitamin C at pH 3 and 5. TEM images showed complexes with a size of approximately 1 μm. DSC and UV spectrophotometry confirmed the presence of vitamin C in the CNCS/VC complexes. The encapsulation efficiency of vitamin C was higher ($\sim$ 91%) at pH 5 compared to pH 3 ($\sim$ 72%). The *in vitro* release of vitamin C from CNCS/VC complexes displayed a sustained release up to 3 weeks with the released vitamin C displaying higher stability

compared to a controlled vitamin C solution. The DPPH method was used to study the scavenging activity and antioxidant kinetics of various CNC samples, CS_{OS}, and vitamin C as control. CNC-CS_{OS} had a higher scavenging activity and antioxidant rate constant compared to oxidized CNC and CS_{OS} and their physical mixture, denoting a synergistic activity against the DPPH radical. Therefore, by loading vitamin C into CNC-CS_{OS} particles, an efficient dynamic antioxidant agent was produced, and vitamin C is released over time with the carrier CS_{OS} also possessing desirable antioxidant properties. The pH, high loading, and stability of vitamin C in CNCS/VC complexes make it an excellent candidate for applications in topical cosmeceuticals.

Chapter 7

Original Contributions and Recommendations

7.1 Original Contributions to Research

Due to the need to reduce the dependence on fossil fuels and diminish environmental pollution, developing novel, biocompatible and biodegradable systems for biomedical applications with unique properties based on green renewable materials is extremely desirable. This thesis aims at developing novel functional materials based on CNC for biomedical applications by exploring the combination of engineering techniques and chemical synthesis. This thesis includes the following parts: (i) amine functionalization of CNC; (ii) surface modification of CNC with CS_{OS}; (iii) evaluating the potentials of CNC, CNC-OX and CNC-CS_{OS} as potential carriers for two cationic model drugs; and (iv) investigation of antioxidant properties of CNC samples and exploring the effectiveness of CNC-CS_{OS} in the delivery of vitamin C. The main findings of each section are summarized in the following:

Preparation, optimization and characterization of amine functionalized cellulose nanocrystals: The surface of CNC was functionalized by amine groups with a high yield using an etherification reaction. Ammonium hydroxide was first reacted with epichlorohydrin (EPH) to produce 2-hydroxy-3-chloro propylamine (HCPA), which was then reacted with the hydroxyl groups on CNC. Optimization of reactant ratios, time, temperature, and refluxing the reaction increased the amine content drastically compared to the results published in literature. Centrifugation of the amine functionalized CNC and studying the supernatant confirmed that there were aminated polymers present due to the

polymerization of EPH. The purified amine CNC found in the sediment possessed a high amine content of 0.6 mmol/g. The amine functionalized CNCs were characterized using elemental analysis, potentiometric titration, and TEM. The positive zeta potential of the amine functionalized CNC at low pH led to increased relative viscosity measurements due to the presence of electrostatic interactions.

Surface modification and characterization of cellulose nanocrystals grafted with chitosan oligosaccharide: A peptidic coupling reaction was used to chemically graft CS_{OS} onto TEMPO-oxidized CNC (CNC-OX). FT-IR and potentiometric titration revealed a degree of oxidation of 0.28 for CNC-OX. The reduction of the C=O peak of CNC-OX in CNC-CS_{OS} in FT-IR and ^{13}C NMR spectra together with the appearance of new amide bonds confirmed the success of the chemical grafting. Moreover, due to the formation of new covalent bonds, an increase in the thermal decomposition temperature of CNC-CS_{OS} was observed. Zeta potential measurements showed a reversal of surface charge for CNC-CS_{OS} from +40 mV to -40 mV when the pH was increased from 4 to 10. AFM and TEM images revealed a loose network structure for CNC-CS_{OS} with a size of approximately 500 nm.

Study of the interactions of two cationic model drugs with cellulose nanocrystals and *in vitro* drug release studies: Two cationic model drugs, namely procaine hydrochloride (PrHy) and imipramine hydrochloride (IMI), were loaded onto CNC and two of its derivatives, CNC-OX and CNC-CS_{OS}. Isothermal calorimetry, transmittance, and zeta potential measurements were used to elucidate the complexation between the drugs and CNC samples. The strongest interaction was observed between IMI and CNC-OX, leading to a large exothermic peak observed in ITC thermogram, which was further confirmed by visual observation of the complexes. Stable drug selective membranes with fast response were prepared for each drug molecule. A drug selective electrode was used to quantify the binding efficiency of the drugs to CNC samples and to monitor *in vitro* release profiles. Different release profiles at varying pH conditions were observed due to the pH responsive properties of the systems and changes in the solubility of drugs. Both drugs were released relatively fast from CNC samples due to the ion-exchange effect. The presence of CS_{OS} chains on the surface of CNC in CNC-CS_{OS} displayed a more sustained release profile at higher pH while increasing the release rate of the cationic drugs at lower pH due to its positive charge. It is believed that these immediate drug release systems could have potential applications in the delivery of local anesthetics and the treatment of wounds in the oral cavity.

Investigating the antioxidant properties of CNC and the potentials of CNC-CS_{OS} as a carrier for the delivery of vitamin C: The antioxidant properties of CNC, CNC-OX and CNC-CS_{OS} were studied against the DPPH radical. It was shown that by grafting CS_{OS} onto CNC, a synergistic antioxidant activity was observed. This could be due to the increased availability of the functional groups in the grafted CS_{OS}. Studying the antioxidant kinetics also revealed a rapid antioxidant activity for CNC-CS_{OS}. Moreover, CNCS/VC complexes were formed between vitamin C and CNC-CS_{OS} via an ionic gelation procedure using TPP at pH 3 and 5. The complexes were studied by TEM, UV spectrophotometry, and DSC. A higher encapsulation efficiency of ∼91% was calculated at pH 5 compared to ∼72% at pH 3. Strong exothermic peaks observed in ITC studies at pH 5 suggested that this could be attributed to additional electrostatic interactions at pH 5. Vitamin C was released gradually from CNCS/VC complexes over 3 weeks and was more stable compared to the controlled vitamin C solution. The stability of vitamin C in the presence of CNC-CS_{OS} was also observed in the ITC plots. Our results showed that the high and fast antioxidant properties of CNC-CS_{OS} make it an excellent candidate for the encapsulation and delivery of vitamin C in topical cosmeceutical formulations. It is speculated that once the vitamin C is released from its carrier (i.e. CNC-CS_{OS}), not only is it more stable, but also additional antioxidant properties can be derived from CNC-CS_{OS}.

7.2 Recommendations for Future Studies

Based on the results from this doctoral research, the following recommendations are proposed for further studies. In the present research, amine functionalized CNC with high yield was prepared and characterized (Chapter 3). Amine CNC can be further functionalized with various biomolecules for different applications. Attempts have been made to synthesize and characterize amine CNC grafted with gallic acid (GA). The chemical structure of GA (3,4,5-trihydroxy benzoic acid), a natural antioxidant found in plants, such as green tea is shown in Figure 7.1 [240]. The carboxylic acid group in the structure of GA allows the possibility of a peptidic coupling reaction with amine groups such as CS [241]. The antioxidant and antibacterial properties of amine CNC-GA need to be explored. Preliminary studies on the conjugation of GA onto CNC-CS_{OS} has also been explored. Comparing the antioxidant properties of GA grafted onto amine CNC surface to those grafted on CS_{OS} chains on the surface of CNC will shed light on the importance of the physical orientation of the antioxidant molecules in the presence of CNC and their synergistic properties.

Chitosan oligosaccharide grafted onto CNC (CNC-CS_{OS}) was synthesized and fully characterized (Chapter 4). This robust novel system was explored as a carrier for two

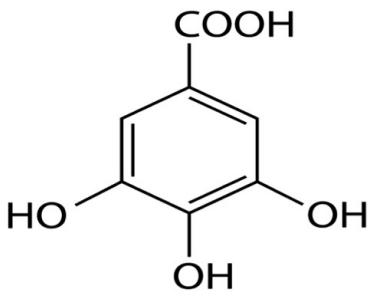

Figure 7.1: Chemical structure of gallic acid (GA).

model cationic drugs (i.e. IMI and PrHy) in Chapter 5. The interactions between these model drugs and CNC-CS_{OS} were investigated using ITC and the *in vitro* drug release profiles were obtained using drug selective electrodes. It is believed that CNC-CS_{OS} can be used for the delivery of a wide range of chemical compounds. CNC-CS_{OS} would form hydrophobic interactions with compounds due to its carbon backbone. Also, depending on the pH CNC-CS_{OS} can be positively or negatively charged which allows the interaction with cationic and anionic compounds. At low pH where the amino groups on CS_{OS} are protonated, the particles are positively charged and negatively charged chemicals can be loaded via electrostatic interactions. Increasing the pH, will deprotonate the amino groups and particles will be negatively charged due to the COO^- and OSO_3^- groups. Therefore, the release of the anionic compound would be triggered. The same situation would apply for the loading of cationic compounds at a high pH and triggering the release by reducing the pH. CNC-CS_{OS} can also form hydrogen bonds with many compounds. Drug selective electrodes can be prepared for a model anionic drug and the potentials of CNC-CS_{OS} as a carrier for anionic drugs can be investigated. Moreover, the pH triggered drug release of the cationic and anionic model drugs can be investigated. The antibacterial properties of CNC-CS_{OS} against gram-positive and gram-negative bacteria can also be explored.

Due to the film forming properties of CNC, thin films of CNC-CS_{OS} can be prepared by different methods such as free casting and spin coating. The physical properties of the thin films in terms of adhesion, friction, and contact angle can be investigated. Furthermore, different drugs can be loaded in the thin films and the *in vitro* release profiles can be studied. Given the mucoadhesive properties of CS, mucoadhesion tests can be performed to identify this property. CNC-CS_{OS} thin films with antibacterial, mucoadhesive, and high drug loading could have potential applications in buccal delivery for treatment of problems in the oral cavity.

CNC-CS_{OS} was used to encapsulate unstable vitamin C and the antioxidant properties of CNC and its derivatives were investigated against DPPH radical (Chapter 6). The antioxidant properties of CNC and its derivatives need to be investigated against other free radicals such as hydroxyl and superoxide radicals. Furthermore, the long-term stability of CNCS/VC complex and its antioxidant activity should to be investigated.

References

[1] Seyedeh Parinaz Akhlaghi, Baoliang Peng, Zhaoling Yao, and Kam Chiu Tam. Sustainable nanomaterials derived from polysaccharides and amphiphilic compounds. *Soft Matter*, 9(33):7905–7918, 2013.

[2] David A LaVan, Terry McGuire, and Robert Langer. Small-scale systems for in vivo drug delivery. *Nature biotechnology*, 21(10):1184–91, October 2003.

[3] Caroline Lemarchand, Ruxandra Gref, and Patrick Couvreur. Polysaccharide-decorated nanoparticles. *European journal of pharmaceutics and biopharmaceutics : official journal of Arbeitsgemeinschaft für Pharmazeutische Verfahrenstechnik e.V*, 58(2):327–41, September 2004.

[4] Arnaud Vonarbourg, Catherine Passirani, Patrick Saulnier, and Jean-Pierre Benoit. Parameters influencing the stealthiness of colloidal drug delivery systems. *Biomaterials*, 27(24):4356–73, August 2006.

[5] M. Miriam de Souza Lima and Redouane Borsali. Rodlike Cellulose Microcrystals: Structure, Properties, and Applications. *Macromolecular Rapid Communications*, 25(7):771–787, April 2004.

[6] My Ahmed Said Azizi Samir, Fannie Alloin, and Alain Dufresne. Review of recent research into cellulosic whiskers, their properties and their application in nanocomposite field. *Biomacromolecules*, 6(2):612–26, 2005.

[7] Merima Hasani, Emily D. Cranston, Gunnar Westman, and Derek G. Gray. Cationic surface functionalization of cellulose nanocrystals. *Soft Matter*, 4(11):2238, 2008.

[8] Latifah Jasmani, Samuel Eyley, Rachel Wallbridge, and Wim Thielemans. A facile one-pot route to cationic cellulose nanocrystals. *Nanoscale*, 5:10207–10211, 2013.

[9] Usha Devi Hemraz, Yaman Boluk, and Rajesh Sunasee. Amine-Decorated Nanocrystalline Cellulose Surfaces: Synthesis, Characterization and Surface Properties. *Canadian Journal of Chemistry*, 91(10):974–981, June 2013.

[10] Shuping Dong and Maren Roman. Fluorescently labeled cellulose nanocrystals for bioimaging applications. *Journal of the American Chemical Society*, 129(45):13810–1, November 2007.

[11] Dwaine F Emerich and Christopher G Thanos. Targeted nanoparticle-based drug delivery and diagnosis. *Journal of drug targeting*, 15(3):163–83, April 2007.

[12] K Fleming, D G Gray, and S Matthews. Cellulose crystallites. *Chemistry (Weinheim an der Bergstrasse, Germany)*, 7(9):1831–5, May 2001.

[13] L Zhu, V Kumar, and G S Banker. Examination of oxidized cellulose as a macromolecular prodrug carrier: preparation and characterization of an oxidized cellulose-phenylpropanolamine conjugate. *International journal of pharmaceutics*, 223(1-2):35–47, July 2001.

[14] John K Jackson, Kevin Letchford, Benjamin Z Wasserman, Lucy Ye, Wadood Y Hamad, and Helen M Burt. The use of nanocrystalline cellulose for the binding and controlled release of drugs. *International journal of nanomedicine*, 6:321–30, January 2011.

[15] S Rossi, M Marciello, M C Bonferoni, F Ferrari, G Sandri, C Dacarro, P Grisoli, and C Caramella. Thermally sensitive gels based on chitosan derivatives for the treatment of oral mucositis. *European journal of pharmaceutics and biopharmaceutics : official journal of Arbeitsgemeinschaft für Pharmazeutische Verfahrenstechnik e.V*, 74(2):248–54, February 2010.

[16] Su Young Chae, Sohee Son, Minhyung Lee, Mi-Kyeong Jang, and Jae-Woon Nah. Deoxycholic acid-conjugated chitosan oligosaccharide nanoparticles for efficient gene carrier. *Journal of Controlled Release*, 109(1-3):330–344, December 2005.

[17] Hezhong Wang, Chen Qian, and Maren Roman. Effects of pH and salt concentration on the formation and properties of chitosan-cellulose nanocrystal polyelectrolyte-macroion complexes. *Biomacromolecules*, 12(10):3708–14, October 2011.

[18] Ruzica Kolakovic, Timo Laaksonen, Leena Peltonen, Antti Laukkanen, and Jouni Hirvonen. Spray-dried nanofibrillar cellulose microparticles for sustained drug release. *International journal of pharmaceutics*, 430(1-2):47–55, July 2012.

[19] Ruzica Kolakovic, Leena Peltonen, Antti Laukkanen, Jouni Hirvonen, and Timo Laaksonen. Nanofibrillar cellulose films for controlled drug delivery. *European journal of pharmaceutics and biopharmaceutics : official journal of Arbeitsgemeinschaft fur Pharmazeutische Verfahrenstechnik e.V*, 82:308–315, June 2012.

[20] Ruzica Kolakovic, Leena Peltonen, Antti Laukkanen, Maarit Hellman, Päivi Laaksonen, Markus B Linder, Jouni Hirvonen, and Timo Laaksonen. Evaluation of Drug Interactions with Nanofibrillar Cellulose. *European journal of pharmaceutics and biopharmaceutics : official journal of Arbeitsgemeinschaft fur Pharmazeutische Verfahrenstechnik e.V*, 85:1238–1244, June 2013.

[21] Xiaodi Guo, Rong-Kun Chang, and Munir A. Hussain. Ion-Exchange Resins as Drug Delivery Carriers. *Journal of Pharmaceutical Sciences*, 98:3886–3902, 2009.

[22] Christopher M Springate, John K Jackson, Martin E Gleave, and Helen M Burt. Clusterin antisense complexed with chitosan for controlled intratumoral delivery. *International journal of pharmaceutics*, 350(1-2):53–64, February 2008.

[23] S. Darr, D.; Combs, S.; Dunston, S.; Manning, T., Pinnell. Topical vitamin C protects porcine skin from ultraviolet radiation-induced damage. *British Journal of Dermatology*, 127:247–253, 1992.

[24] Karen E Burke. Interaction of vitamins C and E as better cosmeceuticals. *Dermatologic therapy*, 20(5):314–21, 2007.

[25] Patricia K Farris. Topical Vitamin C : A Useful Agent for Treating Photoaging and Other Dermatologic Conditions. *American Society for Dermatologic Surgery, Inc.* , 31:814–818, 2005.

[26] Hongyu Piao, Noriho Kamiya, Fude Cui, and Masahiro Goto. Preparation of a solid-in-oil nanosuspension containing L-ascorbic acid as a novel long-term stable topical formulation. *International journal of pharmaceutics*, 420(1):156–60, November 2011.

[27] H Q Mao, K Roy, V L Troung-Le, K a Janes, K Y Lin, Y Wang, J T August, and K W Leong. Chitosan-DNA nanoparticles as gene carriers: synthesis, characterization and transfection efficiency. *Journal of controlled release*, 70(3):399–421, February 2001.

[28] K A Janes, P Calvo, and M J Alonso. Polysaccharide colloidal particles as delivery systems for macromolecules. *Advanced drug delivery reviews*, 47(1):83–97, March 2001.

[29] Hyeon Gyu Jang, Keum-Il; Lee. Stability of Chitosan Nanoparticles for L-Ascorbic Acid during Heat Treatment in Aqueous Solution. *J. Agric. Food Chem*, 56(6):1936–1941, 2008.

[30] Geoffrey Park and John Crank. *Diffusion in polymers*. Academic Press, London, England, 1968.

[31] Theresa M Allen and Pieter R Cullis. Drug delivery systems: entering the mainstream. *Science (New York, N.Y.)*, 303(5665):1818–22, March 2004.

[32] Costas Kaparissides, Sofia Alexandridou, Katerina Kotti, and Sotira Chaitidou. Recent Advances in Novel Drug Delivery Systems. *Journal of Nanotechnology Online*, 2:1–11, 2006.

[33] K Kelley. Nanostructured materials for applications in drug delivery and tissue engineering. *Brain, Behavior, and Immunity*, 22(5):629–629, July 2008.

[34] S Magdassi. Delivery systems in cosmetics. *Colloids and Surfaces A: Physicochemical and Engineering Aspects*, 123-124(97):671–679, May 1997.

[35] Omid C Farokhzad and Robert Langer. Impact of nanotechnology on drug delivery. *ACS nano*, 3(1):16–20, January 2009.

[36] Mansoor M Amiji. Nanotechnology Improving Targeted Delivery Nanotechnology. *Drug Delivery*, pages 53–56, 2007.

[37] Michael Goldberg, Robert Langer, and Xinqiao Jia. Nanostructured materials for applications in drug delivery and tissue engineering. *Journal of Biomaterials Science, Polymer Edition*, 18(3):241–268, January 2007.

[38] H.M. Redhead, S.S. Davis, and L. Illum. Drug delivery in poly(lactide-co-glycolide) nanoparticles surface modified with poloxamer 407 and poloxamine 908: in vitro characterisation and in vivo evaluation. 70(3):353–363, February 2001.

[39] Garheng Kong, Rod D. Braun, and Mark W. Dewhirst. Hyperthermia Enables Tumor-specific Nanoparticle Delivery: Effect of Particle Size. *Cancer Research*, 60:4440–4445, 2000.

[40] Ganeshchandra Sonavane, Keishiro Tomoda, Akira Sano, Hiroyuki Ohshima, Hiroshi Terada, and Kimiko Makino. In vitro permeation of gold nanoparticles through rat skin and rat intestine: effect of particle size. *Colloids and surfaces. B, Biointerfaces*, 65(1):1–10, August 2008.

[41] Annika Vogt, Behazine Combadiere, Sabrina Hadam, Karola M Stieler, Juergen Lademann, Hans Schaefer, Brigitte Autran, Wolfram Sterry, and Ulrike Blume-Peytavi. 40 nm, but not 750 or 1,500 nm, nanoparticles enter epidermal CD1a+ cells after transcutaneous application on human skin. *The Journal of investigative dermatology*, 126(6):1316–22, June 2006.

[42] Irène Brigger, Catherine Dubernet, and Patrick Couvreur. Nanoparticles in cancer therapy and diagnosis. *Advanced drug delivery reviews*, 54(5):631–51, September 2002.

[43] Amol S Amritkar, Hiralal S Chaudhari, Deepak A Narkhede, Dinesh K Jain, and Dheeraj T Baviskar. Nanotechnology for biomedical application. *International Journal of Pharmaceutical Sciences Review and Research*, 8(2):45–53, 2011.

[44] Kwangjae Cho, Xu Wang, Shuming Nie, Zhuo Georgia Chen, and Dong M Shin. Therapeutic nanoparticles for drug delivery in cancer. *Clinical cancer research : an official journal of the American Association for Cancer Research*, 14(5):1310–6, March 2008.

[45] Rajesh Singh and James W Lillard. Nanoparticle-based targeted drug delivery. *Experimental and molecular pathology*, 86(3):215–23, June 2009.

[46] T Govender, T Ehtezazi, S Stolnik, L Illum, and S S Davis. Complex formation between the anionic polymer (PAA) and a cationic drug (procaine HCI): characterization by microcalorimetric studies. 16(7):1125–31, July 1999.

[47] Jayanth Panyam, Deborah Williams, Alekha Dash, Diandra Leslie-Pelecky, and Vinod Labhasetwar. Solid-state solubility influences encapsulation and release of hydrophobic drugs from PLGA/PLA nanoparticles. 93(7):1804–14, July 2004.

[48] B. Magenheim, M.Y. Levy, and S. Benita. A new in vitro technique for the evaluation of drug release profile from colloidal carriers - ultrafiltration technique at low pressure. *Pharmacy International Journal of Pharmaceutics*, 94:115–123, 1993.

[49] Pillai Omathanu and Ramesh Panchagnula. Polymers in drug delivery. *Current Opinion in Chemical Biology*, 5:447–451, 2001.

[50] R Brocchini, S.; Duncan. *Encyclopaedia of Controlled Drug Delivery*. Wiley, New York, 1999.

[51] U. Edlund and A. Albertsson. *Degradable Polymer Microspheres for Controlled Drug Delivery*, volume 157 of *Advanced in Polymer Science*. Springer-Verlag Berlin Heidelberg, 2002.

[52] M.L Hans and a.M Lowman. Biodegradable nanoparticles for drug delivery and targeting. *Current Opinion in Solid State and Materials Science*, 6(4):319–327, August 2002.

[53] L Brannon-Peppas. Recent advances on the use of biodegradable microparticles and nanoparticles in controlled drug delivery. *International Journal of Pharmaceutics*, 116(1):1–9, March 1995.

[54] Li Yan Qiu and You Han Bae. Polymer architecture and drug delivery. *Pharmaceutical research*, 23(1):1–30, January 2006.

[55] Simon J Holland, Brian J Tighe, and Philip L Gould. Polymers for biodegradable medical devices. 1. The potential of polyesters as controlled macromolecular release systems. *Journal of Controlled Release*, 4:155–180, 1986.

[56] Chih-Chang Chu. *Biodegradable Polymeric Biomaterials: An Updated Overview.*. CRC Press, Boca Raton, 2007.

[57] M. Dunne, O.I. Corrigan, and Z. Ramtoola. Influence of particle size and dissolution conditions on the degradation properties of polylactide-co-glycolide particles, August 2000.

[58] S A Wissing, O Kayser, and R H Müller. Solid lipid nanoparticles for parenteral drug delivery. *Advanced drug delivery reviews*, 56(9):1257–72, May 2004.

[59] D F Williams. A model for biocompatibility and its evaluation. *Journal of biomedical engineering*, 11(3):185–91, May 1989.

[60] Brian K Irons and Joseph R Robinson. Bioadhesives in Drug Delivery. In A Pizzi and K. L Mittal, editors, *Handbook of Adhesive Technology, Revised and Expanded*, chapter 48. CRC Press, 2003.

[61] Alfred D. French and Glenn P. Johnson. What crystals of small analogs are trying to tell us about cellulose structure. *Cellulose*, 11(1):5–22, March 2004.

[62] Tsuguyuki Saito and Akira Isogai. Wet Strength Improvement of TEMPO-Oxidized Cellulose Sheets Prepared with Cationic Polymers. *Industrial & Engineering Chemistry Research*, 46(3):773–780, January 2007.

[63] S. Kamel. Pharmaceutical significance of cellulose: A review. *eXPRESS Polymer Letters*, 2(11):758–778, October 2008.

[64] Ilari Filpponen. *The Synthetic Strategies for Unique Properties in Cellulose Nanocrystal Materials*. PhD thesis, Raleigh, North Carolina, 2009.

[65] Dieter Klemm, Brigitte Heublein, Hans-Peter Fink, and Andreas Bohn. Cellulose: fascinating biopolymer and sustainable raw material. *Angewandte Chemie (International ed. in English)*, 44(22):3358–93, May 2005.

[66] Roger Rowell. The Chemistry of Solid Wood. *Advances*, 207, May 1984.

[67] Andreas P. Heiner, Junji Sugiyama, and Olle Teleman. Crystalline cellulose Iα and lβ studied by molecular dynamics simulation. *Carbohydrate Research*, 273:207–223, 1995.

[68] Maren Grunert and William T. Winter. Nanocomposites of Cellulose Acetate Butyrate Reinforced with Cellulose Nanocrystals. *Journal of Polymers and the Environment*, 10:27–30, 2002.

[69] Hans Krässig. *Cellulose: Structure, accessibility and reactivity*. Gordon and Beach Science Publishers, Philadelphia, 1993.

[70] Hanne Hjorth Tø nnesen and Jan Karlsen. Alginate in drug delivery systems. *Drug development and industrial pharmacy*, 28(6):621–30, July 2002.

[71] C. Clasen and W.-M. Kulicke. Determination of viscoelastic and rheo-optical material functions of water-soluble cellulose derivatives. *Progress in Polymer Science*, 26(9):1839–1919, November 2001.

[72] Barbara Hinterstoisser and Lennart Salmén. Application of dynamic 2D FTIR to cellulose. *Vibrational Spectroscopy*, 22(1-2):111–118, February 2000.

[73] Marguerite Rinaudo. Non-covalent interactions in polysaccharide systems. *Macromolecular bioscience*, 6(8):590–610, August 2006.

[74] A Bernkopschnurch, M Hornof, and D Guggi. Thiolated chitosans. *European Journal of Pharmaceutics and Biopharmaceutics*, 57(1):9–17, January 2004.

[75] J. R Rangel-Mendez, Vladimir A. Escobar-Barrios, and Jose L Davila-Rodiguez. Biopolymers. Magdy Elnashr.

[76] C Rouget. Des substances amylacees dans le tissue des animux, specialement les Articules (Chitine). *Comptes Rendus*, 48:792–795, 1859.

[77] Q. Li, E.T. Dunn, E.W. Grandmaison, and M.F.a. Goosen. Applications and Properties of Chitosan. *Journal of Bioactive and Compatible Polymers*, 7(4):370–397, January 1992.

[78] Meera George and T Emilia Abraham. Polyionic hydrocolloids for the intestinal delivery of protein drugs: alginate and chitosan–a review. *Journal of controlled release : official journal of the Controlled Release Society*, 114(1):1–14, August 2006.

[79] A K Singla and M Chawla. Chitosan: some pharmaceutical and biological aspects–an update. *The Journal of pharmacy and pharmacology*, 53(8):1047–67, August 2001.

[80] J K Suh and H W Matthew. Application of chitosan-based polysaccharide biomaterials in cartilage tissue engineering: a review. *Biomaterials*, 21(24):2589–98, December 2000.

[81] K Okuyama. Structural diversity of chitosan and its complexes. *Carbohydrate Polymers*, 41(3):237–247, March 2000.

[82] Marguerite Rinaudo. Main properties and current applications of some polysaccharides as biomaterials. *Polymer International*, 57:397–430, 2008.

[83] Pierre Sorlier, Christophe Viton, and Alain Domard. Relation between solution properties and degree of acetylation of chitosan: role of aging. *Biomacromolecules*, 3(6):1336–42, 2002.

[84] R H Chen and M L Tsaih. Effect of temperature on the intrinsic viscosity and conformation of chitosans in dilute HCl solution. *International journal of biological macromolecules*, 23(2):135–41, August 1998.

[85] Eric Buhler and Marguerite Rinaudo. Structural and Dynamical Properties of Semirigid Polyelectrolyte Solutions: A Light-Scattering Study. *Macromolecules*, 33(6):2098–2106, March 2000.

[86] G Berth. The degree of acetylation of chitosans and its effect on the chain conformation in aqueous solution. *Carbohydrate Polymers*, 47(1):39–51, January 2002.

[87] Shobhan Sabnis and Lawrence H. Block. Improved infrared spectroscopic method for the analysis of degree of N-deacetylation of chitosan. *Polymer Bulletin*, 39(1):67–71, July 1997.

[88] W Wang and D Xu. Viscosity and flow properties of concentrated solutions of chitosan with different degrees of deacetylation. *International journal of biological macromolecules*, 16(3):149–52, June 1994.

[89] T A Sonia and Chandra P Sharma. *Chitosan and Its Derivatives for Drug Delivery Perspective*. Advanced in Polymer Science. Springer-Verlag Berlin Heidelberg.

[90] Akhlaghi, S. P., Saremi, S., Ostad, S. N., Dinarvand, R., Atyabi, F. Discriminated effects of thiolated chitosan-coated pMMA paclitaxel-loaded nanoparticles on different normal and cancer cell lines. *Nanomedicine : nanotechnology, biology, and medicine*, 6(5):689–97, October 2010.

[91] E Khor. Implantable applications of chitin and chitosan. *Biomaterials*, 24(13):2339–2349, June 2003.

[92] Jin-San Moon, Hee-Kyung Kim, Hye Cheong Koo, Yi-Seok Joo, Hyang-mi Nam, Yong Ho Park, and Mun-Il Kang. The antibacterial and immunostimulative effect of chitosan-oligosaccharides against infection by Staphylococcus aureus isolated from bovine mastitis. *Applied microbiology and biotechnology*, 75(5):989–98, July 2007.

[93] Sian C Rowe, Raymond C; Sheskey, Paul J ; Owen. *Handbook of pharmaceutical excipients*, volume 40. John Willey, London, Chicago, 15 edition, July 2003.

[94] Fu-Qiang Hu, Meng-Dan Zhao, Hong Yuan, Jian You, Yong-Zhong Du, and Su Zeng. A novel chitosan oligosaccharide-stearic acid micelles for gene delivery: properties and in vitro transfection studies. *International journal of pharmaceutics*, 315(1-2):158–66, June 2006.

[95] Bengt Rånby. The Colloidal Properties of Cellulose Micelles. *Discussions. Faraday Soc.*, 11:158–164, 1951.

[96] V Favier, H Chanzy, and J Y Cavaille. Polymer nanocomposites reinforced by cellulose whiskers. *Macromolecules*, 28:6365–6367, 1995.

[97] B. G. Rå nby and R. H. Marchessault. Inductive effects in the hydrolysis of cellulose chains. *Journal of Polymer Science*, 36(130):561–564, April 1959.

[98] Roya R Lahiji, Xin Xu, Ronald Reifenberger, Arvind Raman, Alan Rudie, and Robert J Moon. Atomic force microscopy characterization of cellulose nanocrystals. *Langmuir : the ACS journal of surfaces and colloids*, 26(6):4480–8, March 2010.

[99] Qian Xiang, Y. Y Lee, Par O Pettersson, and Robert W Torget. Heterogeneous Aspects of Acid Hydrolysis of α-Cellulose. *Applied Biochemistry And Biotechnology*, 105:505–514, 2003.

[100] Y.H. Fan, L.T.; Gharpuray, M.M. and Lee. Cellulose Hydrolysis. Springer Verlag, Berlin, 1st edition, 1987.

[101] L. Y. Mwaikambo, M. P. Ansell, A. Dufresne, M. Hughes, C. Hill, and P. M. Wild. Current international research into cellulosic fibres and composites. *Journal Of Materials Science*, 36:2107–2131, 2001.

[102] Maren Roman and Derek G Gray. Parabolic focal conics in self-assembled solid films of cellulose nanocrystals. *Langmuir : the ACS journal of surfaces and colloids*, 21(12):5555–61, June 2005.

[103] Stephanie Beck-Candanedo, Maren Roman, and Derek G Gray. Effect of reaction conditions on the properties and behavior of wood cellulose nanocrystal suspensions. *Biomacromolecules*, 6(2):1048–54, 2005.

[104] N. M. Marchessault, R. H; Morehead, F. F; Walter. Liquid crystal systems from fibrillar polysaccharides. *Nature*, 184:632–633, 1959.

[105] Y Shin, I Bae, B Arey, and G Exarhos. Simple preparation and stabilization of nickel nanocrystals on cellulose nanocrystal. *Materials Letters*, 61(14-15):3215–3217, June 2007.

[106] My Ahmed Said Azizi Samir, Fannie Alloin, Jean-Yves Sanchez, and Alain Dufresne. Cellulose nanocrystals reinforced poly(oxyethylene). *Polymer*, 45(12):4149–4157, May 2004.

[107] Hiroyuki Matsumura, Junji Sugiyama, and Wolfgang G. Glasser. Cellulosic nanocomposites. I. Thermally deformable cellulose hexanoates from heterogeneous reaction. *Journal of Applied Polymer Science*, 78(13):2242–2253, December 2000.

[108] Eero Kontturi, Leena-Sisko Johansson, Katri S Kontturi, Päivi Ahonen, Peter C Thüne, and Janne Laine. Cellulose nanocrystal submonolayers by spin coating. *Langmuir : the ACS journal of surfaces and colloids*, 23(19):9674–80, September 2007.

[109] Michael T Postek, András Vladár, John Dagata, Natalia Farkas, Bin Ming, Ryan Wagner, Arvind Raman, Robert J Moon, Ronald Sabo, Theodore H Wegner, and

James Beecher. Development of the metrology and imaging of cellulose nanocrystals. *Measurement Science and Technology*, 22(2):1–10, February 2011.

[110] Xue Min Dong, Tsunehisa Kimura, Jean-François Revol, and Derek G. Gray. Effects of Ionic Strength on the IsotropicChiral Nematic Phase Transition of Suspensions of Cellulose Crystallites. *Langmuir*, 12(8):2076–2082, January 1996.

[111] J F Revol, H Bradford, J Giasson, R H Marchessault, and D G Gray. Helicoidal self-ordering of cellulose microfibrils in aqueous suspension. *International journal of biological macromolecules*, 14(3):170–2, June 1992.

[112] Hezhong Wang. *Chitosan Cellulose Nanocrystal Polyelectrolyte Complex Particles : Preparation , Characterization , and In Vitro Drug Release Properties*. PhD thesis, Virginia Polytechnic Institute and State University, 2009.

[113] Stephanie Beck-Candanedo, David Viet, and Derek G. Gray. Triphase Equilibria in Cellulose Nanocrystal Suspensions Containing Neutral and Charged Macromolecules. *Macromolecules*, 40(9):3429–3436, May 2007.

[114] Youssef Habibi. Key advances in the chemical modification of nanocelluloses. *Chemical Society reviews*, 43:1519–1542, December 2013.

[115] Cécile Goussé, Henri Chanzy, Gérard Excoffier, Ludiwine Soubeyrand, and Etienne Fleury. Stable suspensions of partially silylated cellulose whiskers dispersed in organic solvents. *Polymer*, 43(9):2645–2651, April 2002.

[116] Gaelle Morandi, Lindy Heath, and Wim Thielemans. Cellulose nanocrystals grafted with polystyrene chains through surface-initiated atom transfer radical polymerization (SI-ATRP). *Langmuir : the ACS journal of surfaces and colloids*, 25(14):8280–6, July 2009.

[117] B. L. Peng, N. Dhar, H. L. Liu, and K. C. Tam. Chemistry and applications of nanocrystalline cellulose and its derivatives: A nanotechnology perspective. *The Canadian Journal of Chemical Engineering*, 89(5):1191–1206, June 2011.

[118] Jun Araki, Masahisa Wada, and Shigenori Kuga. Steric Stabilization of a Cellulose Microcrystal Suspension by Poly (ethylene glycol) Grafting. *Cellulose*, 17:21–27, 2001.

[119] Kevin H M Kan, Jian Li, Kushlani Wijesekera, and Emily D Cranston. Polymer-Grafted Cellulose Nanocrystals as pH-Responsive Reversible Flocculants. *Biomacromolecules*, 14(9):3130–9, September 2013.

[120] M. Gelbrich and E Gruber. Topochemically modified cellulose. *Cellulose*, 10:237–250, 2003.

[121] M. F. Semmelhack, Chuen S. Chou, and David A. Cortes. Nitroxyl-mediated electrooxidation of alcohols to aldehydes and ketones. *Journal of the American Chemical Society*, 105(13):4492–4494, June 1983.

[122] P.L. Bragd, H. van Bekkum, and A.C. Besemer. TEMPO-Mediated Oxidation of Polysaccharides: Survey of Methods and Applications. *Topics in Catalysis*, 27(1-4):49–66, February 2004.

[123] Nicolas Bordenave, Stéphane Grelier, and Véronique Coma. Advances on selective C-6 oxidation of chitosan by TEMPO. *Biomacromolecules*, 9(9):2377–82, September 2008.

[124] Denilson da Silva Perez, Suzelei Montanari, and Michel R Vignon. TEMPO-mediated oxidation of cellulose III. *Biomacromolecules*, 4(5):1417–25, 2003.

[125] Suzelei Montanari, Mohamad Roumani, Laurent Heux, and Michel R. Vignon. Topochemistry of Carboxylated Cellulose Nanocrystals Resulting from TEMPO-Mediated Oxidation. *Macromolecules*, 38(5):1665–1671, March 2005.

[126] Youssef Habibi, Henri Chanzy, and Michel R. Vignon. TEMPO-mediated surface oxidation of cellulose whiskers. *Cellulose*, 13(6):679–687, August 2006.

[127] Elsa Lasseuguette. Grafting onto microfibrils of native cellulose. *Cellulose*, 15(4):571–580, February 2008.

[128] Tsuguyuki Saito and Akira Isogai. TEMPO-mediated oxidation of native cellulose. The effect of oxidation conditions on chemical and crystal structures of the water-insoluble fractions. *Biomacromolecules*, 5(5):1983–9, 2004.

[129] D S Suh, K S Lee, P S Chang, and K O Kim. Physicochemical properties of cellulose selectively oxidized with the 2,2,6,6-tetramethyl-1-piperidinyl oxoammonium ion. *Journal of food science*, 72(5):C235–42, June 2007.

[130] T. Saito, I. Shibata, A. Isogai, N. Suguri, and N. Sumikawa. Distribution of carboxylate groups introduced into cotton linters by the TEMPO-mediated oxidation. *Carbohydrate Polymers*, 61(4):414–419, September 2005.

[131] Nadège Follain, Suzelei Montanari, Isabelle Jeacomine, Serge Gambarelli, and Michel R. Vignon. Coupling of amines with polyglucuronic acid: Evidence for amide bond formation. *Carbohydrate Polymers*, 74(3):333–343, November 2008.

[132] S Alila, F Aloulou, D Beneventi, and S Boufi. Self-aggregation of cationic surfactants onto oxidized cellulose fibers and coadsorption of organic compounds. *Langmuir : the ACS journal of surfaces and colloids*, 23(7):3723–31, March 2007.

[133] Fadhel Aloulou, Sami Boufi, Naceur Belgacem, and Alessandro Gandini. Adsorption of cationic surfactants and subsequent adsolubilization of organic compounds onto cellulose fibers. *Colloid and Polymer Science*, 283(3):344–350, June 2004.

[134] L. Chazeau, J. Y. Cavaillé, G. Canova, R. Dendievel, and B. Boutherin. Viscoelastic properties of plasticized PVC reinforced with cellulose whiskers. *Journal of Applied Polymer Science*, 71(11):1797–1808, March 1999.

[135] Jeffrey R Capadona, Kadhiravan Shanmuganathan, Dustin J Tyler, Stuart J Rowan, and Christoph Weder. Stimuli-responsive polymer nanocomposites inspired by the sea cucumber dermis. *Science (New York, N.Y.)*, 319(5868):1370–4, March 2008.

[136] Chengjun Zhou, Qinglin Wu, Yiying Yue, and Quanguo Zhang. Application of rod-shaped cellulose nanocrystals in polyacrylamide hydrogels. *Journal of colloid and interface science*, 353(1):116–23, January 2011.

[137] Xuan Yang, Emilia Bakaic, Todd Hoare, and Emily D Cranston. Injectable polysaccharide hydrogels reinforced with cellulose nanocrystals: morphology, rheology, degradation, and cytotoxicity. *Biomacromolecules*, 14(12):4447–55, December 2013.

[138] J Vincent Edwards, Nicolette Prevost, Alfred French, Monica Concha, Anthony Delucca, and Qinglin Wu. Nanocellulose-Based Biosensors : Design , Preparation , and Activity of Peptide-Linked Cotton Cellulose Nanocrystals Having Fluorimetric and Colorimetric Elastase Detection Sensitivity. *Engineering*, 5(September):20–28, 2013.

[139] J. Vincent Edwards, Nicolette T. Prevost, Brian Condon, Alfred French, and Qinglin Wu. Immobilization of lysozyme-cellulose amide-linked conjugates on cellulose I and II cotton nanocrystalline preparations. *Cellulose*, 19(2):495–506, December 2011.

[140] Barbara Thallinger, Endry N Prasetyo, Gibson S Nyanhongo, and Georg M Guebitz. Antimicrobial enzymes: an emerging strategy to fight microbes and microbial biofilms. *Biotechnology journal*, 8(1):97–109, January 2013.

[141] Khaled A Mahmoud, Keith B Male, Sabahudin Hrapovic, and John H T Luong. Cellulose nanocrystal/gold nanoparticle composite as a matrix for enzyme immobilization. *ACS applied materials & interfaces*, 1(7):1383–6, July 2009.

[142] Muzaffer A. Karaaslan, Guangzheng Gao, and John F. Kadla. Nanocrystalline cellulose/β-casein conjugated nanoparticles prepared by click chemistry. *Cellulose*, 20(6):2655–2665, September 2013.

[143] M. Roman, D. Shuping, A. Hirani, and L Yong Woo. Cellulose Nanocrystals for Drug Delivery. *ACS symposium series*, 1017:81–91.

[144] Xiaolan Zhang, Jin Huang, Peter R. Chang, Junli Li, Yongming Chen, Daxin Wang, Jiahui Yu, and Jinghua Chen. Structure and properties of polysaccharide nanocrystal-doped supramolecular hydrogels based on Cyclodextrin inclusion. *Polymer*, 51(19):4398–4407, September 2010.

[145] N. Rescignano, E. Fortunati, S. Montesano, C. Emiliani, J.M. Kenny, S. Martino, and I. Armentano. PVA bio-nanocomposites: A new take-off using cellulose nanocrystals and PLGA nanoparticles. *Carbohydrate Polymers*, 99:47–58, January 2014.

[146] Ning Lin, Jin Huang, Peter R Chang, Liangdong Feng, and Jiahui Yu. Effect of polysaccharide nanocrystals on structure, properties, and drug release kinetics of alginate-based microspheres. *Colloids and surfaces. B, Biointerfaces*, 85(2):270–9, July 2011.

[147] Xiaolin Yu, Shengrui Tong, Maofa Ge, Lingyan Wu, Junchao Zuo, Changyan Cao, and Weiguo Song. Synthesis and characterization of multi-amino-functionalized cellulose for arsenic adsorption. *Carbohydrate polymers*, 92(1):380–7, January 2013.

[148] Jessica L Cohen, Stephanie Schubert, Peter R Wich, Lina Cui, Joel A Cohen, Justin L Mynar, and Jean M J Fréchet. Acid-degradable cationic dextran particles for the delivery of siRNA therapeutics. *Bioconjugate chemistry*, 22(6):1056–65, June 2011.

[149] Shu-Jyuan Yang, Feng-Huei Lin, Kun-Che Tsai, Ming-Feng Wei, Han-Min Tsai, Jau-Min Wong, and Ming-Jium Shieh. Folic acid-conjugated chitosan nanoparticles enhanced protoporphyrin IX accumulation in colorectal cancer cells. *Bioconjugate chemistry*, 21(4):679–89, April 2010.

[150] Thomas Heinze, Andreas Koschella, Meinolf Brackhagen, and Klaus Nachtkamp. Studies on Non-natural Deoxyammonium Cellulose. *Macromolecular Symposia*, pages 74–82, 2006.

[151] Cíntia Salomão Pinto Zarth, Andreas Koschella, Annett Pfeifer, Susann Dorn, and Thomas Heinze. Synthesis and characterization of novel amino cellulose esters. *Cellulose*, 18(5):1315–1325, June 2011.

[152] Thomas Heinze, Taha Genco, Katrin Petzold-Welcke, and Holger Wondraczek. Synthesis and characterization of aminocellulose sulfates as novel ampholytic polymers. *Cellulose*, 19(4):1305–1313, May 2012.

[153] Thorbjørn Terndrup Nielsen, Véronique Wintgens, Catherine Amiel, Reinhard Wimmer, and Kim Lambertsen Larsen. Facile synthesis of beta-cyclodextrin-dextran polymers by "click" chemistry. *Biomacromolecules*, 11(7):1710–5, July 2010.

[154] Nikolaos Pahimanolis, Ulla Hippi, Leena-Sisko Johansson, Tapio Saarinen, Nikolay Houbenov, Janne Ruokolainen, and Jukka Seppälä. Surface functionalization of nanofibrillated cellulose using click-chemistry approach in aqueous media. *Cellulose*, 18(5):1201–1212, July 2011.

[155] Seyedeh Parinaz Akhlaghi, Richard C. Berry, and Kam C. Tam. Surface modification of cellulose nanocrystal with chitosan oligosaccharide for drug delivery applications. *Cellulose*, 20:1747–1764, May 2013.

[156] Khaled A Mahmoud, Jimmy A Mena, Keith B Male, Sabahudin Hrapovic, Amine Kamen, and John H T Luong. Effect of surface charge on the cellular uptake and cytotoxicity of fluorescent labeled cellulose nanocrystals. *ACS applied materials & interfaces*, 2(10):2924–32, October 2010.

[157] Masuduz Zaman, Huining Xiao, Felipe Chibante, and Yonghao Ni. Synthesis and characterization of cationically modified nanocrystalline cellulose. *Carbohydrate Polymers*, 89(1):163–170, June 2012.

[158] Jui-li Ren, Run-cang Sun, and Chan-fu Liu. Etherification of Hemicelluloses from Sugarcane Bagasse. *Journal of Applied Polymer Science*, 105(6):3301–3308, 2007.

[159] Jun-Li Ren, Feng Peng, Run-Cang Sun, and John F. Kennedy. Influence of hemicellulosic derivatives on the sulfate kraft pulp strength. *Carbohydrate Polymers*, 75(2):338–342, January 2009.

[160] He Liu, Dan Wang, Shibin Shang, and Zhanqian Song. Synthesis and characterization of AgPd alloy nanoparticles/carboxylated cellulose nanocrystals nanocomposites. *Carbohydrate Polymers*, 83(1):38–43, January 2011.

[161] M.I. Khalil, M.K. Beliakova, and A.A. Aly. Preparation of some starch ethers using the semi-dry state process. *Carbohydrate Polymers*, 46(3):217–226, November 2001.

[162] Sylvie Brochu and Guy Ampleman. Synthesis and Characterization of Glycidyl Azide Polymers Using Isotactic and Chiral Poly (epichlorohydrin) s. *Macromolecules*, 29(95):5539–5545, 1996.

[163] Stela Dragan and Luminita Ghimici. Cationic polyelectrolytes, XI* Polymers with quaternary N-atoms in the main chain obtained by condensation polymerization of epichlorohydrin with amines. *Die Angewandte Makromolekulare Chemie*, 192(3317):199–211, 1991.

[164] Firas Azzam, Laurent Heux, Jean-Luc Putaux, and Bruno Jean. Preparation by grafting onto, characterization, and properties of thermally responsive polymer-decorated cellulose nanocrystals. *Biomacromolecules*, 11(12):3652–9, December 2010.

[165] Ilari Filpponen and Dimitris S Argyropoulos. Regular linking of cellulose nanocrystals via click chemistry: synthesis and formation of cellulose nanoplatelet gels. *Biomacromolecules*, 11(4):1060–6, April 2010.

[166] Ilari Filpponen, Eero Kontturi, Sami Nummelin, Henna Rosilo, Erkki Kolehmainen, Olli Ikkala, and Janne Laine. Generic Method for Modular Surface Modification of Cellulosic Materials in Aqueous Medium by Sequential "Click"-Reaction and Adsorption. *Biomacromolecules*, 13(3):736–742, January 2012.

[167] Vitaliy V Khutoryanskiy. Advances in mucoadhesion and mucoadhesive polymers. *Macromolecular bioscience*, 11(6):748–64, June 2011.

[168] Narayan Bhattarai, Hassna R Ramay, Jonathan Gunn, Frederick a Matsen, and Miqin Zhang. PEG-grafted chitosan as an injectable thermosensitive hydrogel for sustained protein release. *Journal of controlled release : official journal of the Controlled Release Society*, 103(3):609–24, April 2005.

[169] Seunglee Kwon, Jae Hyung Park, Hesson Chung, Ick Chan Kwon, and In-san Kim. Physicochemical Characteristics of Self-Assembled Nanoparticles Based on Glycol Chitosan Bearing 5β-Cholanic Acid. *Langmuir*, 19:10188–10193, 2003.

[170] Zhijiang Cai and Jaehwan Kim. Characterization and electromechanical performance of cellulosechitosan blend electro-active paper. *Smart Materials and Structures*, 17(3):1–8, June 2008.

[171] A Isogai and R Atalla. Preparation of cellulose-chitosan polymer blends. *Carbohydrate Polymers*, 19(1):25–28, 1992.

[172] Y Wu. Preparation and characterization on mechanical and antibacterial properties of chitsoan/cellulose blends. *Carbohydrate Polymers*, 57(4):435–440, September 2004.

[173] Chao-Ming Shih, Yeong-Tarng Shieh, and Yawo-Kuo Twu. Preparation and characterization of cellulose/chitosan blend films. *Carbohydrate Polymers*, 78(1):169–174, August 2009.

[174] Ha-Soo Seong, Hyun Suk Whang, and Sohk-Won Ko. Synthesis of a quaternary ammonium derivative of chito-oligosaccharide as antimicrobial agent for cellulosic fibers. *Journal of Applied Polymer Science*, 76(14):2009–2015, June 2000.

[175] Jae Kweon Park, Mi Ja Chung, Ha Na Choi, and Yong Il Park. Effects of the molecular weight and the degree of deacetylation of chitosan oligosaccharides on antitumor activity. *International journal of molecular sciences*, 12(1):266–77, January 2011.

[176] W Arguelles-Monal, M Garciga, and C Peniche-Covas. Study of the stoichiometric polyelectrolyte complex between chitosan and carboxymethyl cellulose. *Polymer Bulletin*, 23:307–313, 1990.

[177] Sosaku Ichikawa, Satoshi Iwamoto, and Jun Watanabe. Formation of biocompatible nanoparticles by self-assembly of enzymatic hydrolysates of chitosan and carboxymethyl cellulose. *Bioscience, biotechnology, and biochemistry*, 69(9):1637–42, September 2005.

[178] Danuta Ciechaska. Multifunctional Bacterial Cellulose / Chitosan Composite Materials for Medical Applications. *Fibers & Textiles in Eastern Europe*, 12:69–72, 2004.

[179] Z Li. Study on antibacterial O-carboxymethylated chitosan/cellulose blend film from LiCl/N, N-dimethylacetamide solution. *Polymer*, 43(4):1541–1547, February 2002.

[180] C Remuñán López, a Portero, J L Vila-Jato, and M J Alonso. Design and evaluation of chitosan/ethylcellulose mucoadhesive bilayered devices for buccal drug delivery. *Journal of controlled release : official journal of the Controlled Release Society*, 55(2-3):143–52, November 1998.

[181] Susana C.M. Fernandes, Carmen S.R. Freire, Armando J.D. Silvestre, Carlos Pascoal Neto, Alessandro Gandini, Lars A. Berglund, and Lennart Salmén. Transparent chitosan films reinforced with a high content of nanofibrillated cellulose. *Carbohydrate Polymers*, 81(2):394–401, June 2010.

[182] João P de Mesquita, Claudio L Donnici, and Fabiano V Pereira. Biobased nanocomposites from layer-by-layer assembly of cellulose nanowhiskers with chitosan. *Biomacromolecules*, 11(2):473–80, March 2010.

[183] João P. de Mesquita, Claudio L. Donnici, Ivo F. Teixeira, and Fabiano V. Pereira. Bio-based nanocomposites obtained through covalent linkage between chitosan and cellulose nanocrystals. *Carbohydrate Polymers*, 90(1):210–217, September 2012.

[184] Hezhong Wang and Maren Roman. Formation and properties of chitosan-cellulose nanocrystal polyelectrolyte-macroion complexes for drug delivery applications. *Biomacromolecules*, 12(5):1585–93, May 2011.

[185] Neha Dhar, Daniel Au, Richard C. Berry, and Kam C. Tam. Interactions of Nanocrystalline Cellulose with an Oppositely Charged Surfactant in Aqueous Medium. *Colloids and Surfaces A: Physicochemical and Engineering Aspects*, September 2012.

[186] P Bulpitt and D Aeschlimann. New strategy for chemical modification of hyaluronic acid: preparation of functionalized derivatives and their use in the formation of novel biocompatible hydrogels. *Journal of biomedical materials research*, 47(2):152–69, November 1999.

[187] J S Pieper, T Hafmans, J H Veerkamp, and T H van Kuppevelt. Development of tailor-made collagen-glycosaminoglycan matrices: EDC/NHS crosslinking, and ultrastructural aspects. *Biomaterials*, 21(6):581–93, March 2000.

[188] N Nakajima and Y Ikada. Mechanism of amide formation by carbodiimide for bioconjugation in aqueous media. *Bioconjugate chemistry*, 6(1):123–30, 1995.

[189] S Sam, L Touahir, J Salvador Andresa, P Allongue, J-N Chazalviel, a C Gouget-Laemmel, C Henry de Villeneuve, a Moraillon, F Ozanam, N Gabouze, and S Djebbar. Semiquantitative study of the EDC/NHS activation of acid terminal groups at modified porous silicon surfaces. *Langmuir : the ACS journal of surfaces and colloids*, 26(2):809–14, January 2010.

[190] Nadège Follain, Marie-France Marais, Suzelei Montanari, and Michel R. Vignon. Coupling onto surface carboxylated cellulose nanocrystals. *Polymer*, 51(23):5332–5344, October 2010.

[191] Richard K. Johnson, Audrey Zink-Sharp, and Wolfgang G. Glasser. Preparation and characterization of hydrophobic derivatives of TEMPO-oxidized nanocelluloses. *Cellulose*, 18(6):1599–1609, August 2011.

[192] Ping-Sheng Liu, Qiang Chen, Xiang Liu, Bo Yuan, Shi-Shan Wu, Jian Shen, and Si-Cong Lin. Grafting of zwitterion from cellulose membranes via ATRP for improving blood compatibility. *Biomacromolecules*, 10(10):2809–16, October 2009.

[193] P Aggarwal. The combustion of starch, cellulose and cationically modified products of these compounds investigated using thermal analysis. *Thermochimica Acta*, 291(1-2):65–72, April 1997.

[194] Jie Yi, Qunxing Xu, Xuefei Zhang, and Hailiang Zhang. Temperature-induced chiral nematic phase changes of suspensions of poly(N,N-dimethylaminoethyl methacrylate)-grafted cellulose nanocrystals. *Cellulose*, 16(6):989–997, August 2009.

[195] Qiang Zhao, Shufang Wang, Xinjian Cheng, Richard C M Yam, Deling Kong, and Robert K Y Li. Surface modification of cellulose fiber via supramolecular assembly of biodegradable polyesters by the aid of host-guest inclusion complexation. *Biomacromolecules*, 11(5):1364–9, May 2010.

[196] Daniel Bondeson, Aji Mathew, and Kristiina Oksman. Optimization of the isolation of nanocrystals from microcrystalline cellulose by acid hydrolysis. *Cellulose*, 13(2):171–180, April 2006.

[197] Jie Yi, Qunxing Xu, Xuefei Zhang, and Hailiang Zhang. Chiral-nematic self-ordering of rodlike cellulose nanocrystals grafted with poly(styrene) in both thermotropic and lyotropic states. *Polymer*, 49(20):4406–4412, September 2008.

[198] Per M. Claesson and Barry W. Ninham. pH-dependent interactions between adsorbed chitosan layers. *Langmuir*, 8(5):1406–1412, May 1992.

[199] Severian Dumitriu. Polysaccharides as Biomaterials. In *Polymeric Biomaterials*, pages 1–61. CRC Canada, Quebec, 2nd edition, 2002.

[200] Kevin J Edgar, Thomas Heinze, and Charles M Buchanan. 1017 Polysaccharide Materials : Performance by Design. In *ACS SYMPOSIUM SERIES 1017*, chapter 4, pages 81–91. 2010.

[201] Sohel Shaikh, Anil Birdi, Syed Qutubuddin, Eric Lakatosh, and Harihara Baskaran. Controlled release in transdermal pressure sensitive adhesives using organosilicate nanocomposites. *Annals of biomedical engineering*, 35(12):2130–7, December 2007.

[202] Rajalaxmi Dash and Arthur J. Ragauskas. Synthesis of a novel cellulose nanowhisker-based drug delivery system. *RSC Advances*, 2(8):3403, 2012.

[203] Hanna Valo, Miia Kovalainen, Päivi Laaksonen, Merja Häkkinen, Seppo Auriola, Leena Peltonen, Markus Linder, Kristiina Järvinen, Jouni Hirvonen, and Timo Laaksonen. Immobilization of protein-coated drug nanoparticles in nanofibrillar cellulose matrices–enhanced stability and release. *Journal of controlled release : official journal of the Controlled Release Society*, 156(3):390–7, December 2011.

[204] Hanna Valo, Suvi Arola, Päivi Laaksonen, Mika Torkkeli, Leena Peltonen, Markus B Linder, Ritva Serimaa, Shigenori Kuga, Jouni Hirvonen, and Timo Laaksonen. Drug release from nanoparticles embedded in four different nanofibrillar cellulose aerogels. *European journal of pharmaceutical sciences : official journal of the European Federation for Pharmaceutical Sciences*, 50(1):69–77, September 2013.

[205] Emrah Yildir, Ruzica Kolakovic, Natalja Genina, Jani Trygg, Martin Gericke, Leena Hanski, Henrik Ehlers, Jukka Rantanen, Mikko Tenho, Pia Vuorela, Pedro Fardim, and Niklas Sandler. Tailored beads made of dissolved cellulose-Investigation of their drug release properties. *International journal of pharmaceutics*, 456(2):417–23, November 2013.

[206] Beng H Tan, P Ravi, Lie N Tan, and Kam C Tam. Synthesis and aqueous solution properties of sterically stabilized pH-responsive polyampholyte microgels. *Journal of colloid and interface science*, 309(2):453–63, May 2007.

[207] Ernesto Freire. Isothermal Titration Calorimetry and Drug Design. *Application Note*, ©MicroCal, 2006.

[208] T. Ohyama and J. A. Cowan. An approach to the evaluation of RNA solution structure and metal coordination chemistry by titration calorimetry. *Journal of Biological Inorganic Chemistry*, 1(1):83–89, February 1996.

[209] T Govender, T Riley, T Ehtezazi, M C Garnett, S Stolnik, L Illum, and S S Davis. Defining the drug incorporation properties of PLA-PEG nanoparticles. *International journal of pharmaceutics*, 199(1):95–110, April 2000.

[210] Alisdair B Boraston, David N Bolam, Harry J Gilbert, and Gideon J Davies. Carbohydrate-binding modules: fine-tuning polysaccharide recognition. *The Biochemical journal*, 382(Pt 3):769–81, September 2004.

[211] C. Wang and K. C. Tam. New Insights on the Interaction Mechanism within Oppositely Charged Polymer/Surfactant Systems. *Langmuir*, 18(17):6484–6490, August 2002.

[212] Parisa Yousefpour, Fatemeh Atyabi, Ebrahim Vashegani Farahani, Ramin Sakhtianchi, and Rassoul Dinarvand. Polyanionic carbohydrate doxorubicin-dextran nanocomplex as a delivery system for anticancer drugs: in vitro analysis and evaluations. *International journal of nanomedicine*, 6:1487–96, January 2011.

[213] Lin Huang, Xiuli Chen, Thanh Xuan Nguyen, Huiru Tang, Liming Zhang, and Guang Yang. Nano-cellulose 3D-networks as controlled-release drug carriers. *Journal of Materials Chemistry B*, 1(23):2976–2984, 2013.

[214] Sheldon R Pinnell, Huanshu Yang, Mostafa Omar, Nancy Monteiro Riviere, Holly V Debuys, Linda C Walker, Yaohui Wang, and Mark Levine. Topical L-Ascorbic Acid : Percutaneous Absorption Studies. *American Society for Dermatologic Surgery, Inc.*, 27:137–142, 2001.

[215] Yasunobu Ochiai, Satoko Kaburagi, Kei Obayashi, Nobuyuki Ujiie, Satoru Hashimoto, Yuri Okano, Hitoshi Masaki, Masamitsu Ichihashi, and Hiromu Sakurai. A new lipophilic pro-vitamin C, tetra-isopalmitoyl ascorbic acid (VC-IP), prevents UV-induced skin pigmentation through its anti-oxidative properties. *Journal of dermatological science*, 44(1):37–44, October 2006.

[216] S Murad, D Grove, K. A. Lindberg, G Reynolds, A Sivarajah, and S. R. Pinnell. Regulation of collagen synthesis by ascorbic acid Biochemistry :. *Proceedings of the National Academy of Sciences of the United States of America*, 78(5):2879–2882, 1981.

[217] Yukako Ogiri, Fang Sun, Shoko Hayami, Aki Fujimura, Kinue Yahahoto, Maki Yaita, and Shosuke Kojo. Very Low Vitamin C Activity of Orally Administered L-Dehydroascorbic Acid. *J. Agric. Food Chem.*, 50:227–229, 2002.

[218] Gregory L W Simpson and B J Ortwerth. The non-oxidative degradation of ascorbic acid at physiological conditions. *Biochimica et biophysica acta*, 1501:12–24, 2000.

[219] B. Idson. Vitamins and the skin. *Cosmetics and toiletries*, 108(12):79–94, 1993.

[220] Wenming Xie, Peixin Xu, and Qing Liu. Antioxidant Activity of Water-Soluble Chitosan Derivatives. *Bioorganic & MedicinalChemistry Letters 11*, 11:1699–1701, 2001.

[221] Ming-Tsung Yen, Joan-Hwa Yang, and Jeng-Leun Mau. Antioxidant properties of chitosan from crab shells. *Carbohydrate Polymers*, 74(4):840–844, November 2008.

[222] Ronge Xing, Song Liu, Zhanyong Guo, Huahua Yu, Pibo Wang, Cuiping Li, Zhien Li, and Pengcheng Li. Relevance of molecular weight of chitosan and its derivatives and their antioxidant activities in vitro. *Bioorganic & medicinal chemistry*, 13(5):1573–7, March 2005.

[223] Youngjin Cho, Jun Tae Kim, and Hyun Jin Park. Size-controlled self-aggregated N-acyl chitosan nanoparticles as a vitamin C carrier. *Carbohydrate Polymers*, 88(3):1087–1092, April 2012.

[224] A. Alishahi, A. Mirvaghefi, M.R. Tehrani, H. Farahmand, S. Koshio, F.a. Dorkoosh, and Maher Z. Elsabee. Chitosan nanoparticle to carry vitamin C through the gastrointestinal tract and induce the non-specific immunity system of rainbow trout (Oncorhynchus mykiss). *Carbohydrate Polymers*, 86(1):142–146, August 2011.

[225] M E W. Brand-Williams, Cuvelier and C Berset. Use of a Free Radical Method to Evaluate Antioxidant Activity. *Lebensm. Wiss. u. Technol*, 30:25–30, 1995.

[226] Janelle Tam, Juewen Liu, and Zhaoling Yao. Effect of microstructure on the antioxidant properties of fullerene polymer solutions. *RSC Advances*, 3:4622–4627, 2013.

[227] L. Y. Lim, Lucy S. C. Wan, and P. Y. Thai. Chitosan Microspheres Prepared by Emulsification and Ionotropic Gelation. *Drug Development and Industrial Pharmacy*, 23(10):981–985, January 1997.

[228] K G H Desai and H J Park. Encapsulation of vitamin C in tripolyphosphate cross-linked chitosan microspheres by spray drying. *Journal of microencapsulation*, 22(2):179–92, March 2005.

[229] Giulia Capuzzi, Pierandrea Lo Nostro, Kavita Kulkarni, and Jack E Fernandez. Mixtures of Stearoyl-6-O-ascorbic Acid and r-Tocopherol : A Monolayer Study at the Gas / Water Interface. *Langmuir*, 12(16):3957–3963, 1996.

[230] E. A. Dikusar, N. G. Kozlov, and L. a. Mel'nichuk. Salts of L-Ascorbic Acid with Certain Substituted Amines and Triphenylphosphine. *Chemistry of Natural Compounds*, 40(4):406–407, July 2004.

[231] X L Tian, D F Tian, Z Y Wang, and F K Mo. Synthesis and Evaluation of Chitosan-Vitamin C complex. *Indian journal of pharmaceutical sciences*, 71(4):371–6, July 2009.

[232] Tian Xiaolin, Tian Dafeng, Wang Zhongyan, and Mo Fengkui. Synthesis and Evaluation of Chitosan-Vitamin C Complexes. *Journal of Applied Polymer Science*, 114(June):2986–2991, 2009.

[233] Su-Il Park and Yanyun Zhao. Incorporation of a high concentration of mineral or vitamin into chitosan-based films. *Journal of Agricultural and Food Chemistry*, 52(7):1933–1939, 2004.

[234] Manuela Curcio, Francesco Puoci, Francesca Iemma, Ortensia Ilaria Parisi, Giuseppe Cirillo, Umile Gianfranco Spizzirri, and Nevio Picci. Covalent insertion of antioxidant molecules on chitosan by a free radical grafting procedure. *Journal of agricultural and food chemistry*, 57(13):5933–8, July 2009.

[235] A. Alishahi, A. Mirvaghefi, M.R. Tehrani, H. Farahmand, S.A. Shojaosadati, F.A. Dorkoosh, and Maher Z. Elsabee. Shelf life and delivery enhancement of vitamin C using chitosan nanoparticles. *Food Chemistry*, 126(3):935–940, June 2011.

[236] Marina R Kasimova. On the Temperature Dependence of Complex Formation between Chitosan and Proteins. *Biomacromolecules*, 12:2534–2543, 2011.

[237] Philip Molyneux. The use of the stable free radical diphenylpicryl- hydrazyl (DPPH) for estimating antioxidant activity. *Songklanakarin J. Sci. Technol.*, 26(2):211–219, 2004.

[238] Szu Kai Chen, Min Lang Tsai, Jin Ru Huang, and Rong Huei Chen. In Vitro Antioxidant Activities of Low-Molecular-Weight Polysaccharides with Various Functional Groups. *Agricultural and food chemistry*, 57(4):2699–2704, 2009.

[239] C. Sanchez-Moreno. Review: Methods Used to Evaluate the Free Radical Scavenging Activity in Foods and Biological Systems. *Food Science and Technology International*, 8(3):121–137, June 2002.

[240] Zhongbing Lu, Guangjun Nie, Peter S Belton, Huiru Tang, and Baolu Zhao. Structure-activity relationship analysis of antioxidant ability and neuroprotective effect of gallic acid derivatives. *Neurochemistry international*, 48(4):263–74, March 2006.

[241] Wanvimol Pasanphan and Suwabun Chirachanchai. Conjugation of gallic acid onto chitosan: An approach for green and water-based antioxidant. *Carbohydrate Polymers*, 72(1):169–177, April 2008.